



UNICA

UNIVERSITÀ
DEGLI STUDI
DI CAGLIARI

**Ph.D. DEGREE IN
ELECTRONIC AND COMPUTER ENGINEERING**

Cycle XXXVII

TITLE OF THE Ph.D. THESIS

Dynamic Radio Access Selection and Slice Allocation for Differentiated Traffic

Management Beyond 5G Networks

Scientific Disciplinary Sector(s)

ING-INF/03

Ph.D. Student: Claudia Carballo González

Supervisor: Prof. Maurizio Murrone

Final exam. Academic Year 2023/2024
Thesis defense session: February 2025

Dedicated to my grandma; wherever she is, I know she always takes care of me.

To my mom for her love, dedication, and constancy: the best mom in the world.

*To my grandfather for always being present and for his exceptional example,
dedication, and love.*

To my father for his advice, support, and love.

*To Ernesto, my favorite person, my love, my support, and my everything. To push
me every day to be better. Together, life is colorful and full of adventure.*

*To my dear in-laws, for always taking care of me and welcoming me as a daughter
in the family.*

*To the rest of my family and friends, thanks for all the shared moments that bind
us and make our relationships unique.*

*To my supervisor, Professor Maurizio Murrone, for the great opportunity that has
represented achieving this professional goal and living in Italy during these three
wonderful years.*

Contents

List of Figures	5
List of Tables	8
Abstract	8
1 Introduction	11
1.1 Research Motivation and Context	11
1.1.1 Beyond 5G Networks	11
1.1.2 The TN-NTN integration	13
1.1.3 The MBS support	14
1.1.4 Native intelligent and softwarized B5G architecture	15
1.1.5 Challenges	16
1.2 Objective	18
1.3 Contributions	19
1.4 Organization of this Document	22
2 Related Works and Theoretical Background	24
2.1 Network Slicing and Softwarized Frameworks	24
2.2 Network Selection and Slicing Resource Allocation	27
2.2.1 Heuristic-based Solutions	27
2.2.2 ML-based Solutions	28
2.3 Load Balancing	30
2.4 QoE-aware RRM Solutions	32
3 System Model and Problem Formulation	36
3.1 General System Model	36
3.2 General Problem Formulation	40
4 Heuristic-based solution for dynamic RAN/NS selection	43
4.1 Considered Scenario	44
4.2 Overview of the Proposed Algorithm	45
4.3 Network Selection Process	47

4.4	Load Balancing Process	50
4.4.1	Collaboration among candidate access networks (CANs) . . .	50
4.4.2	Collaboration among network slices (NSs)	53
4.5	Simulation and Scenarios Deployment	56
4.5.1	Scenario 1	58
4.5.2	Scenario 2	58
4.6	Results and Discussion	59
4.6.1	Results of Scenario 1	59
4.6.2	Results of Scenario 2	61
4.7	Conclusions	64
5	Hybrid terrestrial-airborne connectivity for unicast-MBS	67
5.1	Softwarized E2E 3D architecture	68
5.2	The proposed E-DASA solution	69
5.2.1	Non-Saturated Network	69
5.2.2	Saturated Network	70
5.3	Simulation and Results	71
5.4	Conclusions	74
6	ML-based solution for dynamic RAN selection into O-RAN	76
6.1	Overview of the Proposed Solution	77
6.1.1	The O-RAN Framework	77
6.1.2	eDRANS Overview	78
6.2	Network Selection Process	81
6.3	Load Balancing Process	85
6.4	Results and Discussion	89
6.4.1	Training	89
6.4.2	eDRANS Validation	92
6.5	Conclusions	97
7	F-DRL based Unicast/Multicast Delivery into O-RAN	99
7.1	The O-RAN Framework	100
7.2	Algorithm Overview	102
7.3	Results and Discussion	102
7.4	Conclusions	105
8	QoE-based energy-aware RRM solution	107
8.1	System Overview	107
8.2	Proposed Solution Overview	110
8.2.1	QoE Modeling	110
8.2.2	QoE and Energy-Aware Resource Allocation Algorithm	111
8.3	Performance Evaluation	112
8.3.1	Simulation Settings	112

8.3.2	Results and Analysis	113
8.4	Conclusion	117
9	Conclusions and Future Works	119
9.1	Conclusions and Remarks	119
9.2	Future Works	120
	Appendices	122
A	Main Mathematical Notations	123
B	Publications	126
B.1	Directly Related to the Thesis	126
B.2	Other publications	127
C	Bio	129
D	Acronyms	130
	Bibliography	148

List of Figures

1.1	The envisioned B5G networks; terrestrial network (TN); high-altitude platform (HAP); unmanned aerial vehicle (UAV); wireless fidelity (Wi-Fi); Open-RAN (O-RAN).	12
1.2	The MBS evolution towards 6G and the main features of each Rel; enhanced television (EN-TV); further evolved multimedia broadcast multicast service (FeMBMS); orthogonal frequency-division multiplexing (OFDM).	15
1.3	Challenges towards reaching the envisioned B5G heterogeneous radio access networks (RANs).	16
1.4	Main contributions to handle the defined research problems.	21
2.1	A general overview of the O-RAN architecture.	25
3.1	The general system model B5G RAN.	41
4.1	The DASA algorithm inserted in a softwarized architecture.	44
4.2	The DASA algorithm flowchart.	46
4.3	The utility functions (UFs) for VI, AR, IoT, and GM.	47
4.4	The load balancing mechanism flowchart.	51
4.5	The simulated HetNet environment.	56
4.6	Elements of the DASA validation process.	58
4.7	Best BS for the user UE_{51} in scenario 1.	59
4.8	Th_{sat} values for the user UE_{51} in scenario 1.	60
4.9	ADR for the static GT and the 1 st phase of GT with fixed C_{GC}	61
4.10	Th_{sat} standard deviation for the static GT and the 1 st phase of GT with fixed C_{GC}	62
4.11	Affected users for the 1 st phase of GT and the combination of the 1 st and 2 nd phases.	63
4.12	Residual for the 1 st phase of GT and the combination of the 1 st and 2 nd phases.	64
4.13	ADR for the combination of the 1 st and 2 nd phases of GT.	65
4.14	Average Th_{sat} for the combination of the 1 st and 2 nd phases of GT.	65

4.15	Average Th_{sat} of the base stations (BSs) for the combination of the 1 st and 2 nd phases of GT.	66
5.1	Softwarized E2E 3D architecture.	68
5.2	UFs setting for VI, AR, and WB.	69
5.3	The E-DASA algorithm's validation process.	71
5.4	Th_{sat} and SD average values for 400 users.	72
5.5	Ec average values for an incremental number of users.	73
5.6	ADR for an incremental number of users.	73
5.7	Number of affected users at each saturation point.	74
5.8	Th_{sat} average for TN-airborne unicast/broadcast and TN unicast/broadcast scenarios considering different users' priorities.	75
6.1	The RAN softwarized architecture based on the O-RAN framework.	77
6.2	The eDRANS algorithm flowchart.	80
6.3	The DDQN diagram.	84
6.4	Possible actions to perform during the coalition formation.	87
6.5	Loss function for Adam optimizer, different α values, and mini-batch sizes.	91
6.6	Loss function for Adam and SGD optimizers, and different α values.	92
6.7	Reward average during the training process.	92
6.8	Th_{sat} average for an incremental number of users.	93
6.9	Th_{sat} for different user priorities (eDRANS algorithm).	93
6.10	ADR average for an incremental number of users.	94
6.11	D average for an incremental number of users.	94
6.12	Ec average for an incremental number of users.	95
6.13	Cumulative Ec for an incremental number of users.	95
6.14	The SLA indicator (I) for an incremental number of users.	96
7.1	The O-RAN scenarios [26].	100
7.2	The proposed RAN softwarized architecture based on the O-RAN framework.	101
7.3	Th average per NS for F-DRL multicast (M), F-DRL unicast (U), and Max-SINR.	103
7.4	Th_{sat} average for F-DRL unicast/multicast (U/M), F-DRL (U), and Max-SINR.	104
7.5	ADR average for F-DRL (U/M), F-DRL (U), and Max-SINR.	104
7.6	Ec average for F-DRL unicast/multicast (U/M), F-DRL unicast (U), and Max-SINR.	105
7.7	D average for F-DRL (U/M), F-DRL (U), and Max-SINR.	106
8.1	The considered HetNet deployment scenario.	108
8.2	Average MOS_p^{TV} and Γ^{TV} for highest SF^{TV} and different w values.	113
8.3	Average MOS_p^{SP} and Γ^{SP} for highest SF^{SP} and different w values.	114

8.4	Average MOS_p^{LP} and Γ^{LP} for highest SF^{LP} and different w values.	114
8.5	Average Γ for different numbers of end devices (EDs) in the network.	115
8.6	Average MOS for different a number of EDs in the network.	116
8.7	Average ADR for a different number of EDs in the network.	116
8.8	Average Th_{sat} for a different number of EDs in the network.	117

List of Tables

1.1	Enhanced use cases' requirements.	17
2.1	State-of-the-art summary (QoS-aware RRM solutions).	32
2.2	State-of-the-art summary (QoE-aware RRM solutions); throughput (Th), backlight luminance (BL)	34
3.1	Priority weights ($\varrho_{m,o}^u$) for NS usage.	37
3.2	Possible NS states.	38
4.1	The Saaty-scale values.	48
4.2	Pairwise comparison's matrix for AR.	48
4.3	UFs weights for VI, AR, IoT and GM.	50
4.4	Pairwise comparison's matrix.	52
4.5	Data rates of the considered multimedia applications.	53
4.6	Simulation Parameters (DASA Validation)	57
4.7	NSs states (St_m^b).	57
4.8	Average Th_{sat} for the user U_{51} in scenario 1.	60
4.9	Evaluated cases in scenario 2.	61
4.10	Results of scenario 2 for 200 users.	66
5.1	Services' Th_m^{max} and Th_m^{min} requirements.	69
5.2	The E-DASA simulation parameters.	71
6.1	The w_{Th}, w_D, w_{Ec} values for VI, VR, and IIoT.	79
6.2	eDRANS simulation parameters.	90
6.3	Hyperparameters configuration.	90
8.1	Estimated overall Γ^d per week for TV, LP, and SP [118].	109
8.2	Main simulation parameters.	112
A.1	Main mathematical notations.	123

Abstract

Beyond 5G (B5G) claims a three-dimensional (3D) ecosystem with cooperation between terrestrial networks (TNs) and non-terrestrial networks (NTNs) to achieve seamless coverage, improve capacity, and enable cutting-edge applications with strict quality of service (QoS) and quality of experience (QoE) requirements. This complex environment requires a disaggregated radio access network (RAN) deployment with open interfaces, such as the architecture promoted by the Open-RAN (O-RAN) Alliance. This framework, supporting the slicing paradigm, is a prominent solution to guarantee dynamism and differentiated traffic management. Furthermore, intelligence is critical for future wireless networks to enable machine learning (ML)-based optimization for autonomous RANs, handling ultra-dense heterogeneous environments, and adapting to numerous scenarios.

Multiple types of end devices (EDs) with different mobility behaviors and tariff plans compete for finite resources, making critical an effective strategy to satisfy all requests with at least the minimum QoS requirements according to the service and user profiles. In such a context, each ED must be associated with the most suitable base station (BS) and network slice (NS) in his/her service area, ensuring the always best-connected (ABC) paradigm and seamless connectivity through the effective TNs-NTNs integration.

Bearing the previous explanation, this Ph.D. study aims to dynamically manage RAN selection and slice allocation over the envisioned B5G heterogeneous environment. First, the thesis presents an overview of the research umbrella and the motivation, specifying the objective and contributions in Chapter 1. Then, Chapter 2 overviews the related works and main theoretical concepts, and Chapter 3 establishes the system model and problem formulation. The core content regarding the objectives, contributions, and associated publications are detailed in Chapters 4 to 8.

Chapters 4 and 5 present heuristic algorithms based on multi-attribute decision-making (MADM), whereas Chapters 6 and 7 propose federated deep reinforcement learning (F-DRL) solutions inserted into the O-RAN framework. These proposals dynamically handle the RAN selection and slice allocation over the envisioned B5G environment to satisfy multiple service requests anywhere and anytime. The presented solutions aim to maximize the long-term QoS of all users in the network and optimize the slicing resource utilization based on the defined service level agree-

ment (SLA). In case of overloading, a cooperative game theory (CGT) strategy is applied to adjust resources on demand and avoid abrupt QoS degradation. Additionally, Chapters 5 and 7 analyze the importance of exploiting multicast/broadcast services (MBS) capabilities over a softwarized framework to increase network capacity and avoid congestion. Finally, Chapter 8 proposes a QoE-based energy-aware radio resource allocation process over 5G ultra-dense heterogeneous networks (HetNets). We analyze the trade-off between user perception and electricity consumption, focusing on sustainability.

The proposed solutions handle diverse network conditions, service requests, different types of EDs, mobility patterns, and priorities. Along the Ph.D. study, we conduct several simulations to prove the dynamic adaptation of our proposals in B5G heterogeneous systems while guaranteeing efficient differentiated traffic management. We demonstrate that the ML algorithm behaves similarly to the heuristic proposal, ensuring an efficient learning process based on multiple interactions with the environment. Moreover, we prove the importance of F-DRL solutions to reduce communication overhead, computational complexity (CC), and enhance data privacy, taking advantage of disaggregated and flexible architectures such as O-RAN. On the other hand, we evidence the necessity to save network resources and reduce energy consumption while maintaining satisfactory levels of QoE.

Chapter 1

Introduction

1.1 Research Motivation and Context

1.1.1 Beyond 5G Networks

According to the Ericsson report [1], the fifth-generation (5G) mobile subscriptions reached 1.6 billion by the end of 2023 with 40 % of global population coverage. Additionally, this report forecasts that 5G mobile subscriptions will exceed 5.3 billion in 2029, resulting in significant investments to adequately satisfy the stringent requirements of many different user types. Specifically, the most common 5G services launched by service providers are fixed wireless access (FWA) and enhanced mobile broadband (eMBB), including gaming and augmented reality (AR)/virtual reality (VR)-based applications.

In line with the 5G adoption and accelerated growth, the research community and industry are actively working towards beyond 5G (B5G), pushing the boundaries of wireless communication technologies to meet the evolving demands of users and various industry sectors [2]. The 3rd Generation Partnership Project (3GPP) has recently presented the project update for radio access network (RAN) Release (Rel)-18, marking the start of 5G-Advanced [3]. Some of the most distinguished features expanded in Rel-18 are extended reality (XR), multicast/broadcast services (MBS), beamforming/multiple-input multiple-output (MIMO), mobility enhancements, network power savings, and new radio (NR) coverage improvement with non-terrestrial networks (NTNs) [4, 5]. Moreover, 5G-Advanced will enable suitable artificial intelligence (AI)/machine learning (ML)-based techniques in different levels of the network (e.g., for physical (PHY) layer and RAN enhancements). Apart from the described capabilities that 5G-Advanced will introduce, it will serve as an essential step in developing mobile communications towards sixth-generation (6G).

The envisioned 6G era will represent a complete paradigm shift for global communications, merging the physical, digital, and virtual worlds through immersive human interaction [6]. The 6G architecture must be extremely scalable, disaggre-

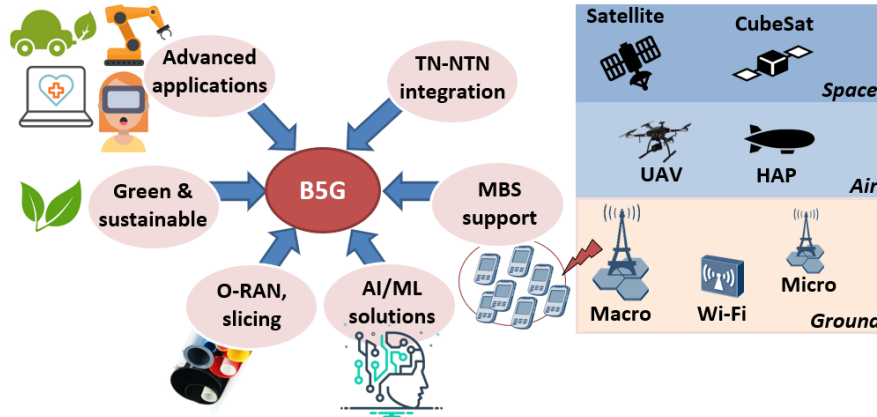


Figure 1.1: The envisioned B5G networks; terrestrial network (TN); high-altitude platform (HAP); unmanned aerial vehicle (UAV); wireless fidelity (Wi-Fi); Open-RAN (O-RAN).

gated, and virtualized, enabling ultra-secure and resilient communications. The future generation of wireless networks must adopt a green and sustainable approach with higher energy efficiency, longer life cycles, and less environmental impact [7].

6G will enable a wide range of cutting-edge applications with stringent quality of service (QoS) and quality of experience (QoE) requirements, directly impacting the industrial, educational, health, and social sectors [8–10]. A significant use case will be immersive experience-sharing communications, including holographic and three-dimensional (3D) video (VI) delivery. Then, 6G will facilitate extreme communication applications such as autonomous driving, telesurgery, mixing robotic technologies, flexible manufacturing, and seamless interaction with immersive applications. Such a wave of multimedia and experience delivery will align with an upcoming connected everything era. 6G massive communication will imply a hyperconnected infrastructure with an unprecedented diversity of end devices (EDs) (e.g., XR equipment, sensors, and cars). Facing these challenging use cases will require advanced capabilities such as 0.1 ms of latency, throughput of up to 1 Gbps , mobility at high speeds of up to 1000 km/h , a capacity density of 500 Mbps/m^2 with connection density of up to 10^8 devices per km^2 . Regarding energy and capacity efficiency, 6G will improve the 5G numbers by up to five and three times, respectively [8].

Bearing the previous explanation, Fig. 1.1 evidences some of the most distinguished features that will characterize the envisioned B5G networks. In the following subsections, we are going deep into the TN-NTN integration, the MBS support, and the necessity of a native intelligent and softwarized architecture with slicing support to satisfy multiple service requests anywhere and anytime successfully. Merging these challenging technologies in future wireless networks is a crucial motivation for this Ph.D. study.

1.1.2 The TN-NTN integration

To meet the tight requirements of future advanced applications, such as holograms and full-sense digital reality, future networks will exploit the millimeter-wave (mmWave) and terahertz (THz) bands with larger bandwidths and smaller footprints. Then, the TN infrastructure will mainly consider an ultra-dense deployment of small base stations (BSs) [11]. Moreover, wireless local area networks (WLANs) technologies, such as Wi-Fi operating at high frequencies, will play a significant role in indoor spaces, from supporting explosive growth in high-bandwidth applications to massive sensor arrays [12].

In contrast, the current study of the International Mobile Telecommunications (IMT)-2030 group positions the enhanced ubiquitous coverage as one of the prominent use cases B5G networks to close the digital divide in access in all countries, regions, and for all humanity [13, 14]. This ambitious goal cannot be possible only with TNs due to their limitations in terms of coverage and deployment [15]. Consequently, to reach the envisioned B5G global connectivity, the future infrastructure must guarantee a 3D ecosystem composed of TNs and NTN. This integration is crucial to offer a cost-effective anywhere and anytime user perception and manage diverse services, types of users, and mobility patterns [2, 16].

NTNs will constitute a critical element in fulfilling the TNs' limitations, especially in remote regions, such as rural areas, deserts, and oceans. Moreover, NTNs can complement the terrestrial infrastructure in overcrowded scenarios and serve as backhaul [15]. NTNs are distinguished as spaceborne or airborne, depending on their altitude, beam footprint size, and orbit. The spaceborne platforms are classified as:

- Geostationary Earth orbiting (GEO), which has a circular orbit at 35786 *km* above the Earth's equator. This kind of platform appears fixed in the sky to ground users with a beam footprint size in diameter ranging from 200 to 1000 *km*.
- Medium Earth orbiting (MEO) with an altitude between 7000 to 20000 *km*. Its beam footprint size in diameter ranges from 100 to 500 *km*.
- Low Earth orbiting (LEO) with an altitude varying from 600 to 1500 *km*, and a beam footprint size in diameter that varies from 100 to 500 *km* [17].

The airborne nodes include:

- HAPs with an altitude between 20 to 50 *km*. The beam footprint size in diameter typically ranges from 5 to 200 *km* based on the antenna beam width and the altitude at which the HAP operates [15, 17].
- UAVs which fly at lower altitudes up to 0.3 *km* above ground level (AGL) [18]. Thanks to their flexibility and quick deployment, a swarm of UAVs can be effectively exploited in emergencies to cover unconnected areas and assist

the terrestrial infrastructure during temporal events that generate peak traffic (e.g., football World Cup and Olympics) [19].

The 3GPP describes the different NTN architecture options deployment [20]. In the transparent mode, the NTN nodes repeat the received waveform signal unchanged, and the BS (e.g., gNodeB (gNB)) functionalities are on the ground [15]. In contrast, regenerative NTNs execute all or part of the BS functions on board the spaceborne or airborne platforms. This configuration allows the creation of faster scheduling decisions and shorter round-trip-time (RTT) concerning transparent mode [21]. In the case of regenerative NTNs with functional split, the radio unit (RU) and distributed unit (DU) functionalities could be on board, whereas the central unit (CU) could be on the ground [22].

1.1.3 The MBS support

Another essential characteristic B5G is the MBS support. Early warning dissemination, massive internet of things (IoT) updates, and live events such as the Olympics generate peak traffic, making it unfeasible to handle limited wireless spectrum resources with only unicast capabilities. With MBS, multiple concurrent EDs requesting the same content can be treated as a multicast/broadcast group and share the same network resources efficiently. Moreover, MBS reduces network delay and the risks of congestion and failures [19, 23].

In Rel-17, the 3GPP started standardizing MBS as a native 5G capability [24]. The standardization has been conducted for the overall 5G system architecture, including the next-generation RAN (NG-RAN) and the 5G core network (5GC). It introduces new functionalities into the 5GC, ensuring compatibility with legacy infrastructures and lossless handover. This recommendation supports individual and shared MBS traffic delivery. Moreover, it describes the broadcast transmission in the radio resource control (RRC) states connected and idle, whereas the multicast transmission in the connected RRC state [15, 25].

Current Rel-18 enhances unicast and MBS convergence for efficient resource utilization over ultra-dense heterogeneous networks (HetNets) (i.e., TNs-NTNs integration). Furthermore, it considers the multicast capability extension to users in RRC inactive state [25].

Fig. 1.2 shows the evolution of the envisioned MBS towards 6G networks [26]. As previously discussed, B5G systems will enable groundbreaking use cases like 360-degree VR streaming, XR, and holographic communications, requiring the MBS capabilities for efficient resource utilization and adequate computing performance. Tailored group-oriented communications are essential to streaming challenging services to numerous users distributed in a small or wide area and offloading popular information to the network edge [6]. The future MBS architecture must guarantee decentralized and distributed caching and edge computing capabilities to reduce delay and backhaul data traffic [15]. Moreover, new specifications must be oriented

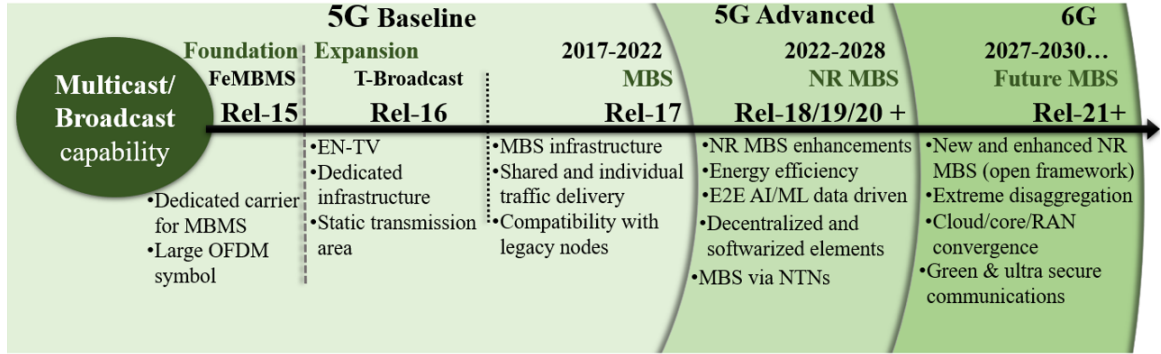


Figure 1.2: The MBS evolution towards 6G and the main features of each Rel; enhanced television (EN-TV); further evolved multimedia broadcast multicast service (FeMBMS); orthogonal frequency-division multiplexing (OFDM).

to develop end-to-end (E2E) AI/ML designs to handle complex MBS scenarios and increase energy efficiency.

1.1.4 Native intelligent and softwarized B5G architecture

The envisioned B5G systems claim for network architectures with native AI as an endogenous characteristic to handle highly dynamic and heterogeneous environments, as previously described. The B5G baseline networks must be extremely disaggregated, scalable, and virtualized, guaranteeing diverse entities' efficient and private interaction through open interfaces [7, 27].

Under these circumstances, the architecture proposed by the O-RAN Alliance has gained momentum. It leverages the increasingly software-defined network (SDN) implementations and networking functions. Instead of legacy interfaces that are vendor-specific and controlled by major industry players, it defines generic modules and open interfaces for data collection, distribution, and processing [28, 29]. The O-RAN enables an effective ML closed-loop workflow to dynamically conduct several optimization actions (e.g., network selection, load balancing, and scheduling policies) directly impacting QoS and QoE [2].

In this softwarized framework, the network slicing paradigm is a paramount feature for assurance and service provisioning [30, 31]. It allows dynamism, isolation, and prioritization by creating several logical network slices (NSs) utilizing a shared physical infrastructure. Network slicing leverages the SDN/network function virtualization (NFV) orchestration framework to dynamically instantiate, modify, and terminate NSs so that each slice is the combination of multiple chained virtual network functions (VNFs) to support the service that the slice delivers to multiple end-users [32]. Critical concerns in the slicing planning are how many NSs to deploy and what features to share across multiple NSs. Then, each NS can host several

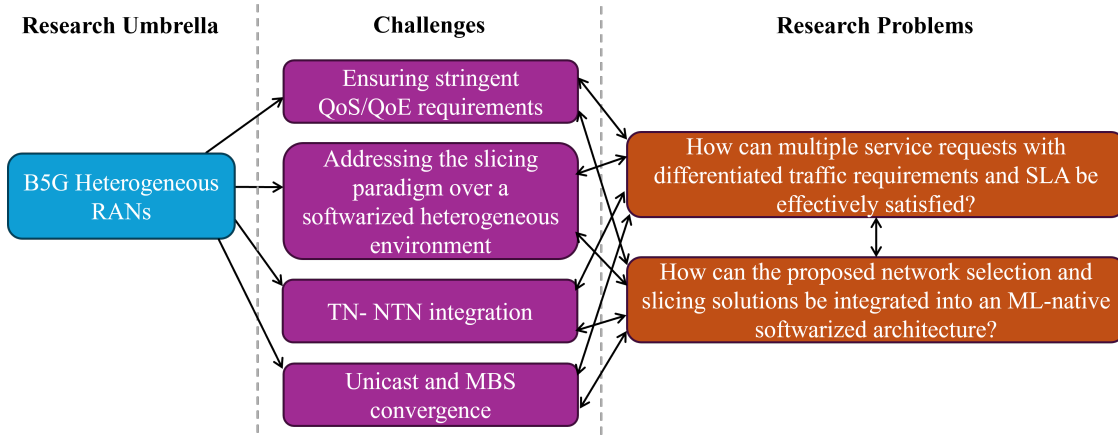


Figure 1.3: Challenges towards reaching the envisioned B5G heterogeneous RANs.

service instances, which can be associated with various network segments (e.g., RAN and core) [15]. The NSs can be tailored to accommodate various application scenarios (i.e., unicast/multicast/broadcast applications) and enable differentiated traffic management. Resources can be dynamically assigned based on service requirements, network load conditions, and users' priority according to the defined service level agreement (SLA) [2, 33].

The SLA is an official contract between the service provider and the tenant to establish service-specific QoS metrics, responsibilities, and priorities for every part. The SLA contracts differ according to the user's financial capacities (i.e., green, best effort, dedicated QoS) [34]. During the arrangement, the user chooses an SLA level based on his/her needs (i.e., QoS requirements, security) and the price he/she is willing to pay. Then, the service provider must fulfill minimum QoS requirements (i.e., threshold values) to avoid an SLA violation. For example, higher QoS and superior user perception should be ensured at higher prices.

1.1.5 Challenges

Despite the enormous advantages of the envisioned B5G wireless systems, their current development stage is far from the expected requirements with multiple open challenges. Fig. 1.3 illustrates the challenges and research problems identified under the B5G heterogeneous RANs umbrella that motivates this investigation.

We identify as a primary challenge the necessity of ensuring the stringent QoS and QoE requirements of future cutting-edge applications B5G networks. Each application is characterized by different key performance indicators (KPIs) that make the radio resource management (RRM) and, particularly, the dynamic slice allocation, a very complex process. Table 1.1 summarizes the requirements of enhanced use cases expected to be enabled by B5G networks [25, 26, 35, 36]. As defined, multimedia applications like VR require a high data throughput and extreme reliability.

Use Case	Throughput	Latency	Reliability
Video resolution of 4000 pixels (4K)	20-50 Mbps	15-35 ms	--
Video resolution of 8000 pixels (8K)	100-140 Mbps	15-35 ms	99.99999 %
AR entertainment	0.02-1 Gbps	20 ms	99.99999 %
VR entertainment	0.02-3 Gbps	5-10 ms	99.99999 %
XR	0.025-5 Gbps	5-7 ms	99.99999 %
Digital twin of smart city	10 Mbps	5-10 ms	99.99999 %
AR smart healthcare	10 Gbps	5 ms	99.999999 %
Holographic	4-10 Tbps	sub ms	--
eHealth/remote surgery	1 Gbps	< 1 ms	99.99999 %
Industrial automation	Gbps order	0.1-1 ms	99.9999999 %
Autonomous mobility	--	< 1 ms	99.99999 %

Table 1.1: Enhanced use cases' requirements.

On the other hand, applications like remote surgery and autonomous mobility are very sensitive to latency.

Multiple types of EDs with different mobility behaviors and tariff plans compete for finite resources, making critical an effective strategy to satisfy all requests with at least the minimum QoS requirements. The differentiated traffic management must leverage the slicing paradigm over a softwarized heterogeneous environment, where decentralized and intelligent solutions must be correctly designed to reduce communication overhead and computational complexity (CC) and preserve data privacy.

In such a context, each ED must be associated with the most suitable BS in his/her service area, ensuring the always best-connected (ABC) paradigm and seamless connectivity through the effective TNs-NTNs integration. This ultra-dense heterogeneous environment endows flexibility and improves service area and capacity [15]. However, several BSs at different altitudes, working at different frequencies and with diverse mobility behaviors (e.g., UAVs acting as aerial BSs) and processing capabilities, raise the RRM complexity. Specifically, using high frequencies improves capacity but reduces coverage with a substantial impact on mobility, increasing the risk of frequent handovers. Path losses, signal penetration, and blocking effects are critical concerns in these high-frequency bands (e.g., sub-THz) [16, 37, 38].

Particularly, NTN presents several challenges caused by their altitude and movement that must be effectively handled (e.g., propagation delay and path-loss, Doppler effect, inference risk, and handover issues) [16, 17]. Additionally, regenerative NTNs are more complex than transparent systems. As the BS functionalities are partially or fully integrated on board, power consumption, security, CC, overhead, and storage capacity are more significant concerns, sensibly impacting deployment costs and performance.

On the other hand, MBS is a key enabler technology B5G, especially for a dense

user deployment requesting bandwidth-demanding applications. Nevertheless, ensuring a fair and effective resource allocation with MBS delivery is more complicated than unicast because the users of the multicast group (MG) experience diverse reception conditions [26]. Group-oriented multicast applications suffer a high probability of QoS/QoE degradation due to the limitations of the users with the worst channel quality conditions. Moreover, multicasting at high frequencies and handling complex mobility behaviors (e.g., cars-mounted devices and pedestrian users coexistence) increase system complexity. These two factors are closely related to fast variations in the users' reception conditions and the MG diversity.

Considering the challenges above, the main research problem of this Ph.D. study is how to effectively satisfy multiple service requests with differentiated traffic management and no SLA violations in B5G HetNets, ensuring adequate QoS/QoE and optimizing slicing resource utilization. Additionally, we analyze how to integrate dynamic network selection and slice allocation solutions into an ML-native softwarized architecture, taking advantage of the disaggregated and open RAN components. Addressing these research problems and dealing with the identified critical challenges represent advancing the knowledge and state-of-the-art contributions regarding the envisioned B5G heterogeneous RANs.

1.2 Objective

Once the research overview and motivation have been presented, this Subsection defines the main goal and specific objectives (SOs) that guide this Ph.D. study. In such a context, this research aims to **dynamically manage RAN selection and slice allocation over the envisioned B5G heterogeneous environment**. To reach the Ph.D. main goal and face the presented challenges, we define several SOs:

- **(SO-1) Analysis of the existing RRM solutions in 5G and beyond heterogeneous RANs.** Detailed state-of-the-art analysis and definition of the principal theoretical concepts covered in the research. We delve into the network selection and slicing resource allocation processes under diverse network conditions to maximize QoS/QoE. Moreover, we analyze the insertion of RRM solutions into a native intelligent and softwarized architecture as the one promoted by the O-RAN Alliance to provide disaggregation, scalability, and dynamism.
- **(SO-2) Definition of the system model and problem formulation for addressing the network selection and slicing resource allocation tasks inserted into the B5G heterogeneous environment.** Definition of the mathematical notations used along the manuscript, constraints, and recreated network conditions.
- **(SO-3) Design a heuristic solution to conduct the network selection and resource allocation tasks under diverse B5G network conditions**

as our superior bound strategy. Definition of the optimization function based on QoS metrics, such as throughput, delay, and energy consumption. We consider several terrestrial BSs, unicast NSs, multiple EDs, tariff plans, and mobility behaviors.

- **(SO-4) Extend SO-3 to handle TNs-NTNs integration and diverse unicast, multicast, and broadcast NSs over B5G networks.** Analysis of the resource allocation improvement utilizing airborne nodes and MBS capabilities.
- **(SO-5) Extend SO-3 by proposing an ML-based network selection and resource allocation algorithm to handle complex and ultra-dense B5G HetNets.** Integration of the proposed solution into the O-RAN framework. Definition of the optimization function based on QoS metrics. Definition of the training and inference entities' location, state, and action spaces, and reward function. We consider terrestrial-airborne BSs cooperation, unicast/multicast NSs, multiple EDs, tariff plans, and mobility behaviors.
- **(SO-6) Design a QoE-based energy-aware resource allocation solution with a special focus on VI service delivery.** We propose a heuristic solution to dynamically conduct RRM over B5G HetNets. We define the electricity consumption and the perceived QoE as the optimization metrics. We consider diverse types of EDs (i.e., television (TV), laptop (LP), and smartphone (SP)) and mobility behaviors.

1.3 Contributions

The research's main contributions and related publications can be summarized as follows:

- The proposed heuristic solution represents the superior bound for this Ph.D. study, proving the dynamic slicing resource allocation for diverse network conditions, user preferences, tariff plans, and service constraints. The network selection process employs multi-attribute decision-making (MADM), distinguishing each service type's most critical QoS attributes and ensuring an efficient traffic differentiation over a heterogeneous RAN. During overload situations, we utilize a cooperative game theory (CGT) strategy based on the BSs collaboration to provide an efficient slice reallocation on-demand, avoiding abrupt throughput degradations.

Related Publications:

C. C. González, E. F. Pupo, L. Atzori and M. Murrone, "Dynamic access control and slice allocation algorithm for diverse traffic demand over 5G heterogeneous networks," 2021 IEEE International Symposium on Broadband

Multimedia Systems and Broadcasting (BMSB), Chengdu, China, 2021, pp. 1-6, doi: 10.1109/BMSB53066.2021.9547129 [39].

C. C. González, E. F. Pupo, L. Atzori and M. Murrone, “Dynamic Radio Access Selection and Slice Allocation for Differentiated Traffic Management on Future Mobile Networks,” in *IEEE Transactions on Network and Service Management*, vol. 19, no. 3, pp. 1965-1981, Sept. 2022, doi: 10.1109/TNSM.2022.3150978 [30].

- We demonstrate the positive impact on optimizing network resources and maximizing QoS by combining the slicing paradigm, MBS capabilities, and the temporal deployment of airborne nodes to assist the terrestrial infrastructure during overcrowded scenarios. Specifically, the proposal maximizes the number of users served with adequate QoS and minimizes the throughput loss when the network saturates in scenarios where multiple users request the same content simultaneously, leveraging the MBS capability.

Related Publications:

C. C. González, S. Pizzi, M. Murrone and G. Araniti, “Multicasting Over 6G Non-Terrestrial Networks: A Softwarization-Based Approach,” in *IEEE Vehicular Technology Magazine*, vol. 18, no. 1, pp. 91-99, March 2023, doi: 10.1109/MVT.2022.3232919 [15].

C. C. González, E. F. Pupo, J. Montalban, S. Pizzi, E. Iradier and M. Murrone, “Hybrid Terrestrial-Airborne Connectivity for Unicast/Broadcast Services Beyond 5G,” 2023 *IEEE International Symposium on Broadband Multimedia Systems and Broadcasting (BMSB)*, Beijing, China, 2023, pp. 1-6, doi: 10.1109/BMSB58369.2023.10211608 [19].

- The proposed ML-based network selection is based on federated deep reinforcement learning (F-DRL), which is well-suited for handling complex and ultra-dense heterogeneous environments as expected in B5G systems. We insert the ML solution in the O-RAN framework to exploit their disaggregated elements and open interfaces effectively, facilitating an ML control loop from training to model deployment. The proposal demonstrates the effectiveness of integrating terrestrial and airborne BSs to improve network capacity. Moreover, it tackles overload situations by employing CGT among resource blocks (RBs) in the selected BS. This enables balancing resources among active users and accepting new clients while guaranteeing satisfactory QoS levels. Overall, the proposal provides a comprehensive solution that handles the complexities of network selection, slice allocation, and RRM in a dynamic and heterogeneous B5G environment. Results demonstrate that our proposal behaves similarly to the heuristic solution in terms of QoS metrics while enhancing data privacy and reducing communication overhead. Additionally, we analyze the advantages of using MBS capabilities to save network resources and effectively satisfy

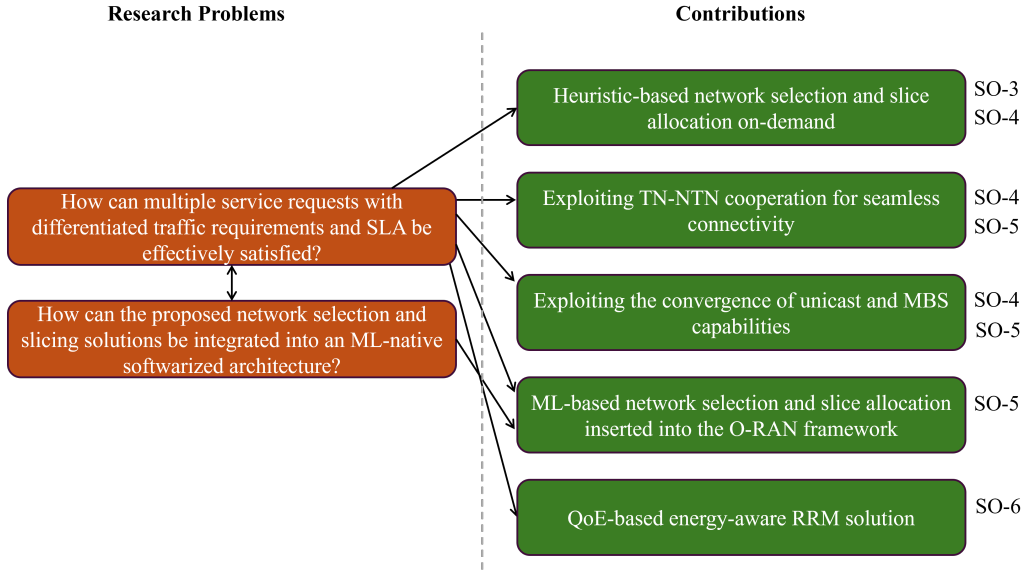


Figure 1.4: Main contributions to handle the defined research problems.

multiple concurrent users.

Related Publications:

C. C. González, E. F. Pupo, E. Iradier, P. Angueira, M. Murrioni and J. Montalban, “Network Selection over 5G-Advanced Heterogeneous Networks Based on Federated Learning and Cooperative Game Theory,” in *IEEE Transactions on Vehicular Technology*, vol. 73, no. 8, pp. 11862-11877, Aug. 2024, doi: 10.1109/TVT.2024.3373638. [2].

C. C. González, E. F. Pupo, J. Montalban, E. Iradier, P. Angueira, and M. Murrioni, “Federated Learning-based Unicast/Multicast Service Delivery over 6G O-RAN Framework,” 2024 *IEEE International Symposium on Broadband Multimedia Systems and Broadcasting (BMSB)*, Toronto, ON, Canada, 2024, pp. 1-6, doi: 10.1109/BMSB62888.2024.10608261. [40].

C. C. González, E. F. Pupo, D. Pereira-Ruisánchez, L. Atzori and M. Murrioni, “Deep Reinforcement Learning for Dynamic Radio Access Selection over Future Wireless Networks,” 2022 *IEEE International Symposium on Broadband Multimedia Systems and Broadcasting (BMSB)*, Bilbao, Spain, 2022, pp. 1-6, doi: 10.1109/BMSB55706.2022.9828746 [41].

- The proposed QoE-aware RRM solution ensures a dynamic resource allocation strategy over B5G HetNets for multiple EDs with different mobility behaviors requesting VI applications. We study the trade-off between maximizing QoE and reducing electricity consumption instead of only considering the QoS metrics. Our findings demonstrate that allocating additional RBs does not always

increase the perceived quality, but it often consumes more electricity and increases the risk of overloading.

Related Publications:

C. C. González, E. F. Pupo, G. Bingol, A. Floris, S. Porcu, M. Murrone, and L. Atzori, “A QoE-based Energy-aware Resource Allocation Solution for 5G Heterogeneous Networks,” 2024 International Conference on Quality of Multimedia Experience (QoMEX’24), Karlshamn, Sweden, 2024, pp. 29-35, doi: 10.1109/QoMEX61742.2024.10598282. [42].

The defined research goal and SOs guided the investigation process, enabling the characterization and addressing of the identified research problems. Fig. 1.4 shows the interrelation between the two research problems and the main contributions, classifying the contributions regarding the SOs. The contributions derived from each SO are explained and supported by the results and analysis of the upcoming chapters.

1.4 Organization of this Document

The thesis is structured in nine chapters, plus the appendices and bibliography. First, Chapter 1 presents an overview of the research umbrella and the motivation, establishes the objective and contributions, and finally gives the thesis outline. Chapter 2 overviews the existing related works and main theoretical concepts to understand the remainder of the paper better. Then, Chapter 3 establishes the system model and problem formulation. The core content regarding the objectives, contributions, and associated publications are detailed in Chapters 4 to 8 as follows:

- Chapter 4 presents the heuristic-based solution for dynamic network selection and slice allocation over a B5G heterogeneous environment. The proposal is evaluated through link-level simulations (LLSs) recreating multiple terrestrial RANs and service requirements mapped into unicast NSs, diverse network conditions, several types of EDs, mobility behaviors, and tariff plans.
- Chapter 5 extends the solution presented in the previous Chapter, analyzing the advantages of exploiting TNs-NTNs integration and the convergence of unicast and multicast/broadcast NSs.
- Chapter 6 presents an ML-based RRM solution to handle network selection and slice allocation over a B5G heterogeneous environment. The Chapter analyzes the integration of the proposed ML solution into the O-RAN framework. The proposal is evaluated through LLSs recreating terrestrial and airborne RANs, diverse service requirements, network conditions, types of EDs, mobility behaviors, and tariff plans. The validation process is designed to compare

the F-DRL with heuristic and traditional deep reinforcement learning (DRL) solutions.

- Chapter 7 extends the solution presented in the previous Chapter, analyzing the benefits of exploiting the MBS capabilities. Moreover, we propose the integration of the ML solution into a novel O-RAN scenario for B5G networks. The validation process is designed to demonstrate efficient resource utilization using MBS.
- Chapter 8 presents a QoE-aware RRM solution for dynamic resource allocation over B5G HetNets, considering diverse EDs requesting VI applications. The proposal is validated through LLSs, analyzing the trade-off between maximizing QoE and reducing electricity consumption instead of only considering the QoS metrics.

Finally, the general conclusions and future research directions are drawn in Chapter 9. The thesis concludes with the appendices, including the main mathematical notations and the list of acronyms. At the end, the bibliography is presented.

Chapter 2

Related Works and Theoretical Background

Chapter 1 presented an overview of the research umbrella, motivation, considered objectives and contributions, and finally gave the thesis outline. As we analyzed in Subsection 1.1.5, selecting the most suitable BS to satisfy multiple service requests in B5G networks is a necessary task due to the limited nature of resources and the ultra-dense heterogeneous conditions of RANs, EDs, and applications mapped into diverse NSs. This topic has been in the crosshairs of many researchers, industry, and standardization entities looking to optimize QoS/QoE while saving network resources, enhancing privacy, and reducing CC.

Bearing the previous explanation, this Chapter surveys the state-of-the-art related to the slicing paradigm and softwarized frameworks, the network selection and slicing resource allocation processes, and the load-balancing strategy during overload situations. Moreover, we discuss literature studies related to QoE-aware RRM solutions instead of only QoS optimization approaches.

2.1 Network Slicing and Softwarized Frameworks

B5G communication systems must be disaggregated, softwarized, and dynamic to deal with a highly complex and ultra-dense heterogeneous environment. Open interfaces and intelligent controllers must guarantee reliable E2E communication between multiple entities at different altitudes and with diverse characteristics and priorities. Built on top of emerging technologies such as SDN and NFV, network slicing must manage the computing, storage, and network resources to meet the extremely diversified requirements of enhanced applications.

From this perspective, Barakabitze *et al.* [43] reviewed the standardization efforts for 5G slicing supported by SDN and NFV technologies. This work represents a deep state-of-the-art analysis, highlighting architectural approaches in practical

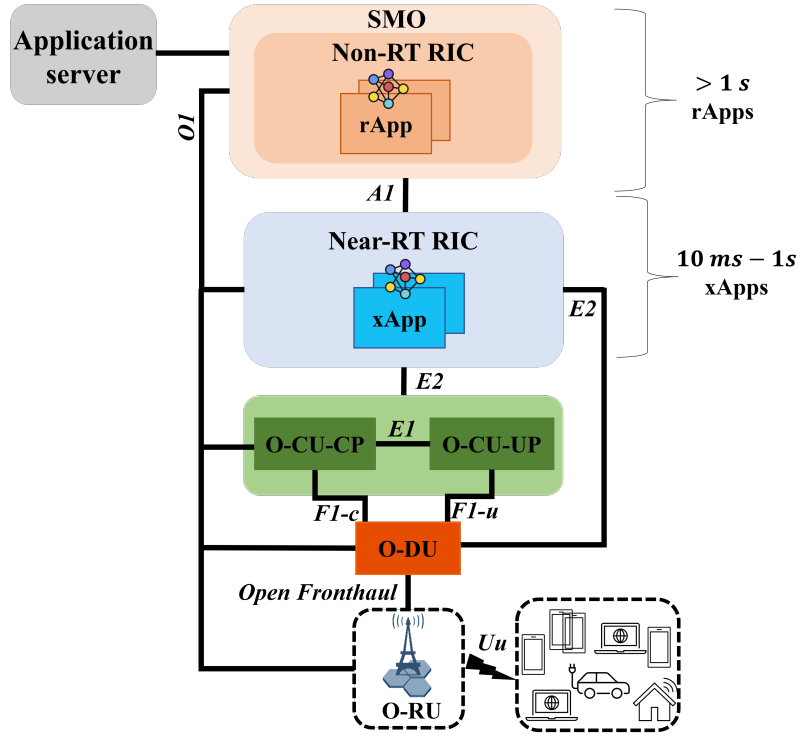


Figure 2.1: A general overview of the O-RAN architecture.

implementations and deployment strategies. Taleb *et al.* [44] proposed a network slicing management and orchestration architecture incorporating SDN and NFV components to the 3GPP slicing management. In [45], the authors proposed a QoS framework for network slicing based on SDN and NFV technologies. Their proposal is based on monitoring network status to compute the best resource allocation path. Yousaf *et al.* [46] presented a mobility management extension for NFV orchestration to dynamically adapt the NSs capacity and select the suitable template for slice instantiation and the correct mobility scheme according to the users' mobility behavior. The authors of [47] introduced an architecture that combines SDN, NFV, and satellite slicing to distribute network resources on demand. In addition, they defined several services that must be attended to considering available capacity and QoS requirements. In [48], the authors explained the E2E slicing process from service requests to NSs deployment and life-cycle management. Further, Park *et al.* [49] analyzed the main use cases and technology trends associated with network slicing, detailing the organizations and open-source projects involved in the slicing development.

In this era of software-defined infrastructure, the architectural framework endorsed by the O-RAN Alliance has significantly gathered pace. O-RAN is an ML-native framework that uses virtualized and disaggregated elements interconnected through open interfaces (Fig. 2.1) to conduct dynamic tasks. Its mission is to re-

shape the RAN industry towards fully interoperable mobile networks, guaranteeing a smooth collaboration between multiple vendors and network elements. It can operate with numerous deployment configurations offering custom solutions [29, 49].

In the O-RAN framework, the BS functionalities are disaggregated into the Open-RAN central unit (O-CU)-control plane (CP), O-CU-user plane (UP), Open-RAN distributed unit (O-DU), and Open-RAN radio unit (O-RU). Then, these functional units can be flexibly deployed at different network locations and hardware platforms. Additionally, the slicing paradigm aids this architecture, mapping multiple service types into numerous NSs to dynamically manage differentiated traffic and ensure the defined SLA [6, 34].

Two critical elements in the O-RAN architecture are the RAN Intelligent Controllers (RICs) identified as Non-Real Time RIC (Non-RT RIC) and Near-Real Time RIC (Near-RT RIC) [50]. The Non-RT RIC is a Service Management and Orchestration (SMO) framework component. It can implement RAN optimization's actions (e.g., forecasting traffic load) through microservices termed *rApps* on a time scale superior to 1 s [29]. It trains and updates ML models that will be executed nearer to the end-user (e.g., Near-RT RIC). Moreover, the Non-RT RIC realizes long-term monitoring of RAN slices via the *O1* interface and sends *A1* policies and enrichment information to the Near-RT RIC to drive slices and E2E SLA assurance.

The Near-RT RIC is deployed at the network's edge and operates in control loops between 10 ms and 1 s. It conducts monitoring tasks through the *E2* interface to detect whether the performance is out of the target KPIs indicated via *A1* policies or to collect new service requests. Furthermore, the Near-RT RIC can execute RAN optimization actions (e.g., handover management, load balancing) through microservices termed *xApps* based on *E2*, *O1*, and *A1* information.

The papers [28, 29, 51] presented a comprehensive overview of the O-RAN specifications, describing its architecture, proposed scenarios, and interfaces. Moreover, they discussed how the RICs can be used to effectively manage the 3GPP-defined RANs in different timescales according to specific use cases. Particularly, we discussed in [52] the insertion in the envisioned 6G O-RAN framework of ML-based RRM solutions integrating unicast and MBS capabilities. This research covered essential aspects at the intersection of MBS, ML-based RRM solutions, and the disaggregated O-RAN architecture, identifying possible scenarios as feature extensions of O-RAN B5G networks.

The above papers represent a good benchmark for understanding how this Ph.D. study could be integrated into different state-of-the-art softwarized frameworks. These works distinguish the high value of merging slicing and softwarization technologies over next-generation wireless networks. In such a context, the O-RAN framework is an excellent option to develop intelligent and disaggregated ML-based RRM solutions that allow satisfying multiple service requests with adequate QoS and QoE in B5G systems.

2.2 Network Selection and Slicing Resource Allocation

This Section discusses how selecting the most suitable BS and NS combination over a heterogeneous infrastructure is complicated but meaningful since multiple types of EDs request various services with tight QoS requirements simultaneously. Numerous users compete for finite resources; then, it is necessary for an effective strategy to improve user satisfaction and optimize resource utilization [53]. We present some of the most recent works on network selection and slicing resource allocation processes, divided into heuristic and ML-based solutions.

2.2.1 Heuristic-based Solutions

Desogus *et al.* [54] presented the Traffic tYpe-based DifferEntiated Reputation (TYDER) algorithm, a network selection method based on MADM and analytical hierarchy process (AHP). They considered network reputation in the context of diverse application requirements: VI, gaming, navigation, and IoT. Montalban *et al.* [55] proposed a similar approach based on MADM to address multiple users' requests within a convergent architecture that encompasses broadcast, broadband, and cellular services. This proposal makes the decision based on a combination of throughput, delay, packet success rate, and spectral efficiency parameters. In [56], the authors presented a multi-criteria analysis to evaluate and rank IoT applications. They also used MADM and AHP methods, combining parameters such as cost, number of customers, privacy, and availability. In general, MADM enables making a preference-based decision over the available alternatives that are characterized by multiple attributes. Then, AHP helps to define the attributes' weight values [54].

The above investigations represent an excellent approach to the network selection task. However, they did not address the simultaneous users' requests of multiple service instances. Moreover, the authors' approach did not include the network slicing paradigm. Instead, in [57], the authors presented a multi-criteria analysis to select the best NS among candidate slice instances. Furthermore, the proposal considered memory and central processing unit (CPU) resources, as well as throughput and delay.

Alternatively, Bakmaz *et al.* [58] proposed a technique for order preference by similarity to the ideal solution (TOPSIS) to select the best NS among available slices. TOPSIS considers the following steps: normalization, weighting calculation, and alternative ranking [59]. In [60], the authors proposed a genetic algorithm (GA) [61] to select the optimal BS and NS. The proposal is validated by comparing it with the traditional received signal strength (RSS) criterion [62] and the greedy algorithm [63]. However, they considered that an NS could be only associated with one BS for proving the proposal. Moreover, they assumed that users only request one service flow, limiting the slicing advantages.

References [57, 58, 60] represent a good approach to NS's access and handover process. Nevertheless, they did not inquire into the different behavior of QoS metrics for several possible applications in the selection process. On the other hand, none of the previous papers, except [55], exploited the potentialities of combining unicast and MBS capabilities.

Contrary, Montalban *et al.* demonstrated in [64] how integrating a broadcast-oriented RAN architecture into a heterogeneous environment solves the exponential growth of multimedia data traffic and improves the energy efficiency of future wireless networks. The authors of [65] proposed a heuristic solution to serve users with good reception conditions via unicast transmissions and users with poor channel quality conditions via multicast. Khalid *et al.* [66] presented an adaptive multicast resource allocation algorithm based on the multicast traffic demand while giving the unused resources to unicast traffic. The works [55, 64–66] represent good approaches for analyzing the advantages of multicast/broadcast capabilities. However, they did not exploit the slicing potential to enable differentiated traffic management in a complex and dynamic environment. Furthermore, none of the above papers discussed the importance of TNs-NTNs integration for an adequate anywhere and anytime service perception [15].

2.2.2 ML-based Solutions

In the context of B5G networks, the increasing complexity of massive, dynamic, and heterogeneous systems has rendered heuristic algorithms impractical [67]. A significant drawback is their high CC since handling extensive data is required for a complete (if possible) system knowledge [41, 68]. Traditional algorithms like MADM iterate among all possibilities to find the best solution for each generated event. Therefore, it is challenging to formulate an accurate mathematical model to get global optimal results in a short time [69]. Consequently, recent papers have shifted their focus towards solving network selection through ML approaches. Although ML methods have a high cost of offline training, they can quickly make near-optimal decisions once trained. Moreover, ML solutions do not depend on accurate mathematical models, which makes them appealing for very complex network scenarios [68, 70].

Particularly, DRL increases attention thanks to its capacity to solve complex problems with a large state space, automating sequential decision-making tasks. It does not require extensive datasets since it learns optimal policies through multiple trial-and-error interactions with the environment [41, 67]. In [41], the authors proposed a centralized double deep Q-network (DDQN) algorithm aided by dynamic NS allocation to serve multiple users with different priorities and service preferences. Zhang *et al.* [71] considered a centralized agent to manage user association and resource allocation over a heterogeneous environment. However, centralized schemes could suffer scalability issues in real deployments, and only small networks or some straightforward applications can benefit from this strategy [53].

The authors of [72] presented a distributed algorithm where each BS, based on its local information, shows its willingness to attend the service request. Additionally, a superior entity makes a random final decision among all available BSs. This proposal is suboptimal because it does not guarantee that the best BS is always selected. Sun *et al.* [73] proposed a distributed DRL mechanism with slicing deployment to minimize the long-term handover cost while ensuring the user's QoS. The agents consider the priority, throughput, delay, and CPU usage. As a weak point, the considered NS's bandwidth allocation was static. Thus, this paper does not exploit the potential of dynamic slicing allocation for different network conditions. In general, distributed ML strategies reduce the overhead and complexity regarding centralized systems. However, the no round-trip fashion between an aggregated unit and the agents limits the generated local models to only use the individual information without any benefit from peer's data [74]. In the case of [75], a DRL multi-agent solution is proposed, in which the BSs are the agents to manage resource allocation and reduce frequent handovers. The authors offered an effective combination of states from adjacent BSs, and their coefficients are jointly computed to improve results. Nevertheless, this solution does not inquire about privacy issues.

Recent studies have been focused on F-DRL to overcome the limitations of centralized and distributed ML processes. This solution is highly appropriate for complex environments, benefiting from collaborative ML training while preserving data privacy and considerably reducing communication overhead compared with traditional ML approaches (e.g., centralized ML models).

In [76], the authors presented an algorithm based on F-DRL and game theory (GT), where multiple multi-access edge computing (MEC) domains collaborate on building an efficient learning model preserving privacy and adjusting the virtual resources over industrial IoT scenarios. Liu *et al.* [77] introduced a device association scheme for RAN slicing. They leveraged a hybrid F-DRL approach to enhance throughput and reduce handover costs. The authors of [78] employed a user-centric F-DRL algorithm to select the proper BS and RBs for delivering the requested service. Nevertheless, this strategy raises concerns regarding selecting agents for the training phase, particularly in environments with diverse types of EDs, battery limitations, and varying mobility patterns. Additionally, the effectiveness of user decisions relies on a higher-level entity that ultimately determines whether to accept the proposed BS association by the user. This introduces complexity, mainly because multiple users compete for the same resources.

Wang *et al.* [79] proposed a support vector machine (SVM)-federated learning solution where multiple high-altitude balloons cooperate as local agents in building an SVM model to determine the user association that reduces overall energy and time consumption. In [80], the authors presented an F-DRL algorithm inserted in the O-RAN architecture to take advantage of this disaggregated framework. According to the number of NSs at each BS, multiple parallel layers are deployed in the RIC to enhance local resource allocation. The action space is a set of discrete numbers of RBs, assuming the presence of a preliminary admission mechanism such as presented

in [78]. Abouaomar *et al.* [81] proposed an F-DRL algorithm where multiple mobile network operators (MNOs) collaborate to improve the performance of their RAN slicing models based on the O-RAN architecture. In [82], the authors presented an F-DRL solution where several BSs participate in training a common ML model to tailor the power allocation of their users. Even considering diverse mobility behaviors, [82] does not apply user association and eventual handover process. The papers [76–82] did not include either user priority differentiation or a heterogeneous RAN infrastructure (TNs-NTNs integration), which represents one of the future wireless networks’ pillars [15, 83].

2.3 Load Balancing

Load balancing is a crucial and challenging strategy for optimizing slicing resource utilization and satisfying multiple users’ requests B5G networks. This process becomes even more critical in overload situations, where dynamic resource reallocation is required to accept new clients while current users’ satisfaction is not abruptly degraded. However, none of the previously analyzed works considered resource adjustment during overloading.

Different, the authors of [84] focused on the principles of load balancing in 5G network slicing. They categorized different mathematical models of resource allocation, dividing them into game-theoretic economic models [85], prediction models [86–88], and robustness and failure recovery models [89, 90]. Specifically, the GT approach has been extensively used in networking research problems, and it is suitable to apply in allocation problems over B5G HetNets [84, 91, 92]. This mathematical framework is a powerful tool to model players’ interaction, attempting to make decisions that maximize each entity’s utility. In particular, Han *et al.* [93] described the potential of CGT to handle a wide range of applications in wireless communication systems. Additionally, one of the main branches of the CGT is the coalition formation, deeply described in [94–97].

The authors of [98] proposed a heuristic network selection algorithm based on MADM and offered a CGT solution for load balancing. Anedda *et al.* [99] dealt with overloading by gradually decreasing the throughput of current users to accept new customers on the network. This solution is based on the Markov decision process (MDP). Additionally, they considered different users’ priorities (business and typical) and several screen resolutions. The papers [98, 99] only focused on VI content delivery without exploiting the slicing paradigm.

Botez *et al.* [100] presented a heuristic solution for real-time monitoring and dynamic path adjustment only in case of congestion. The proposal was focused on 5G backhaul networks for slices with very low latency requirements. The defined thresholds are adapted based on congestion severity, and the optimal path is recalculated as needed. In [101], the authors proposed a deep-learning model for congestion control. This proposal aims to select the proper NS according to the service requests

and network conditions. If a particular NS fails or exceeds a defined threshold in terms of capacity (93 %), the incoming traffic is automatically assigned to a master NS. As a weak point, each NS is configured with fixed resources, and there is no applied resource adjustment to already users in the overloaded NS.

Zhang *et al.* [102] presented a heuristic greedy strategy for data traffic control. This solution makes a congestion judgment at each time step, identifying the overloaded links. Then, some part of the traffic of these links is migrated to alleviate saturation and avoid data losses. However, the proposal did not consider bit rate adaptation of current clients in overloaded links to free up resources and attend to new clients. The authors of [83] analyzed the TNs-NTNs integration to increase coverage and capacity. They proposed a heuristic load-balancing solution in which some traffic of an overloaded cell is migrated to a neighbor cell or another BS (e.g., satellite) with enough resources. Initially, the users are randomly distributed among terrestrial cells without applying a network selection process. The NTN infrastructure only assists the TN when overloaded. The proposal is limited to the number of BSs without considering bit rate adaptation.

Considering the works analyzed in Subsection 2.2.1 and in this current Subsection as benchmarks, Chapter 4 presents the Dynamic radio Access selection and Slice Allocation (DASA) algorithm [30]. This proposal is an integral solution to handle the network selection and the load balancing strategies based on MADM and CGT. It takes advantage of slicing, SDN, and NFV potentials, allowing an adequate QoS and management of critical services. Moreover, DASA considers users with different priorities requesting multiple services simultaneously, guaranteeing a dynamic and efficient slice allocation over 5G HetNets and beyond. Further, as an evolution of the DASA algorithm, Chapter 5 presents a heuristic solution that exploits the MBS capabilities and the TNs-NTNs integration to improve network capacity and coverage [19].

On the other hand, compared with the works presented in Subsections 2.2.1, 2.2.2 and in this current Section, our proposal enhanced Dynamic Radio Access Network Selection (eDRANS) (Chapter 6) stands out as an integral solution inserted in the emerging O-RAN architecture [2]. It addresses the challenge of dynamic network selection and slice allocation over a heterogeneous environment to satisfy multiple users with diverse priorities, mobility patterns, and service requirements. It is considered the cooperation among terrestrial and airborne nodes to improve network capacity and coverage. One of the advantages of eDRANS is its foundation on the F-DRL approach, which is well-suited for handling large and diverse state spaces while enhancing data privacy and reducing communication overhead. The algorithm makes a preference statement for BSs without overloading, selecting the BS that maximizes QoS for each user in the network. Furthermore, eDRANS tackles overload situations by employing CGT among RBs in the selected BS. This enables balancing resources among active users and accepting new clients while guaranteeing satisfactory QoS levels. Overall, the eDRANS proposal provides a comprehensive solution that handles the complexities of network selection, slice allocation, and

Paper	eDRANS [2, 40]	DASA [19, 30]	[55]	[78]	[80]	[98]	[99]	[101]
Action target	BS selection/ NS allocation	BS selection/ NS allocation	BS selection	BS selection/ RB allocation	NS allocation	BS selection/ RB adjustment	RB allocation	NS selection/ allocation
Method	F-DRL +CGT	MADM +CGT	MADM	F-DRL	F-DRL	MADM	MDP	SVM
Overload	✓	✓	×	×	×	✓	✓	✓
O-RAN	✓	×	×	✓	✓	×	×	×
RAN slicing	✓	✓	×	×	✓	×	×	✓
User priority	✓	✓	×	×	×	×	✓	×
TN-airborne	✓	[19] ✓, [30] ×	×	×	×	×	×	×
MBS	[2] ×, [40] ✓	[19] ✓, [30] ×	✓	×	×	×	×	×

Table 2.1: State-of-the-art summary (QoS-aware RRM solutions).

resource management in a dynamic and heterogeneous environment.

Chapter 7 represents a variation of the eDRANS proposal, examining the advantages of exploiting MBS delivery [40]. Moreover, the proposed ML model is inserted into a novel O-RAN scenario for B5G networks.

Table 2.1 summarizes the distinguished features of eDRANS and DASA proposals compared with some of the state-of-the-art works. As mentioned before, DASA represents the superior bound of this Ph.D. study because it iterates among all possibilities to select the BS that maximizes the QoS in the coverage area of each ED. In the case of eDRANS, it is an ML-based solution inserted into the O-RAN framework to handle complex and heterogeneous environments, reduce CC, and enhance data privacy with a negligible QoS degradation regarding DASA.

2.4 QoE-aware RRM Solutions

In the expected B5G systems, which open the doors to immersive and interactive services, a purely network-centric approach will not fully capture the real user experience and the diverse nature of advanced applications. These strategies focus on measurable technical aspects to only optimize QoS, often disconnected from subjective expectations and individual user preferences [103]. Specifically, the QoE is defined as “the degree of delight and annoyance of the user of an application or

service” [104]. Then, the user experience is affected by the network performance and further aspects, such as the device characteristics, the context, and the user’s preferences and expectations. For this reason, the same QoS can be perceived with a different QoE on the user’s side. Consequently, future networks must shift towards a user-centric approach that prioritizes QoE, while optimizing network resource usage and reducing energy consumption [7].

Particularly, the rapid advancement of technology has led to an exponential increase in VI streaming performance, significantly enhancing the user QoE. Nevertheless, this progress has come at the cost of higher electricity consumption. Indeed, while the delivery of VI content at the highest quality undoubtedly contributes to providing satisfactory QoE, it also leads the E2E VI delivery chain to massive energy usage, posing a substantial challenge to the goal of sustainable development adopted by the United Nations Member States, which is aimed to minimize greenhouse gas (GHG) emissions by 2030¹.

The research [105] evidenced that the carbon emissions of 5G networks are about 50 % less than those of the fourth-generation (4G) in terms of information transmission bit. However, [106] reported that since the 5G bandwidth is still underutilized in short burst flows, it consumes $1.67\times$ more energy than 4G when the ED is running the same Web loading sessions. Additionally, the study in [107] analyzed that higher data traffic increases electricity consumption, whereas smaller devices (i.e., smaller size and screen resolution) consume less electricity. Therefore, a purely QoE-aware RRM strategy may lead to excessive electricity consumption because the resources would be allocated to provide the highest quality content without regard to sustainability. This is the main limitation of most literature studies focused on network management implementing QoE resource allocation algorithms [108–110].

The paper [108] presented a QoE-centric analysis for multimedia services over 5G networks with a particular focus on the QoS/QoE correlation. Barakabitze *et al.* [109] performed a dynamic link resources management in softwarized 5G networks to optimize QoE. The QoS/QoE correlation was constructed based on an exponential mapping function. The authors of [110] proposed a user association procedure selecting the BS that provides the highest QoE. In this case, the video multimethod assessment fusion (VMAF) strategy evaluates the VI user perception. As a drawback, VMAF is a full-reference objective quality metric with high CC, requiring access to detailed VI information that is generally inaccessible by MNOs [111]. On the other hand, Rahdari *et al.* [112] presented a non-linear fuzzy RRM approach, evaluating the QoE based on transmission rate and service price.

Bearing the previous explanation, the MNOs must adopt energy-efficient architectures to reduce their power consumption and take on social responsibility to decrease the carbon footprint [115]. On the other hand, recent research evidenced the tendency of more users to be more attentive to sustainability. They could slightly sacrifice QoE, always maintaining adequate service perception while decreasing car-

¹<https://sdgs.un.org/2030agenda>

Paper	Our proposal [42]	[109]	[110]	[112]	[113]
Action target	BS selection and RBs allocation	Resources allocation	BS selection and power allocation	Resources allocation	Best download network selection
RRM Method	MADM	Heuristic	GA	Non-linear fuzzy	Heuristic
QoE model	Obtained through subjective test	QoS/QoE correlation	VMAF	QoS/QoE correlation	ITU-T P.1201 [114]
QoE factors	Th and BL	bandwidth, user priority, video codec	video features	Th and service price	video features
Network	Wi-Fi and 5G	5G	5G	5G	Wi-Fi, 3G and Bluetooth
ED types	TV, LP, and SP	Not specified	SP	Not specified	SP
Mobility behavior	static and random directional mobility	Not specified	Not specified	Not specified	Not specified
Sustainability	✓	×	×	×	✓

Table 2.2: State-of-the-art summary (QoE-aware RRM solutions); throughput (Th), backlight luminance (BL)

bon emissions [116, 117]. In such a context, the paper [118] presented a subjective QoE assessment, demonstrating that streaming lower-quality VI would not necessarily lead to a noticeable QoE decrease, whereas it would save a relevant amount of energy and network resources. Then, the QoE-aware RRM solutions must find the right balance between assigning RBs for adequate ED perception (not necessarily the maximum QoE value) while reducing unnecessary electricity consumption.

The authors of [119] proposed an energy management system for energy/QoE-efficient request redirection of content delivery network (CDN) clusters. The QoE is estimated based on its correlation with QoS, considering the number of instantaneous requests. Abbas *et al.* [113] presented user-centric traffic splitting strategies in HetNets to achieve a high QoE level for VI-on-demand applications with low cost and energy consumption. The authors analyzed the user accessibility through Wi-Fi, third-generation (3G) wireless networks, and Bluetooth communication. Nevertheless, they did not examine the stringent conditions in B5G networks.

Different, Chapter 8 presents a QoE-aware RRM solution to dynamically allocate resources in 5G heterogeneous scenarios [42]. Unlike the previous works, the proposed solution aims to identify the trade-off between the overall QoE perceived by the different types of EDs (i.e., TV, LP, and SP) when visualizing VI content and the overall network energy consumption. Then, we define a score function considering the combined impact of both metrics. The QoE is obtained based on previous subjective tests conducted on [118]. Table 2.2 summarizes the distinguished features of our proposal compared with some of the state-of-the-art works.

Chapter 3

System Model and Problem Formulation

This Chapter defines the system model and the general problem formulation of the proposed algorithms for addressing the network selection and resource allocation tasks over B5G heterogeneous RANs. We first define the main mathematical notations, constraints, and recreated network conditions. Then, we present the general problem formulation of the proposed solutions in the manuscript. For better understanding, Table A.1 summarizes the main mathematical notations used throughout the document.

3.1 General System Model

We consider that the network serves a set of U user equipments (UEs), randomly distributed in the service area, denoted by \mathbb{U} with the sub-index $u \in \{1, 2, \dots, U\}$. We assume that according to the provider and tenants' defined SLA [34, 99], the users can belong to one of the priority levels $p^u = \{1, 2\}$. Priority high ($p^u=1$) corresponds to premium clients paying more to guarantee the best possible QoS level. In contrast, priority low ($p^u=2$) corresponds to regular users who pay less and are satisfied with the minimum quality according to the service's requirements. We distinguish four types of EDs: TV, LP, sensor (SN) and SP with $d \in \{TV, LP, SN, SP\}$. Particularly, the TVs, LPs, and SNs have static mobility, whereas SPs are static or follow a random way-point (RWP) mobility. The SNs have high priority due to their critical application type, and the rest of the EDs can have one of the possible priority levels.

We recreate a B5G heterogeneous RAN environment with a set of B BSs defined by \mathbb{B} , and the sub-index $b \in \{1, 2, \dots, B\}$. $\mathbb{B} = \mathbb{T} \cup \mathbb{N}$, where \mathbb{T} is the group of TN-BSs, whereas \mathbb{N} is the set of NTN-BSs. Each BS_b has a capacity defined in terms of RBs of a fixed bandwidth (BW_{RB_b} , expressed in MHz) and operates at

Usage	PS	SS_1	SS_2	SS_3	SS_4	SS_5	SS_6	SS_7
1	8/8							
2	6/8	2/8						
3	6/8	2/12	1/12					
4	6/8	3/24	2/24	1/24				
5	4/8	4/20	3/20	2/20	1/20			
6	4/8	5/30	4/30	3/30	2/30	1/30		
1	4/8	6/42	5/42	4/42	3/42	2/42	1/42	
1	4/8	7/56	6/56	5/56	4/56	3/56	2/56	1/56

Table 3.1: Priority weights ($\varrho_{m,o}^u$) for NS usage.

some specific frequency f_b . An RB is the smallest frequency resource the BS can allocate, corresponding to 12 consecutive and equally spaced subcarriers for an RB bandwidth $BW_{RB_b} = 12 \times \Delta f_b$. As defined by the 5G NR standard, we assume numerology (μ) for the subcarrier spacing value defined as $\Delta f_b = 15 \times 2^\mu$, expressed in kHz [120].

The set of M NSs denoted by \mathbb{M} , with the sub-index $m \in \{1, 2, \dots, M\}$, can be available or not in different BSs. They can host several service instances defined by the QoS parameters and specific demanding resources (e.g., high-data-rate applications). The set of NSs to accommodate the UE_u request is denoted by \mathbb{M}_u , where $\mathbb{M}_u \subseteq \mathbb{M}$. On the other hand, the set of L possible services is defined by \mathbb{L} , with the sub-index $l \in \{1, 2, \dots, L\}$. Each service considered is characterized by different KPIs (e.g., throughput, delay, and energy consumption). Therefore, we assume each service is mapped into a different NS.

The notation φ_o^u specifies each requested service by the UE_u . According to the services' preferences, the most important for the user UE_u is classified as primary service (PS), and the rest as secondary services (SSs). This preference relation is represented by the sub-index o , where $o = 1$ identifies the PS and $o > 1$ represents the SSs in order of preference.

The $\varrho_{m,o}^u$ is the priority value of the requested NS_m by the UE_u . The highest priority slice for the user hosts his/her PS, and we assign to this slice the highest weight. At the same time, the priority of the SSs is weighted in decreasing order according to the user request (i.e., $\varrho_{m,o=2}^u > \varrho_{m,o=3}^u$). The 3GPP defines that the UE does not need to support more than eight NSs simultaneously [121]. Therefore, we assume the priority weights of the users' requested services according to Table 3.1. The $\varrho_{m,o}^u$ follows the rule expressed in

$$\sum_{m \in \mathbb{M}_u} \varrho_{m,o}^u = 1. \quad (3.1)$$

The available RBs (RB_b^{av}) in the BS_b must be dynamically assigned considering the number of requests, users' priorities, mobility behavior, and QoS constraints.

St_m^b	Accessible	Activated
0	×	×
1	✓	×
2	✓	✓

Table 3.2: Possible NS states.

The variable $\psi_m^b \in \{0,1\}$ denotes the availability of resources for the NS_m in the BS_b , where 0 means that the number of RB_b^{av} are insufficient to assign the minimum throughput (Th) required by the user for the NS_m (Th_m^{min}). The accessibility of the NS_m via the BS_b is denoted by $\kappa_m^b \in \{0,1\}$, where 0 means that the NS_m is unavailable from the BS_b due to the impossibility to access the service (e.g., a security reason) or missing functionality. Additionally, $\varkappa_{b,m}^u$ details the historical association of the user UE_u with the NS_m via BS_b .

From the previous explanation, we define the possible states of NS_m in the BS_b as $St_m^b \in \{0,1,2\}$, where the meaning of these values is displayed in Table 3.2. For example, the NS_m is activated in the BS_b if it is accessible and is being used ($St_m^b = 2$). This information is contained in the NS Repository in the SMO framework.

To evaluate the network conditions to satisfy each requested service (with preference o configured in the NS_m), we define the individual score $S_{b,m,o}^u \in [0,1]$. The score for each requested service is represented by utility functions (UFs) and their respective weights (w). The UFs represent the most sensitive attributes that characterize the QoS: Th , delay (D), jitter (J), packet loss ratio (PLR), and energy consumption (Ec). The weights denote the importance of such QoS parameters. The individual score is defined as follows

$$S_{b,m,o}^u = \sum_{uf \in \mathbb{UF}} w_{m,uf}^u \times UF_{m,uf}^u, \quad (3.2)$$

and

$$\sum_{uf \in \mathbb{UF}} w_{m,uf}^u = 1, \quad (3.3)$$

where uf is the sub-index to iterate through the set \mathbb{UF} and their corresponding weights. The cardinality of \mathbb{UF} is denoted by n , representing the number of sensitive attributes associated with each service. The AHP [122] determines the w values according to the relevance's relation among them for the different analyzed services. Specific details will be covered in Chapters 4 and 6.

The Th that a UE_u can receive regarding BS_b ($Th_{b,m}^u$) depends of the user reception conditions and the assigned RBs ($RB_{b,m}^u$) from the RB_b^{av} . This term, expressed in Mb/s, is defined as

$$Th_{b,m}^u = e_{ffb}^u \times RB_{b,m}^u \times BW_{RB_b}, \quad (3.4)$$

where $RB_{b,m}^u \leq RB_b^{av}$. The e_{ffb}^u is the efficiency (in b/s/Hz) corresponding to the modulation and coding scheme (MCS) received by the UE_u regarding BS_b . The

reception conditions bound the maximum modulation efficiency supported by the user, s.t. channel quality indicator (CQI), CQI_b^u [52].

The CQI values range from 0 to 15, where 0 means that the user is out of the BS service area, 1 is for the users' lowest channel quality, and 15 is for the best reception conditions. This research assumes the U users are in the service area (i.e., $1 \leq CQI_b^u \leq 15$). The reported CQI_b^u is directly related to the signal-to-interference-plus-noise ratio (SINR) experienced by each UE_u . This SINR is higher than or equal to the minimum SINR ($SINR_{min}$) required to decode the MCS associated with the reported CQI correctly. Each MCS has associated a specific code rate and e_{fb}^u value according to Table 5.2.2.1-3 in [120]. We assume perfect CQI estimation, and the impact of imperfect CQI estimation is out of the scope of this research.

$D_{b,m}^u$, expressed in seconds (s), is the delay experimented by the user to access the required service through the BS_b , and it is calculated as

$$D_{b,m}^u = D_{b,m}^{u,Tx} + D_{b,m}^{u,Q}, \quad (3.5)$$

where $D_{b,m}^{u,Tx}$ is the transmission delay, and $D_{b,m}^{u,Q}$ is the queuing delay.

$Ec_{b,m}^u$, expressed in joule (J), is the energy consumption calculated by the user accessing the requested service via the BS_b

$$Ec_{b,m}^u = P^u \times D_{b,m}^u, \quad (3.6)$$

where P^u , expressed in watt (W), is the power consumed by the user UE_u for the specific service reception. $D_{b,m}^u$ is inversely proportional to $Th_{b,m}^u$; consequently, a higher $Th_{b,m}^u$ means a lower value of $Ec_{b,m}^u$ accessing the requested service.

$PLR_{b,m}^u$ (dimensionless) is defined by

$$PLR_{b,m}^u = MissedPackets_{b,m}^u / TotalPackets_{b,m}^u, \quad (3.7)$$

where $MissedPackets$ is the number of lost packets from the total number of transmitted packets ($TotalPackets$) [54].

To obtain the jitter, expressed in seconds, we apply

$$J_{b,m}^u = D_{peak}_{b,m}^u + 2 \times F_c \times Rrms_{b,m}^u, \quad (3.8)$$

where D_{peak} is the deterministic jitter according to systematic effects (e.g., inter-symbol interference and periodic jitter). $Rrms$ is the random jitter resulting from accumulating random processes, requiring statistical analysis to be quantified. Additionally, F_c is a factor tabulated according to different bit error rate (BER) tolerances [123].

As we can observe, the UFs (e.g., $Th_{b,m}^u$ and $D_{b,m}^u$) have different units of magnitude that make a fair comparison impossible [54]. Therefore, we normalize them (e.g., $Th_{b,m}^{u, Norm}$ and $D_{b,m}^{u, Norm}$) to ensure their proportional contribution to the $S_{b,m,o}^u$.

In this work, we consider the UFs upward and downward (UF^{up}, UF^{down}) equations [124–126] expressed by

$$UF^{up} = \begin{cases} 0, & \text{if } x < x_{min} \\ 1 - \frac{x_{max} - x}{\delta' \times (x_{max} - x_{min})}, & \text{if } x_{min} \leq x \leq x_{max} \\ 1, & \text{otherwise.} \end{cases} \quad (3.9)$$

$$UF^{down} = \begin{cases} 1, & \text{if } x < x_{min} \\ 1 - \frac{x - x_{min}}{\delta' \times (x_{max} - x_{min})}, & \text{if } x_{min} \leq x \leq x_{max} \\ 0, & \text{otherwise,} \end{cases} \quad (3.10)$$

where equation 3.9 represents the upward criteria and describes the Th . On the contrary, equation 3.10 denotes the downward criteria and describes the D , J , Ec , and PLR . The variables x_{min} and x_{max} are the minimum and maximum tolerable values defined for each service. The functions are dimensionless and range from 0 to 1. The variable $\delta' \geq 2$ is a tuned steepness parameter depending on the application type [124].

On the other hand, the throughput satisfaction ($Th_{sat,b}^u$) is a dimensionless value that ranges between 0 and 1. It computes the ratio between the assigned $Th_{b,m}^u$ and the maximum Th (Th_m^{max}) supported by the requested service. Additionally, the $Th_{sat,b}^{average}$ value is obtained averaging the $Th_{sat,b}^u$ of all users in the BS_b . A $Th_{sat,b}^u = 1$ means that the BS_b is capable of assigning to the UE_u the number of necessary resources to achieve Th_m^{max} , s.t. reception conditions and RB_b^{av} .

Each QoS metric has a specific minimum and maximum tolerable value according to the service profile and the user priority. Then, if the minimum constraints are met, the SLA is satisfied and expressed with the indicator $I_{b,m}^u = 1$, otherwise $I_{b,m}^u = 0$. Particularly, the satisfaction degree (SD) (SD_b^u) is the ratio between the number of assigned NSs and the total requested NSs by the user UE_u .

3.2 General Problem Formulation

As we explained in Chapter 1, in the highly complex and heterogeneous B5G environment, each UE_u must be associated with one or more NSs via TN or NTN, guaranteeing an adequate QoS and QoE. Then, the main challenge that we face in our research is how to effectively satisfy multiple service requests in B5G HetNets considering diverse types of users, mobility patterns, and tariff plans, guaranteeing improved user satisfaction and optimizing resource utilization.

As Fig. 3.1 shows, the BSs must be connected to intelligent controllers through open interfaces to perform dynamic optimization actions, such as network selection, MG formation, and load balancing. In general, the resource allocation process must always be oriented to satisfy the minimum constraints for each UE_u (s.t. user priority and application profile) without exceeding the necessary resources to obtain the Th_m^{max} . Moreover, due to the finite number of resources and the dynamic variations

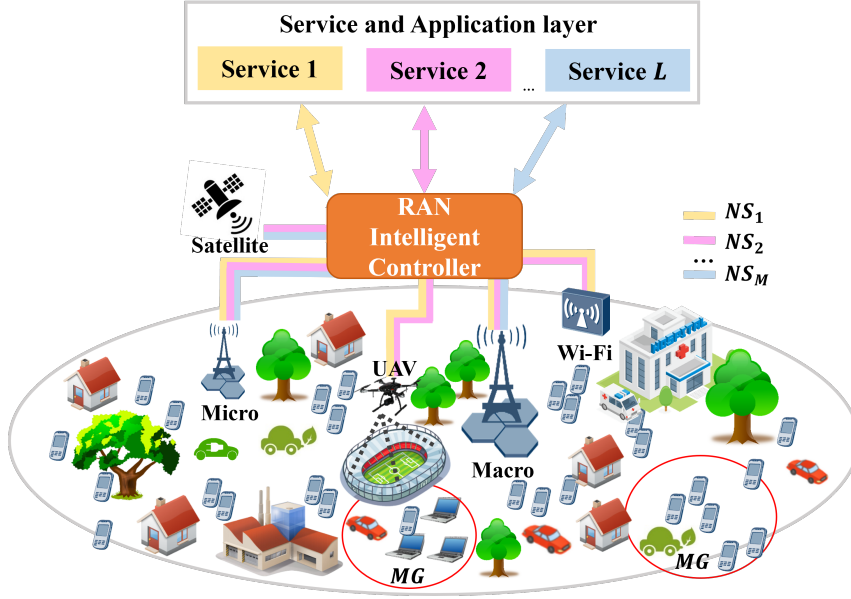


Figure 3.1: The general system model B5G RAN.

in the service requests, predefining RBs for each NS may lead to inefficient resource usage with a negative impact on QoS/QoE. Then, we consider a slicing model without fixing the resources for each NS. On the other hand, the users requesting the same content simultaneously (e.g., massive IoT updates and live video streaming) can benefit from the MBS capabilities, forming a MG to use the same NS resources efficiently. In this case, the user with the worst reception conditions bound the RRM process.

In a softwarized heterogeneous environment, the envisioned monitoring system must detect new users' service requests, existing users' service updates, or existing users' CQI variation according to a certain threshold. Then, the proposed algorithms select the most suitable BS to satisfy each user according to his/her priority and service constraints. In general, each algorithm can be formulated as a long-term utility optimization problem to maximize the score function (SF) $SF_b^{u,t}$, $\forall u \in \mathbb{U}$:

$$\max \lim_{T \rightarrow \infty} \sum_{t=1}^T \sum_{u=1}^U SF_{b,m}^{u,t}, \quad (3.11)$$

where t represents a specific transmission time interval (TTI), and T is the total number of TTIs. Particularly, the algorithms presented in Chapters 4, 5, 6, and 7 aim to maximize the QoS and optimize slicing resource allocation. In these cases, the SF combines multiple QoS metrics and the accessibility of the NS_m via the BS_b (κ_m^b), distinguishing diverse network conditions, user types, mobility behaviors, service constraints, and slice accessibility. Chapters 4 and 5 present heuristic solutions, whereas Chapter 6 and 7 propose a ML-based algorithm that guarantees enhancing privacy and reducing communication overhead.

On the other hand, the heuristic algorithm presented in Chapter 8 aims to optimize resource allocation in a heterogeneous environment, analyzing the trade-off between the QoE and the electricity consumption. Then, the SF is defined as a combination of these two metrics. This solution is focused on VI streaming applications, considering diverse types of EDs and mobility behaviors. Further details will be given in the next Chapters.

Chapter 4

Heuristic-based solution for dynamic network selection and slice allocation B5G systems

This Chapter presents a novel Dynamic radio Access selection and Slice Allocation (DASA) algorithm over 5G HetNets and beyond. This algorithm is an integral solution to handle BS selection and slice allocation for diverse network conditions, leveraging emerging technologies like SDN, NFV, and the slicing paradigm. The proposed solution, analysis, and conclusions respond to **SO-3**. The main contributions can be summarized as follows:

1. DASA integrates the network selection and load balancing mechanisms, efficiently managing slice allocation in B5G heterogeneous wireless networks. The algorithm considers users requesting multiple services simultaneously. It takes advantage of the MADM method and the slicing paradigm by dynamically handling diverse QoS requirements, network conditions, user preferences, and tariff plans.
2. The load balancing process is based on CGT, applying two collaborative phases: among BSs and among NSs. This procedure guarantees an efficient slice reallocation on-demand, avoiding abrupt throughput degradations of active users in the network.
3. The proposal recreates a heterogeneous environment composed of several terrestrial BSs, unicast NSs, and multiple users. Comprehensive simulation results are obtained by optimizing resource utilization, considering critical features such as throughput, delay, energy consumption, overloading, and NS availability. The validation is focused on DASA flexibility and the efficient utilization of network resources during the network selection and load-balancing strategies. The DASA validation demonstrates the differentiated treatment

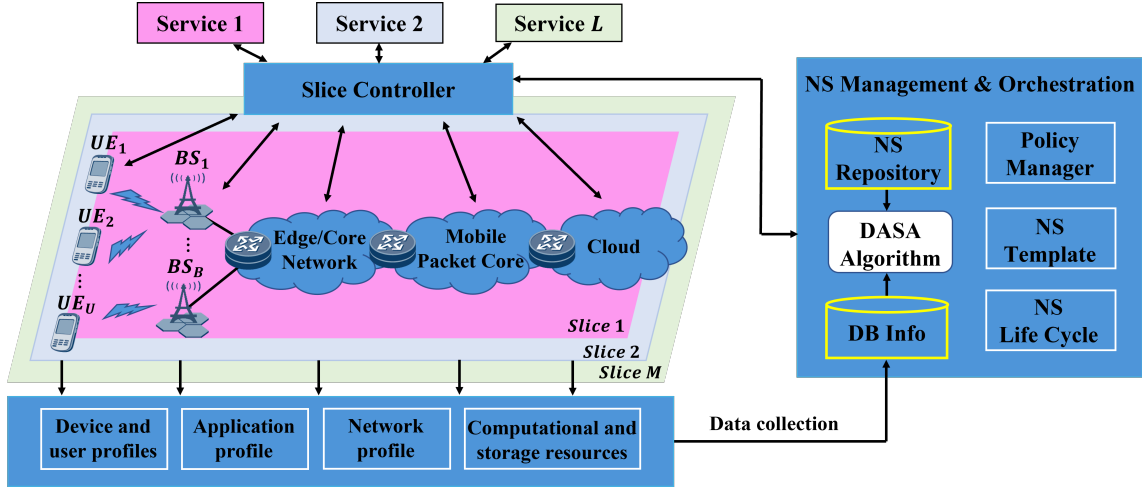


Figure 4.1: The DASA algorithm inserted in a softwarized architecture.

between premium and regular clients, ensuring a superior QoS for the users with high priority. Moreover, the algorithm achieves an efficient resource re-allocation, affecting a minimum number of users at each saturation point.

4.1 Considered Scenario

The proposed algorithm considers an E2E slice deployment based on the softwarization technologies SDN and NFV with particular application to the RAN domain. The proposed solution is set on the reference architecture [127, 128], shown in Fig. 4.1, which includes the RAN with several BSs, the transport network layer, the mobile packet core network, and the cloud computing infrastructure.

The architecture considers different service types (i.e., Services 1- L in Fig. 4.1) demanding specific resources and attributes, and it provides an E2E connection service according to the users' requests. Particularly, we consider four services: VI, AR, IoT, and cloud gaming (GM), characterized by specific functionalities and resources. Therefore, a user can request from one to four of these services simultaneously. We assume that each service is associated with one NS (i.e., one NS for each of the four typologies of service).

In this softwarized system, DASA is integrated into the NS Management and Orchestration module, interacting with the Slice Controller during the network selection and load balancing processes. The Slice Controller has complete control of the network. It oversees the coordination of service requests and drives resource allocation.

The DASA algorithm is triggered when the Slice Controller detects a new user's services request (e.g., connecting a group of IoT devices, streaming 360-degree VI),

when a user wants to change the service type and requirements, or when it is necessary a handover process or a resource reallocation due to the degradation of the current network's QoS below a certain threshold. Depending on application and user profiles, these thresholds are imposed on throughput, delay, jitter, packet loss ratio, and energy consumption.

The objective of the DASA module is to select the best combination of access network (i.e., which BS to be associated) and NSs to satisfy the user's requests and handle a load balancing strategy during an overload situation. DASA requires access to the Database Information (DB Info) and the NS Repository to determine the best combination to satisfy the user's requests and maximize the resulting QoS. The former gathers in real-time the following data:

- User profile: contains the users' preferences and their tariff plans.
- Device profile: specifies the device characteristics, such as the screen resolution, current position, and mobility behavior.
- Network profile: collects information about identification (ID), type, and the available wireless networks' QoS.
- Application profile: details the services/NSs performance that users are currently using.

Following the General Data Protection Regulation (GDPR) [129], it is important to highlight that collected data must be kept anonymous to protect users' privacy. Specifically, an identification number is associated with the user terminal, which is not linked to any information that may identify the user. Additionally, this data is collected once user consent is given.

The NS Repository contains information about the active NSs in each architecture layer, their supported service instances, and the allocated virtual and physical resources. This information is used to check if the slice to accommodate a requested service exists (St_m^b).

DASA sends the results to the NS Life-Cycle, which manages the topology and resources update and the creation and deletion of NSs. The NS creation is based on the NS Template, which stores the attributes that characterize the topology of NS services. Additionally, the Policy Manager oversees the NS policies enforcement, such as the access rules and the creation and expiration times.

4.2 Overview of the Proposed Algorithm

DASA selects the best combination of BS and NSs over a heterogeneous environment to fulfill users' requests and optimize network resource usage. Fig. 4.2 shows the DASA algorithm flowchart, highlighting the most critical processes detailed in the following Sections 4.3 and 4.4.

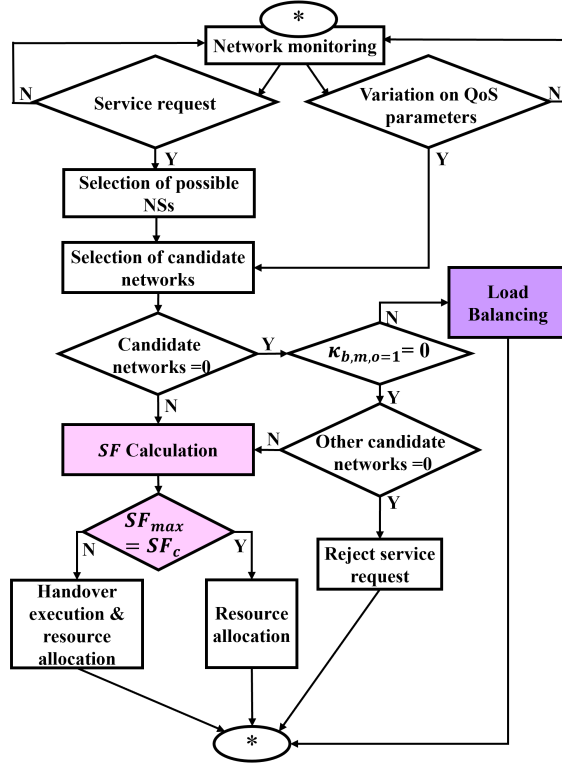


Figure 4.2: The DASA algorithm flowchart.

As mentioned, DASA is triggered when the Slice Controller detects a new user request or the variation on QoS parameters according to a certain threshold, s.t. service performance, and user's priority. According to Fig. 4.2, if there are new service requests, first, the algorithm identifies the NSs able to accommodate the petition. Then, it selects the candidate access networks (CANs) among the available BSs in the user's coverage area (i.e., small-cell, macro-cell, or Wi-Fi access point (AP)).

The BS_b is considered a CAN if it supports at least the NS corresponding to the user's PS. The reception conditions and RB_b^{av} must guarantee at least the Th_m^{min} required for the PS. Additionally, the $D_{b,m,o}^u$, $J_{b,m,o}^u$, $PLR_{b,m,o}^u$, and $EC_{b,m,o}^u$ of the user accessing the PS ($o = 1$) via BS_b must be less than or equal to the maximum admissible values.

Once the CANs have been identified, DASA determines the best access network to fulfill the user request. The algorithm computes a SF SF_b^u for each CAN, and the BS_b with the highest value (SF_{max}) is selected. If the SF_{max} value does not belong to the user's current network (SF_c), the handover process will be executed.

If there are no CANs due to the NS's inaccessibility to the PS ($\kappa_{m,o=1}^b = 0$), DASA selects other CANs that support the SSs, and it applies the rest of the algorithm according to Fig. 4.2. On the contrary, if there are no CANs due to a

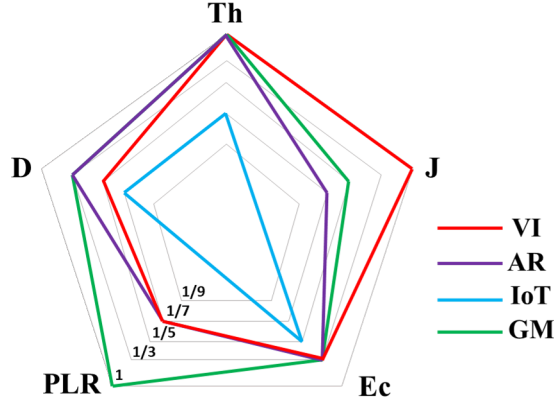


Figure 4.3: The UFs for VI, AR, IoT, and GM.

lack of resources for the PS ($\psi_{m,o=1}^b = 0$), the load balancing mechanism is activated (details in Section 4.4).

When the network has enough capacity, DASA assigns the maximum resources and does not consider the user's priority. On the other hand, during a load balancing mechanism, the algorithm applies different strategies to adjust the Th from the current value to the imposed threshold according to the service performance and the user's tariff plan. This resource allocation strategy is applied according to the defined SLA among providers and tenants.

DASA never assigns more resources than the maximum required by the service (Th_m^{max}). The algorithm ensures the maximum possible $Th_{b,m}^u$ for the UE_u according to the service requirements, tariff plan, $e_{ff_b}^u$, and RB_b^{av} .

4.3 Network Selection Process

As highlighted in Fig. 4.2, the most important element of the network selection process is the SF_b^u calculation for each CAN to select the most suitable combination of BS and NSs. The SF_b^u is a dimensionless function $\in [0, 1]$ based on MADM to combine multiple normalized attributes considering the NSs accessibility, resource availability, user, and application profiles. The $SF_{b,m}^u = 1$ means that the BS_b can satisfy the request maximizing the QoS. As we assumed in Subsection 4.1, an NS only allocates one service. Therefore, the SF_b^u is defined by

$$SF_b^u = \sum_{m \in \mathbb{M}_u} \psi_{m,o}^b \times \kappa_{m,o}^b \times \varrho_{m,o}^u \times S_{b,m,o}^u \quad (4.1)$$

The notations used are presented in Section 3.2. As we previously described, the individual score $S_{b,m,o}^u$ for each requested service (equation 3.2) is represented by UFs (equations 3.9 and 3.10) and their respective weights (equation 3.3).

Fig. 4.3 shows the considered services and the sensitive attributes that affect their QoS in different proportions. We consider $n = 3$ for IoT and $n = 5$ for VI,

Scale	Definition
1	Equal importance
3	Moderate importance of one over another attribute
5	Strong importance
7	Very strong importance
9	Extreme importance
1/3	Little less critical one over another
1/5	Fairly less importance
1/7	Definitely less importance
1/9	Extremely less importance

Table 4.1: The Saaty-scale values.

	<i>Th</i>	<i>D</i>	<i>Ec</i>	<i>J</i>	<i>PLR</i>
<i>Th</i>	1	3	3	7	7
<i>D</i>	1/3	1	1	5	5
<i>Ec</i>	1/3	1	1	5	5
<i>J</i>	1/7	1/5	1/5	1	1
<i>PLR</i>	1/7	1/5	1/5	1	1

Table 4.2: Pairwise comparison's matrix for AR.

AR, and GM, where n is the number of comparable UFs in the set UF as previously defined.

In the case of the analyzed multimedia services, *Th* is the attribute with the most significant impact. According to the IoT scenario, the applications can be classified into machine or human-oriented, delay-sensitive or not, and with different *Th* requirements [130]. In this proposal, as shown in Fig. 4.3, we assume IoT applications characterized by a massive number of connected devices transmitting a low data rate and non-delay sensitive data (e.g., smart grid, smart home, and smart city applications).

To define each service's weights (presented in equation 3.9), we apply the AHP and the Saaty-scale [122], used in many scenarios of multi-criteria decisions. The AHP allows decomposing a complex problem into a hierarchical structure to be easier to solve. The Saaty scale permits the establishment of priorities among pairs according to their relevance. Table 4.1 shows the possible assigned values according to [122]. The pairwise comparison matrix is defined as

$$V = \begin{bmatrix} v_{1,1} & \cdots & v_{1,n} \\ \vdots & \ddots & \vdots \\ v_{n,1} & \cdots & v_{n,n} \end{bmatrix}, \quad (4.2)$$

where $v_{i,j}$ represents the importance criterion among different UFs according to the

Algorithm 1: Score Function Calculation

Input: *ServiceType* = List of services request; *CANs* = List of CANs;
Initialize: $SF_{max} = 0$; $SF_b^u = 0$, $b \in CANs$.
Output: Return the best CAN (SF_{max}).
foreach b *in* *CANs* **do**
 foreach m *in* *ServiceType* **do**
 if *ServiceType* == *VI* **then**
 $S_{b,m,o}^u = 0.36 \times (Th_{b,m,o}^{u, Norm} + J_{b,m,o}^{u, Norm}) + 0.16 \times Ec_{b,m,o}^{u, Norm} + 0.08 \times$
 $D_{b,m,o}^{u, Norm} + 0.04 \times PLR_{b,m,o}^{u, Norm}$
 end
 if *ServiceType* == *AR* **then**
 $S_{b,m,o}^u = 0.47 \times Th_{b,m,o}^{u, Norm} + 0.21 \times (D_{b,m,o}^{u, Norm} + Ec_{b,m,o}^{u, Norm}) + 0.055 \times$
 $(J_{b,m,o}^{u, Norm} + PLR_{b,m,o}^{u, Norm})$
 end
 if *ServiceType* == *IoT* **then**
 $S_{b,m,o}^u = 0.6 \times Ec_{b,m,o}^{u, Norm} + 0.2 \times (Th_{b,m,o}^{u, Norm} + D_{b,m,o}^{u, Norm})$
 end
 if *ServiceType* == *GM* **then**
 $S_{b,m,o}^u = 0.34 \times (Th_{b,m,o}^{u, Norm} + PLR_{b,m,o}^{u, Norm}) + 0.13 \times (D_{b,m,o}^{u, Norm} +$
 $Ec_{b,m,o}^{u, Norm}) + 0.06 \times J_{b,m,o}^{u, Norm}$
 end
 end
 $SF_b^u = \sum_{m \in M_u} \psi_{m,o}^b \times \kappa_{m,o}^b \times \varrho_{m,o}^u \times S_{b,m,o}^u$
 if $SF_b^u > SF_{max}$ **then**
 $SF_{max} = SF_b^u$
 end
end

Saaty-scale values.

Table 4.2 details the pairwise comparison's matrix for AR. *Th* is the most important factor (value 1). In contrast, *D* and *Ec* are a little less critical (value 1/3 with respect to *Th*), and *PLR* and *J* are less important (value 1/7 concerning *Th*). Later, it is necessary to obtain the normalization matrix and, finally, the weight w for each UF, defined as

$$V_{norm} = \begin{bmatrix} \frac{v_{1,1}}{\sum v_{i,1}} & \frac{v_{1,2}}{\sum v_{i,2}} & \dots & \frac{v_{1,n}}{\sum v_{i,n}} \\ \frac{v_{2,1}}{\sum v_{i,1}} & \frac{v_{2,2}}{\sum v_{i,2}} & \dots & \frac{v_{2,n}}{\sum v_{i,n}} \\ \vdots & \vdots & \ddots & \vdots \\ \frac{v_{n,1}}{\sum v_{i,1}} & \frac{v_{n,2}}{\sum v_{i,2}} & \dots & \frac{v_{n,n}}{\sum v_{i,n}} \end{bmatrix}, \quad (4.3)$$

Weight/service	w_{Th}	w_D	w_{Ec}	w_J	w_{PLR}	$\sum_{uf \in \mathbb{UF}} w_{m,uf}^u$
VI	0.36	0.08	0.16	0.04	0.36	1
AR	0.47	0.21	0.21	0.055	0.055	1
IoT	0.2	0.2	0.6	-	-	1
GM	0.34	0.13	0.13	0.34	0.06	1

Table 4.3: UFs weights for VI, AR, IoT and GM.

$$w_i = \frac{\sum_{j=1}^n v_{i,j}}{n}. \quad (4.4)$$

Table 4.3 summarizes the obtained weights for each analyzed service and its fundamental factors for the QoS through the AHP. Finally, the SF process calculation is described in Algorithm 1, dynamically adapted to user preferences and network conditions.

4.4 Load Balancing Process

The load balancing mechanism is applied if there are no CANs due to limited resources. Our proposal is based on CGT to benefit more users through dynamic resource allocation. We define the coalition set as $\mathbb{C} = \{C_1, C_2, \dots, C_z\}$, where C_z is a subset of cooperative players, and $\nu(C_z)$ is the characteristic function that describes the payoff associated with the coalition C_z .

The game initiation trigger is the reach of a saturation point in the network and if a new service request is received. This mechanism runs in two consecutive phases:

1. Collaboration among CANs (named *CANs** during the load balancing process), based on a canonical game [93, 96], to determine the most suitable BS to satisfy the new service request.
2. Collaboration among NSs on the selected BS, based on a dynamic coalition formation game [93], to free up resources according to the required *Th* and the conditions of current users. The overall UF aims to maximize the number of users connected to the network with a QoS higher than or equal to the minimum requirements according to their tariff plans. Fig. 4.4 shows the load balancing flowchart, whose details are presented in the following Subsections 4.4.1 and 4.4.2.

4.4.1 Collaboration among CANs

When the network reaches the overload situation, and a new user has a service request, the DASA algorithm selects the *CANs** to determine the best BS to free up resources and attend the petition. The collaboration among the possible BSs

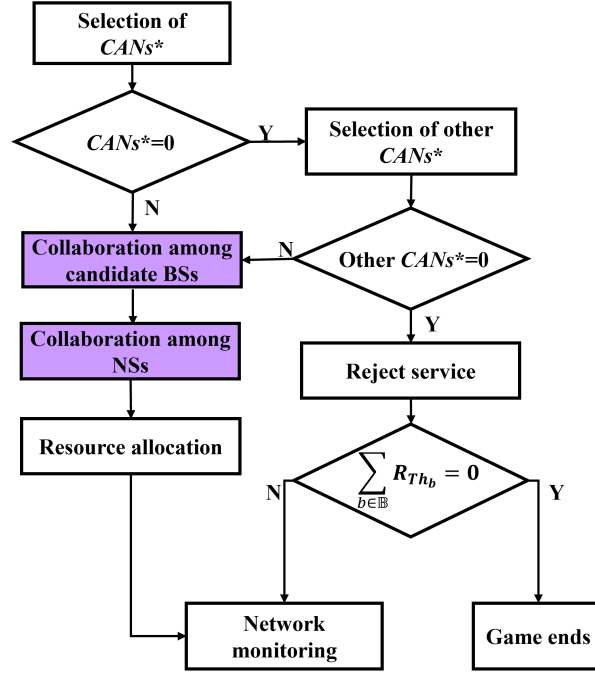


Figure 4.4: The load balancing mechanism flowchart.

(players) represents a canonical coalition game or grand coalition (GC) structure. It assumes that forming a larger coalition (C_{GC}) among the $CANs^*$ cannot be worse than acting alone. Therefore, this formation is characterized by the superadditive property, which means that the payoff $\nu(C_{GC})$ is always higher than or equal to the payoff value of any disjoint set of coalitions.

The $CANs^*$ are the access networks that meet the requirements of the CANs, except that they do not have enough available resources to satisfy the new request. Moreover, the $CANs^*$ must comply

$$R_{Th_b} \geq Thmin_{m,o=1}^u, \quad (4.5)$$

where R_{Th_b} represents the potential resources that BS_b can release until all users belonging to it have the minimum possible Th .

The normalization of R_{Th_b} ($R_{Th_b}^{Norm}$) is expressed by

$$R_{Th_b}^{Norm} = \begin{cases} 0, & \text{if } R_{Th_b} < Thmin_{m,o=1}^u \\ 1, & \text{if } R_{Th_b} \geq \sum_{m \in \mathbb{M}_u} Thmax_m^u \\ \frac{R_{Th_b}}{\sum_{m \in \mathbb{M}_u} Thmax_m^u}, & \text{otherwise.} \end{cases} \quad (4.6)$$

The $CANs^*$ are evaluated according to the fraction of the supported services request between the total requested services (Θ), $R_{Th_b}^{Norm}$ and $Th_{sat,b}^u$ values to select the access network that could better satisfy the new service request.

	$R_{Th_b}^{Norm}$	Θ	$Th_{sat,b}^{average}$
$R_{Th_b}^{Norm}$	1	3	3
Θ	1/3	1	1
$Th_{sat,b}^{average}$	1/3	1	1

Table 4.4: Pairwise comparison's matrix.

Algorithm 2: Collaboration among BSs

Input: *ServiceType* = List of services request; *CANs** = List of *CAN** or *CAN*_{others}*;
Initialize: $SF_{max}^* = 0$; $SF_b^{u*} = 0$, $b \in CANs^*$.
Output: Return the best CAN to attend the new service request.
foreach b *in* *CANs** **do**
 $SF_b^* = 0.2 \times (\Theta + Th_{sat,b}^{average}) + 0.6 \times R_{Th_b}^{Norm}$
 if $SF_b^{u*} > SF_{max}^*$ **then**
 $SF_{max}^* = SF_b^{u*}$
 end
end

According to the new user request and similar users in the network, the algorithm follows a fairness rule among the *CANs**, looking to satisfy the new request with the best QoS possible. Moreover, the BSs play a collaborative attitude trying to balance their resources, avoiding that $Th_{sat,b}^{average}$ abruptly decreases in one access network versus the others. Therefore, it guarantees a stable and fair GC, where the players are not encouraged to leave this structure.

According to the above assumptions, the $SF_{b,u}^*$ for each *CAN** is calculated by

$$SF_{b,u}^* = 0.2 \times (\Theta + Th_{sat,b}^{average}) + 0.6 \times R_{Th_b}^{Norm}. \quad (4.7)$$

Equation 4.7 is determined by MADM and AHP combination, where $R_{Th_b}^{Norm}$, Θ and $Th_{sat,b}^{average}$ are the UFs and range from 0 to 1. In this case, we assume that $R_{Th_b}^{Norm}$ is a little more critical for the decision criteria concerning Θ and $Th_{sat,b}^{average}$ (Table 4.4). Therefore, the w values (i.e., 0.2 and 0.6) represent the relevance attributed to each associated parameter resulting from equations 4.2, 4.3, and 4.4.

The *CAN** with the SF_{max}^* is the BS with the best conditions to satisfy the services request. Therefore, $SF_{b,u}^*$ quantifies the preferences between different outcomes [131]. One BS has a stronger preference respect to others (e.g., $BS_1 \succ BS_2$) if $SF_b^*(BS_1) > SF_b^*(BS_2)$.

If there are not *CANs** due to insufficient resources to release for the PS or $\kappa_{m,o=1}^b = 0$, DASA selects the *CANs*_{others}* that support the SSs. In this case, the *CANs*_{others}* are the players who cooperate to determine the best BS to serve the new user request. R_{Th_b} must be higher than or equal to the minimum Th required from

	VI (Mbps)		AR (Mbps)		GM (Mbps)	
	Max	Min	Max	Min	Max	Min
4K	13	10.4	30	28	40	35
2K	7.549	5.816	27.5	25.5	30	25
FHD	3.676	2.804	25	23	20	15
HD	2.674	1.229	22.5	20	10	8

Table 4.5: Data rates of the considered multimedia applications.

one of the SSs. The above collaboration among BSs is described in Algorithm 2.

4.4.2 Collaboration among NSs

This phase is based on a dynamic coalition formation, implemented according to [93]. This kind of cooperation is an efficient strategy to optimize the network's social welfare. It is subject to environmental changes such as network conditions, number of players, and their characteristics. The main elements of this phase of the game are:

- Set of players, which are the available NSs in the selected BS, and the action space is the combination of all resources (services) of users belonging to this access network.
- The coalition set $\mathbb{C} = \{C_1, C_2, \dots, C_z\}$, where C_z is the subset of players cooperating to reallocate slice resources and accepting new users in the network. The coalition must guarantee that the Th of the served users is higher than or equal to a certain threshold defined by their priorities and application characteristics.
- Actions' sequences $\lambda_{\Lambda, \Lambda+1}$ available to perform on a current user UE_u . These actions represent the transition strategy from the assigned Th to the minimum Th possible. VI, AR, and GM are considered high-demanding data rates multimedia services. Therefore, the actions consider the transition through the states $\Lambda = \{4K, 2K, FHD, HD\}$ (i.e., 4K, resolution of 2000 pixels (2K), full high-definition (FHD), high-definition (HD)). Table 4.5 shows the data rate constraints for each resolution according to [99, 132–135]. On the other hand, we consider IoT applications with low data rate demand. According to [130], we assume the states $\Lambda = \{1 \text{ Mbps}, 500 \text{ kbps}, 100 \text{ kbps}\}$. The presented sequential actions allow for gradually decreasing the Th without abruptly affecting users' QoS. Moreover, a user whose Th has been affected due to an overload situation can revert to the previous state when new network resources are available.

- Minimum cost F that represents the minimum resources (decision point) that NSs need to free up to satisfy the new services request and to guarantee a minor impact on the current users' satisfaction. Therefore, the coalition is considered only if the sum of released resources (Th_r) of its members is higher than or equal to the required Th by a new service request. F depends on the new user's tariff plan, network conditions, and current Th of similar users. To affect as little as possible the users' perception, the resulting delta aggregated data rate (ADR) ($\Delta ADR = ADR_{\Lambda+1} - ADR_{\Lambda}$) must be as low as possible. DASA must guarantee that available resources later of accepting a new user, in an overload situation, be zero or close to zero. The residual value is defined by

$$\mathfrak{a} = \begin{cases} \frac{\sum_{m \in \mathbb{M}_u} Th_{b,m,o}^u}{\sum_{z \in \mathbb{U}} Th_r^z}, & \text{if } Th_r^T \geq F \\ 0, & \text{otherwise.} \end{cases} \quad (4.8)$$

where $Th_r^T = \sum_{z \in \mathbb{U}} Th_r^z$ is the total released resources to guarantee at least the minimum requirement (i.e., F). Additionally, $\sum_{m \in \mathbb{M}_u} Th_{b,m,o}^u$ is the total assigned Th to the new user. If $\mathfrak{a} = 1$, the algorithm frees up precisely what the new user needs. As mentioned, DASA never assigns more resources than the maximum required by the services.

- The characteristic function $\nu(C_z)$ plays a critical role because it quantifies the cooperation cost in terms of residual value and number of affected users. In this case, $\nu(C_z) \in [0, 1]$, and it is defined by

$$\nu(C_z) = \begin{cases} 0.75 \times U_{aff}^{Norm} + 0.25 \times \mathfrak{a}, & \text{if } Th_r^T \geq F \\ 0, & \text{otherwise.} \end{cases} \quad (4.9)$$

U_{aff}^{Norm} is the normalized value of affected users at each saturation point represented by

$$U_{aff}^{Norm} = 1 - \frac{U_{aff}}{U}. \quad (4.10)$$

The cheapest winning coalition is the coalition that satisfies the new service petition, minimizing the number of affected users and the residual value. The $\nu(C_z)$ ponders a little more affecting the fewest number of users.

- Rule of order ρ to determine the sequential coalition formation game. It is developed according to the following fairness assumptions:
 1. It considers two priorities: the services' preferences (PS or SSs) and the tariff plan. The former means that the services with low preference have a minor impact (cost). The latter means that users with low priority pay less and, therefore, are the first to experience reduced resources.
 2. First in, first out (FIFO) policy is also applied. The users that stay longer in the network reduce first their resources.

Algorithm 3: Collaboration among NSs

Input: $ActionSpace$ = List of users and services;
 \mathcal{F} = Minimum required resources;
 $\mathbb{C} = \{C_1\{GM\}, C_2\{AR\}, C_3\{VI\}, C_4\{IoT\}, C_5\{GM, AR\}, \dots, C_{11}\{GM, AR, VI\}, \dots, C_{15}\{GM, AR, VI, IoT\}\}$;
Initialize: $\nu_{win} = 0$; $Th_r^T = 0$; $U_{aff} = 0$;
Output: Return the cheapest winning coalition and released resources.

```

foreach  $s$  in  $\mathbb{C}$  do
  foreach  $z$  in  $ActionSpace$  do
     $Th_r^T = Th_r^T + Th_r^z$ 
     $U_{aff} = U_{aff} + 1$ 
    if  $Th_r^T \geq \mathcal{F}$  then
       $\nu(C_c) = 0.75 \times U_{aff}^{Norm} + 0.25 \times \vartheta$ 
      if  $\nu(C_c) > \nu_{win}$  then
         $\nu_{win} = \nu(C_c)$ 
      end
    end
  end
  if  $Th_r^T < \mathcal{F}$  then
     $\nu(C_c) = 0$ 
  end
end

```

3. The Th is sequentially reduced to avoid an abrupt $Th_{sat}^{average}$ affectation following the defined set of actions.

According to the above assumptions, all served users by the game's players are ranked by priority, the number of services used, and time on the network. Therefore, regular users who have been on the network longer using the largest number of services (four in this case) will be chosen for the game initiation. When all users' services with low priority have the minimum Th possible, and the overload situation persists, the Th of users with high priority decreases, always maintaining superior $Th_{sat,b}^u$ concerning regular users. They pay more and, therefore, demand a better perception, according to the defined SLA.

As mentioned, this work considers four different services. Then, to apply the collaboration among the NSs (four players), we define 15 combinations of possible coalitions: from the NSs acting alone ($C_1 = \{VI\}, \dots, C_4\{IoT\}$) to the $C_{15} = \{GM, AR, VI, IoT\}$, where C_{15} is the GC (C_{GC}) of the four NSs.

The coalition formation game is generally non-superadditive. It means that we cannot guarantee that always the $\nu(C_{15})$ value is higher than or equal to any other coalition in \mathbb{C} . Therefore, we consider a dynamic coalition formation iterating over \mathbb{C} to find the coalition that better satisfies the new services request each time.

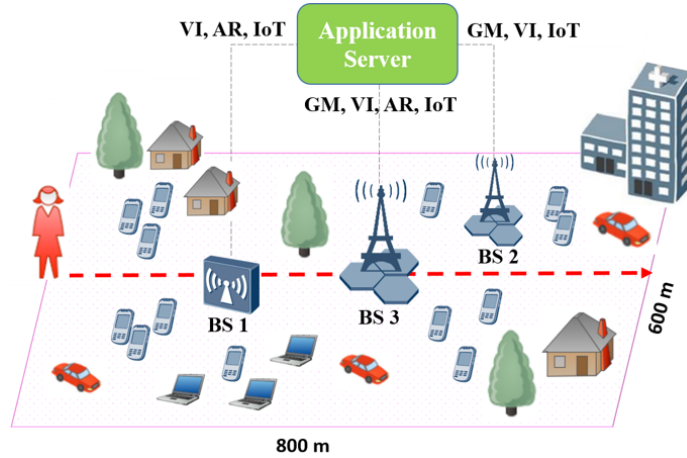


Figure 4.5: The simulated HetNet environment.

This mechanism ensures a stable condition, freeing up resources with the minimum number of affected users and the minimum residual value.

The game is finite, and it ends when all services have the minimum Th possible. At this point, it is unfeasible to free up more resources and accept new users. This condition is transitory until resources are released (i.e., a current user leaves the network). The above collaboration among NSs is described in Algorithm 3.

4.5 Simulation and Scenarios Deployment

This Section presents the simulation method, scenario deployment, and validation process of the DASA algorithm. The simulation framework is based on a dual tool:

- OMNeT++ combined with Simu5G and INET [136] libraries are used as a network-level simulator to evaluate the network configuration and obtain the periodical QoS attributes.
- Python is used to implement DASA and evaluate its performance. The resulting data from OMNeT++ simulations are inputs to this algorithm.

The simulated scenario is shown in Fig. 4.5. It recreates a smart city (800×600 m) with a heterogeneous environment composed of one IEEE 802.11ac AP (BS_1), one micro-cell 5G NR (BS_2), and one macro-cell 5G NR (BS_3). The AP and the micro-cell coverage radius is 250 m, whereas for the macro-cell, the radius is 500 m. We simulate both technologies for 40 MHz of bandwidth in the frequencies of 5 GHz and 3.5 GHz for the 802.11ac and 5G NR, respectively. The BS_1 is located in the position (250, 250), the BS_2 in (550, 350), and the BS_3 in (400, 300). Table 4.6 shows the main simulation parameters. On the other hand, Table 4.7 describes the

Attributes	Cellular Network		WLAN Network
Technology	5G NR		802.11 ac
Radio transmitters (TxS)	2		1
Frequency	3.5 GHz		5 GHz
Transmission	macro-cell	micro-cell	
Power	25 dBm	10 dBm	
Radius Cell	500 m	250 m	
Bandwidth	40 MHz		
Mobility type	Stationary/RWP/ Linear mobility (1 m/s)		
Channel Model	Rayleigh		

Table 4.6: Simulation Parameters (DASA Validation)

NS/BS	BS_1	BS_2	BS_3
VI	1	1	1
AR	1	0	1
IoT	1	1	1
GM	0	1	1

Table 4.7: NSs states (St_m^b).

NSs accessible by the BSs and their respective states ($St_{b,m}$). Initially, we assume only the $St_{b,m}$ equal to 0 or 1.

In the simulations, we recreate U users randomly positioned in the grid. The number of users and their mobility behavior vary according to the recreated scenario and their type (e.g., SN, SP). We assume users with different device characteristics and tariff plans (45 % of premium clients and 55 % of regular clients). They can request from one to four services: VI, AR, IoT, and GM. According to user preferences, one service is the PS, and the rest are SSs. This information is an input of the algorithm. Then, DASA dynamically calculates the best CAN for each user, assigning the resources based on the network conditions and the priority of requested services and users.

The main elements of the DASA validation process can be found in Fig. 4.6. We set up the network-level simulation in OMNeT++ according to the defined scenario and network parameters. We use the resulting network parameters, the QoS attributes, and the device profile as inputs of the DASA algorithm. Additionally, we recreate the NS Repository information, the user, and the application profiles conforming the inputs to run the DASA algorithm and evaluate its performance. The validation consists of evaluating two major processes, the network selection and the load balancing mechanisms, through two scenarios presented below.

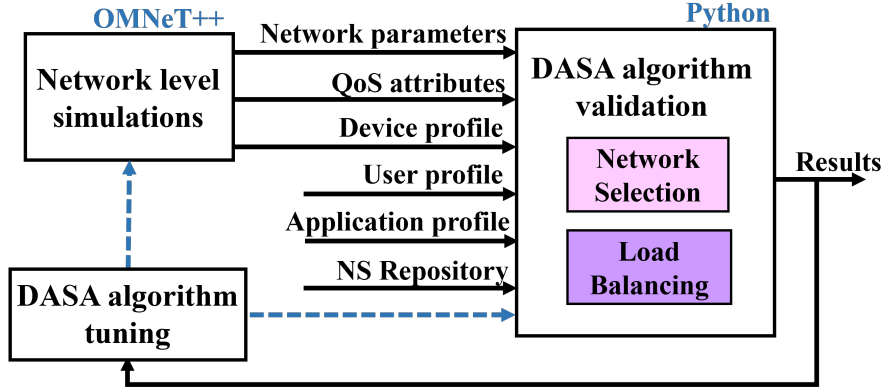


Figure 4.6: Elements of the DASA validation process.

4.5.1 Scenario 1

Scenario 1 aims to evaluate the DASA network selection process. We consider 50 background users randomly positioned in the above-mentioned area around the three BSs, and with a mobility type RWP [137]. They can request from one to four services simultaneously. Moreover, we recreate a new regular user (UE_{51}) walking through a linear path of 800 m from position (0, 300) to (800, 300) at 1 m/s, as shown in Fig. 4.5. The user UE_{51} changes the service petition every 100 seconds to analyze the algorithm's performance under different conditions. The simulation duration is 800 seconds to allow the user to complete the route.

This scenario evaluates the dynamic behavior of the network selection process leading to the constant changes of the QoS attributes of the mobile users. The algorithm must ensure all users have the maximum Th possible according to their priorities and network conditions. The traffic generated by the background users significantly influences the available resources for the user walking along the route, especially at the extremes of the BSs' coverage area due to the relatively low signal level.

4.5.2 Scenario 2

In this scenario, the number of users has been progressively increased to evaluate the network selection and load balancing mechanisms. The network hosts a new user every two seconds, and the process lasts 400 seconds, for a total population of 200 users. The users are randomly positioned in the above-mentioned area around the three BSs and with a mobility type stationary or RWP.

With enough resources, DASA maintains all users' maximum Th_{sat} value according to network conditions and application profile. On the contrary, the algorithm performs the load-balancing mechanism when the first saturation point occurs. The users with low priority experience a gradual reduction in their Th until they have the minimum possible value. In this second relevant point, DASA decreases the

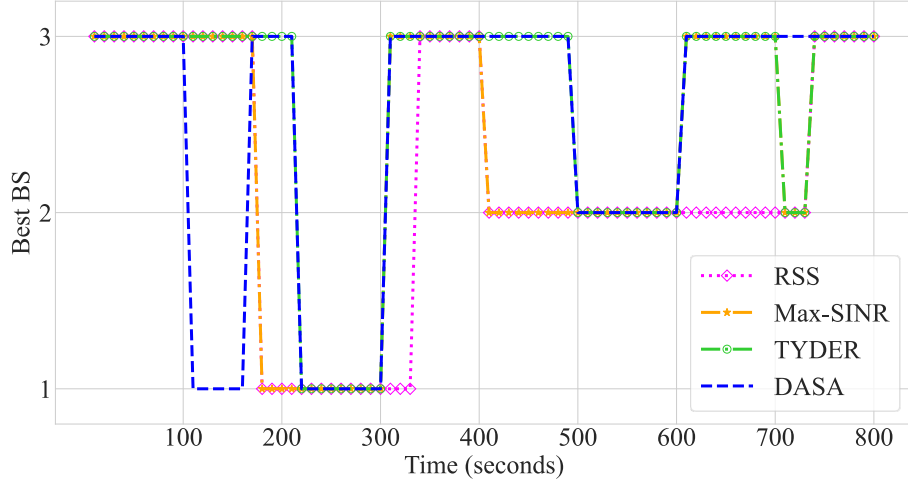


Figure 4.7: Best BS for the user UE_{51} in scenario 1.

resources from users with high priority accepting more clients and maintaining an adequate QoS according to the SLA. Finally, when all users have the minimum possible resources, the game ends, and it is unfeasible to accept more clients.

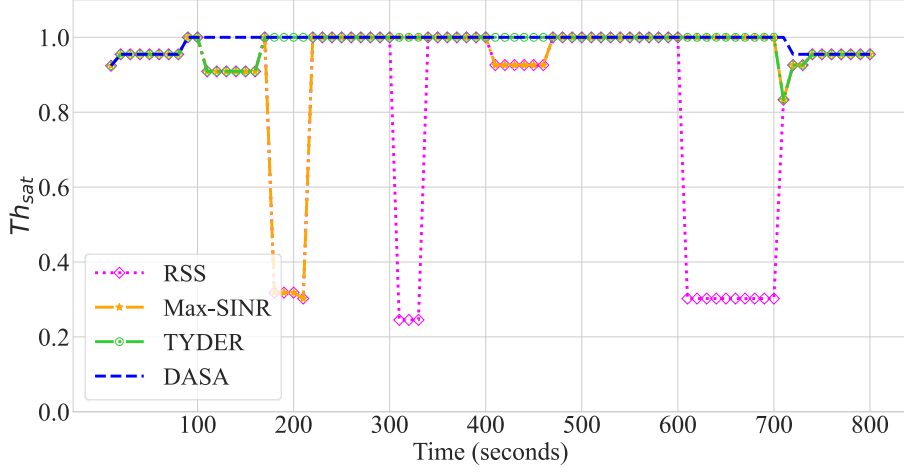
4.6 Results and Discussion

This section shows the results from the simulated scenarios (Section 4.5), validating the DASA algorithm performance in a heterogeneous environment for the network selection and management of resource allocation during an overload situation.

4.6.1 Results of Scenario 1

Scenario 1 evaluates the Th_{sat} and the dynamic network selection behavior for the user UE_{51} along the route, under the influence of dynamic background traffic. The generated figures show the results of a single simulation run. DASA is compared with three state-of-the-art methods: the traditional RSS criterion, TYDER [54], and maximum SINR (Max-SINR) [73]. TYDER calculates the network reputation in terms of QoS parameters to select the most suitable BS that satisfies an individual traffic type requested by the user. Therefore, we assume that TYDER only guarantees the best conditions for the PS. On the other hand, the Max-SINR method is a variation of the traditional RSS handover process. In this case, we assume that Max-SINR selects the BS with the highest SINR, supporting the major number of requested services with the PS included. The selected BS must also guarantee at least the minimum required Th for the PS.

Fig. 4.7 shows the access network selection behavior to satisfy the user UE_{51} request along the route, applying DASA, RSS, TYDER, and Max-SINR. Fig. 4.8

Figure 4.8: Th_{sat} values for the user UE_{51} in scenario 1.

Algorithm	DASA	TYDER	Max-SINR	RSS
$Th_{sat}^{average}$	0.981	0.943	0.922	0.805
CI (95% CV)	(0.975-0.987)	(0.928-0.958)	(0.910-0.934)	(0.771-0.839)

Table 4.8: Average Th_{sat} for the user U_{51} in scenario 1.

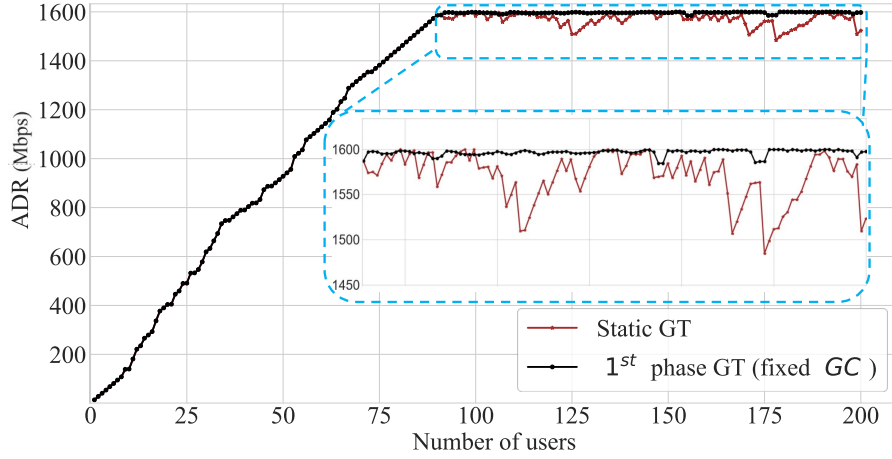
shows the resulting Th_{sat} values experienced by the user UE_{51} due to the network selection process. DASA always selects the best combination of access network/NSs, considering the user priority, network conditions, and the NS accessibility at each BS (Table 4.7). Fig. 4.8 shows how DASA outperforms the other methods, providing a maximum Th_{sat} for the user UE_{51} , except at the extremes of the route. At these points of the simulated area, the user request is GM, VI, and IoT, and the BSs cannot guarantee the necessary channel quality and RBs to assign the maximum Th . All the analyzed methods give the same result in this cell-edge area.

On the other hand, the RSS criterion has the worst performance. This method only uses the SINR value for making the decisions, whereby the target BS might be unable to provide the required services. For example, between 300 and 400 seconds of the simulation, the requested services by UE_{51} are GM and VI. In this condition, RSS selects the BS_1 although this BS does not support GM, resulting in the Th_{sat} degradation shown in Fig. 4.8. Moreover, the Th_{sat} value is considerably affected when RSS selects the BS_2 during the request of AR and VI (between 600 to 700 seconds of the simulation) because this BS does not support AR.

Max-SINR performs better than RSS because it considers the accessibility of the requested services. However, although the target BS supports the user request, the achievable QoS metrics may be insufficient. This situation is evident during 180 to 210 seconds of the simulation when the RSS and Max-SINR methods select BS_1 without considering the QoS performance.

Cases	1 st phase	2 nd phase
Static GT	Without GT	Fixed C_{GT}
1 st phase (fixed C_{GT})	Collaboration among $CANs$	Fixed C_{GT}
2 nd phase (fixed C_{1-4})	Collaboration among $CANs$	Fixed C_{1-4}
1 st + 2 nd phases	Collaboration among $CANs$	Collaboration among NSs

Table 4.9: Evaluated cases in scenario 2.

Figure 4.9: ADR for the static GT and the 1st phase of GT with fixed C_{GC} .

TYDER selects the most suitable BS according to the QoS metrics demanded by the PS. Therefore, this algorithm might not guarantee the maximum Th_{sat} for the Ss during high-traffic conditions. This is shown, for example, during 110 to 160 seconds of the simulation, when the UE_{51} request is AR, VI, and IoT. TYDER, RSS, and Max-SINR select the BS_3 , although this BS does not offer the best QoS conditions for all the requested services.

Additionally, Table 4.8 shows the $Th_{sat}^{average}$ for the user UE_{51} along the route resulting from 50 simulation runs, as well as the confidence interval (CI) guaranteeing a 95 % confidence value (CV). DASA outperforms TYDER, Max-SINR, and RSS by 3.8 %, 5.9 %, and 17.6 %, respectively, proving its advantages in terms of dynamic network selection and slice allocation.

4.6.2 Results of Scenario 2

Scenario 2 evaluates the network selection and load balancing mechanisms in terms of ADR, Th_{sat} , and SD (SD). The generated figures show the results of a single simulation run. For better understanding, we summarized the evaluated cases in Table 4.9.

Fig. 4.9 shows the ADR resulting in applying the collaboration among CANs (first phase of GT) and without cooperation. Both cases are analyzed by fixing

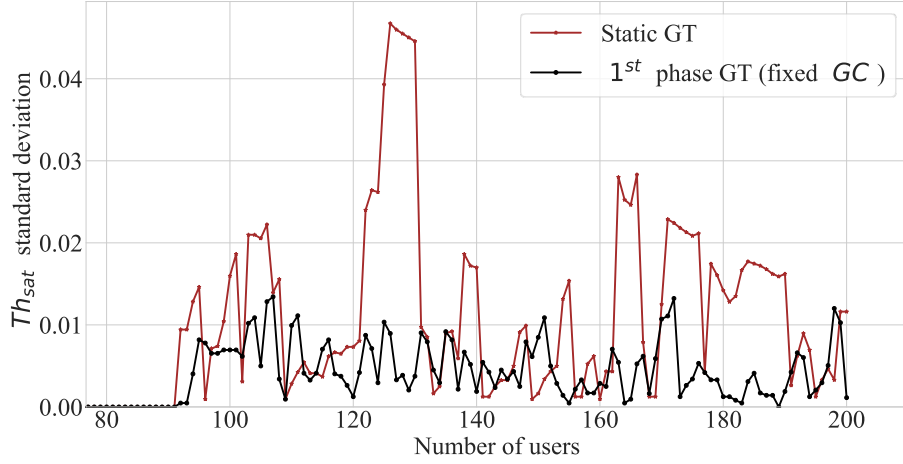


Figure 4.10: Th_{sat} standard deviation for the static GT and the 1st phase of GT with fixed C_{GC} .

the GC structure $C_{GC}\{\text{GM, AR, VI, IoT}\}$ to reduce the resources and handle the congestion control mechanism. Fig. 4.10 shows the Th_{sat} standard deviation among the three BSs for the two analyzed cases.

The figures show the improvement of applying the first phase of our GT proposal. Since the first saturation point is reached, the ADR behavior is more stable around the system's maximum capacity due to the collaboration among BSs. This result means efficient use of the potential released resources. Moreover, the Th_{sat} standard deviation is significantly less when the CANs collaborate, proving that one BS is not affected more than others. It maintains a balance among the resources of the CANs following a fairness strategy.

Fig. 4.11 and 4.12 show the comparison between three different cases. Two of them apply only the first phase and maintain static the NS coalition: one represents the GC (C_{GC}), and the second is another fixed coalition structure (C_{1-4}). In the case of C_{1-4} , DASA applies the reduction of resources starting from C_1 to C_4 , independently. The third case denotes the collaboration among CANs and NSs (first and second phases of GT).

The above comparison proves that the GC structure does not always perform best. Therefore, the superadditive property is not met in the collaboration among NSs. A dynamic coalition selection at each saturation point guarantees the best payoff affecting a smaller number of users and less residual (Θ). For 200 users, the two cases of the first phase of GT (fixed C_{1-4} and C_{GC}) affect 187 and 177 users during the load balancing process, respectively. In contrast, combining the first and second phases affects 159 users. Additionally, the Θ value has the worst performance for the first phase of GT with the fixed C_{1-4} coalition, contrary to the combination of the first and second phases that shows values closest to 1.

Once we validate the outperformance of the first and second phases of GT, we

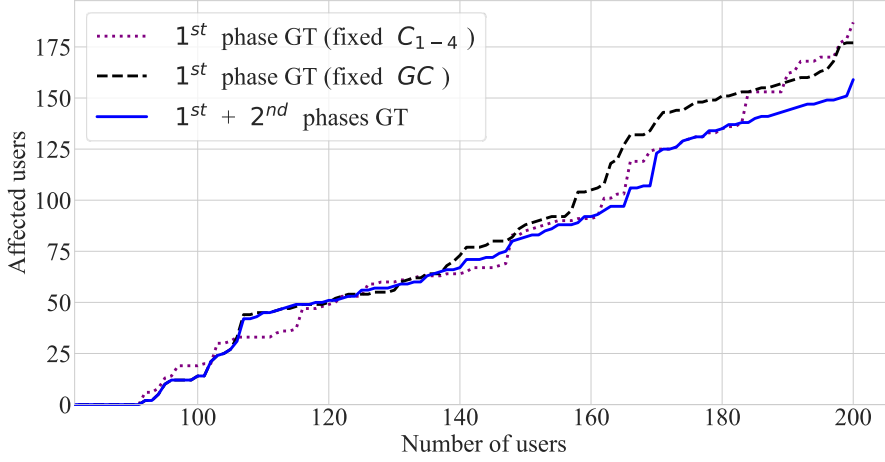


Figure 4.11: Affected users for the 1st phase of GT and the combination of the 1st and 2nd phases.

extend the population size to reach the full saturation point. Fig. 4.13 and 4.14 evaluate the proposal in terms of ADR and $Th_{sat}^{average}$. It is shown that all users experience the maximum Th_{sat} value until the network reaches the first saturation point. At this point, the regular clients reduce their Th , whereas the premium clients maintain the best Th_{sat} . When the current regular users do not have enough resources to free up and accept a new user, the premium clients experience a reduction in their resources. If residual resources are available on the network during the congestion control process, affected users can revert to the previous state.

For this scenario and this specific simulation run, the full saturation occurs with 275 users in the network. At this point, all users have the minimum QoS according to their priorities. The game ends, and any new service request is rejected unless new resources are released. Fig. 4.14 shows that users with high priority always maintain better QoS than users who pay less.

Fig. 4.15 illustrates the $Th_{sat}^{average}$ behavior for each BS. It demonstrates how the CAN with the highest Th_{sat} is always selected at each saturation point, except when the BS does not support the requested services. Note that when UE_{141} requests AR, the selected CAN is BS_1 because even though BS_2 has higher Th_{sat} , it does not support the requested service.

Finally, Table 4.10 summarizes the values of $Th_{sat}^{average}$ and $SD^{average}$ for a total of 200 users resulting from 50 simulation runs with a 95 % CV. The combination of the first and second phases improves the $Th_{sat}^{average}$ regarding the static GT case and the first phase of GT with the fixed coalitions structures C_{1-4} and C_{GC} by 6.5 %, 4.8 %, and 3.9 %, respectively. At the same time, the combination of the first and second phases of GT improves the $SD^{average}$ by 7.2 %, 3 %, and 1.8 %, respectively. These results prove the advantages of applying two collaborative phases of GT among BSs and among NSs.

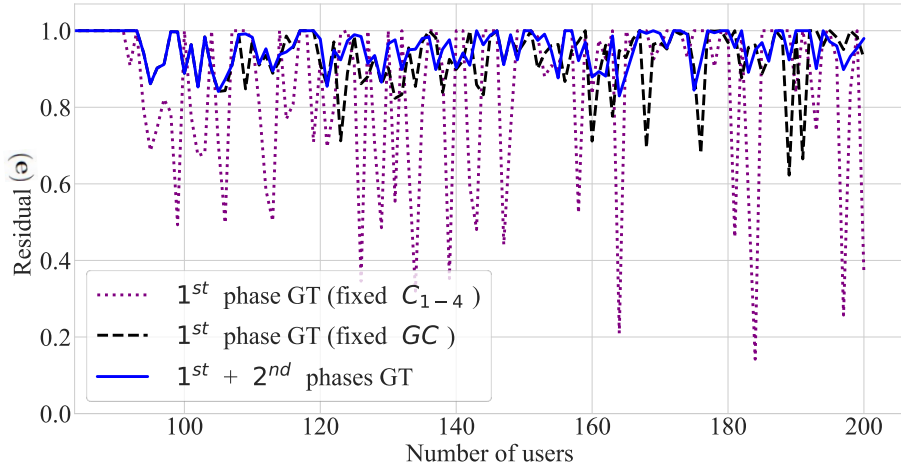


Figure 4.12: Residual for the 1st phase of GT and the combination of the 1st and 2nd phases.

4.7 Conclusions

DASA is an integral solution to handle the network selection and dynamic slice allocation during diverse network conditions, such as overloading. It integrates the NS paradigm, SDN, and NFV as crucial technologies to introduce dynamism in traffic management for future wireless networks.

The proposed algorithm is based on MADM and AHP to combine multiple attributes and face the complex problem of network selection over 5G HetNets and beyond. DASA applies differentiated traffic management of the critical services VI, AR, IoT, and GM according to the throughput, delay, jitter, packet loss ratio, and energy consumption metrics. Moreover, the proposal considers users with different tariff plans, device resolutions, and service preferences. The above assumptions guarantee the selection of the most efficient combination of BSs/NSs to satisfy each user request. On the other hand, DASA applies a CGT approach to drive the load balancing during overload situations. It considers two cooperative phases among BSs and among NSs, ensuring the maintenance of a balance in the Th_{sat} and accepting more users in the network. The premium clients always benefit over the regular ones, as evident in the simulation results.

The algorithm is evaluated through network-level simulations integrating OM-NeT++ with Simu5G and Python tools. The outperformance of the proposed dynamic network selection algorithm is demonstrated through Th_{sat} values concerning RSS, TYDER, and Max-SINR methods. Finally, combining two phases of collaboration during the load balancing mechanism improves the algorithm performance, avoiding the abrupt Th reduction and affecting a small number of users at each saturation point.

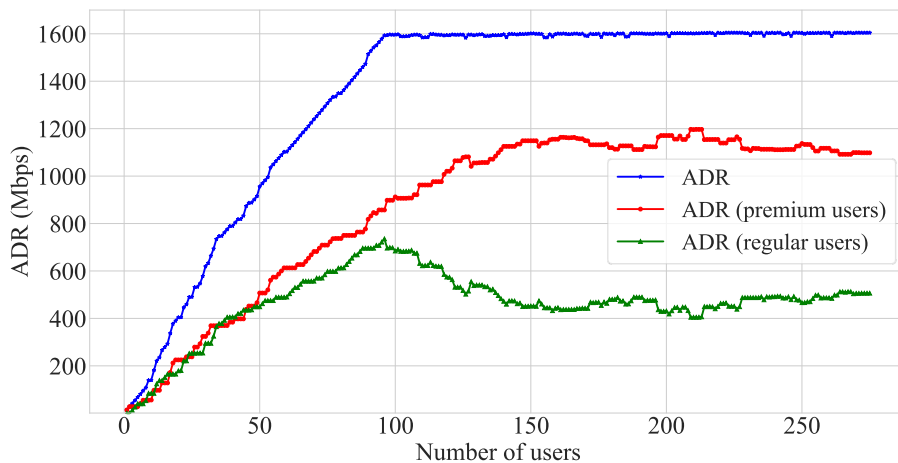


Figure 4.13: ADR for the combination of the 1st and 2nd phases of GT.

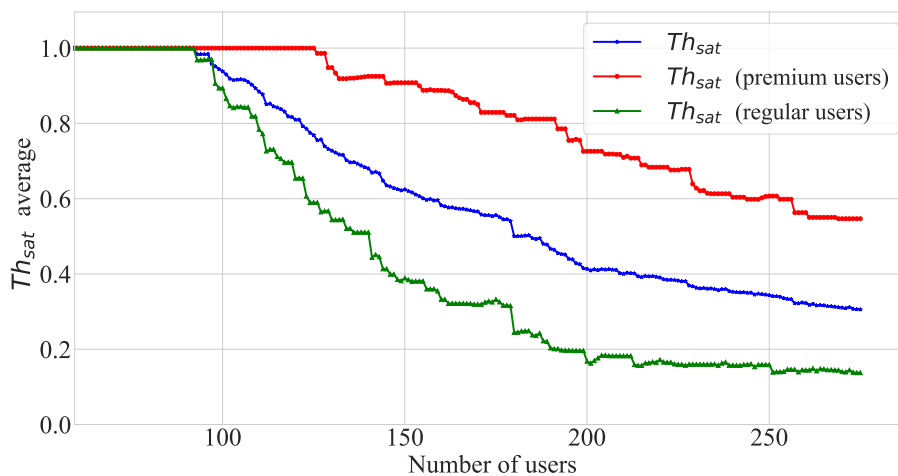


Figure 4.14: Average Th_{sat} for the combination of the 1st and 2nd phases of GT.

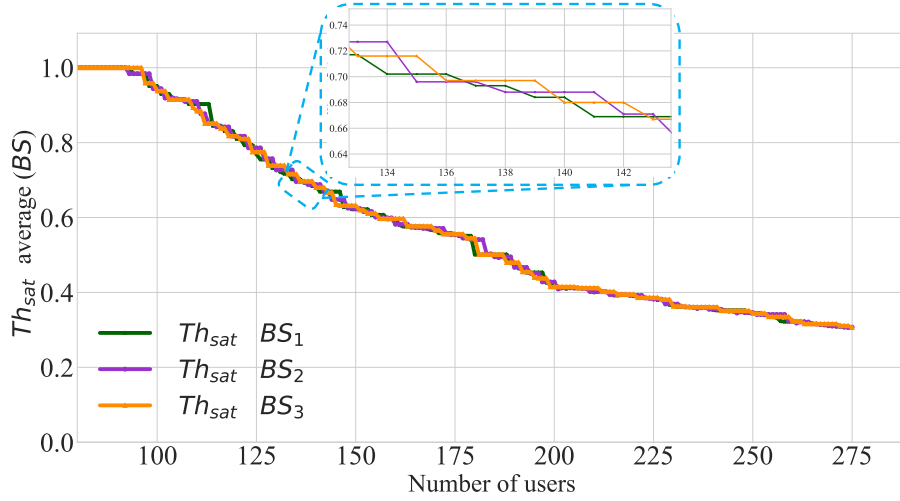


Figure 4.15: Average Th_{sat} of the BSs for the combination of the 1st and 2nd phases of GT.

Metric/phase	Static GT	1 st (C_{1-4})	1 st (C_{GC})	1 st + 2 nd
$Th_{sat}^{average}$	0.394	0.411	0.420	0.459
CI (95% CV)	(0.387-0.401)	(0.404-0.418)	(0.406-0.434)	(0.452-0.466)
$Th_{sat}^{average}$ (premium)	0.687	0.680	0.697	0.713
CI (95% CV)	(0.675-0.699)	(0.647-0.713)	(0.673-0.722)	(0.691-0.735)
$Th_{sat}^{average}$ (regular)	0.158	0.210	0.211	0.243
CI (95% CV)	(0.148-0.169)	(0.177-0.243)	(0.172-0.223)	(0.223-0.263)
$SD^{average}$	0.915	0.957	0.969	0.987
CI (95% CV)	(0.905-0.925)	(0.948-0.966)	(0.959-0.979)	(0.981-0.993)
$SD^{average}$ (premium)	0.960	0.962	0.973	0.988
CI (95% CV)	(0.946-0.974)	(0.956-0.968)	(0.960-0.986)	(0.983-0.993)
$SD^{average}$ (regular)	0.865	0.952	0.966	0.987
CI (95% CV)	(0.845-0.885)	(0.940-0.964)	(0.959-0.973)	(0.982-0.992)

Table 4.10: Results of scenario 2 for 200 users.

Chapter 5

Hybrid terrestrial-airborne connectivity for unicast-MBS convergence B5G networks

This Chapter extends **SO-3** to handle TNs-NTNs integration and the convergence of unicast and MBS capabilities. We propose the enhanced DASA (E-DASA) algorithm to choose the best RAN to satisfy the user requests and optimize slicing resource utilization over B5G networks. This new proposal is inserted into a softwarized system and exploits the broadcast capability, TN-airborne connectivity, and CGT to handle overload situations. Inspired by the algorithm presented in Chapter 4, this solution is analyzed as a particular use case in a football stadium. The proposal, analysis, and conclusions respond to **SO-4**. In summary, the technical contributions include the following:

1. The proposed solution is based on MADM and CGT, ensuring a dynamic RAN selection and slicing allocation in a softwarized hybrid TNs-NTNs ecosystem serving multiple users. The algorithm considers the integration of terrestrial and airborne nodes, diverse traffic performance (i.e., unicast and broadcast services), different users' priorities, and mobility behaviors as inputs.
2. Comprehensive simulation results are obtained and described as one of the most promising use cases of an E2E 3D architecture. The results show how combining unicast/broadcast delivery and employing airborne elements as temporary nodes improves the network capacity in scenarios where multiple users request the same content simultaneously. Specifically, the proposal maximizes the number of users served and minimizes the Th loss when the network saturates, taking advantage of network slicing and broadcast capabilities.

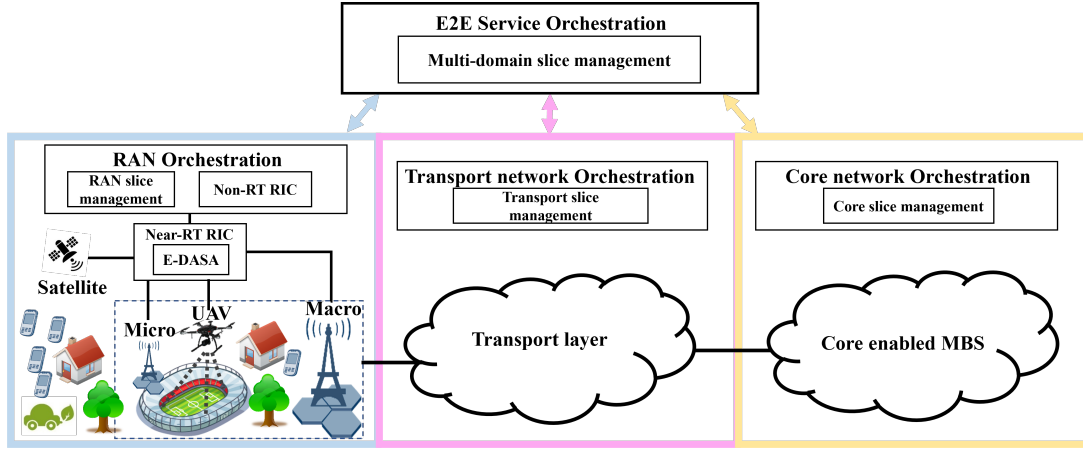


Figure 5.1: Softwarized E2E 3D architecture.

5.1 Softwarized E2E 3D architecture

The following Section comprehensively explains the softwarized system model and 3D architecture. Fig. 5.1 shows the main blocks of an E2E 3D deployment based on softwarization and network slicing technologies. In particular, our proposal covers the RAN domain taking advantage of the O-RAN architecture [138]. The proposed algorithm is located in the Near-RT RIC, which selects the best RAN to satisfy each service request and optimize resource utilization. The Near-RT RIC is one of the main elements of the O-RAN architecture [29] as we described in Section 2.1.

We analyze the proposed solution by recreating a particular use case in a football stadium. We consider that the network serves a set of U football spectators (set \mathbb{U} with the sub-index $u \in \{1, 2, \dots, U\}$), located in a particular section of the arena. The users are mostly stationary, with a minor subgroup moving during the play. The users are randomly distributed into two priority levels $p^u = \{1, 2\}$ according to their tariff plan.

As defined in Section 3.2, we consider a set of B BSs defined by \mathbb{B} , where \mathbb{T} is the set of TN-BSs, and \mathbb{N} is the set of NTN-BSs (i.e., NTNs acting as aerial BSs). We study the TNs-TNs integration, employing the airborne elements as temporary nodes to opportunistically assist the TNs and improve the network capacity during specific game moments.

In this work, we analyze the following services:

- Real-time VI to guarantee that users with a bad location in the stadium can follow the play.
- AR to view real-time data insights and enhance the fan experience, such as how fast a player is sprinting.
- Web browsing (WB) allows fans to consult statistics and the simultaneous plays' results.

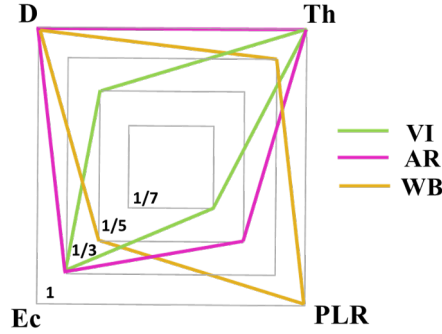


Figure 5.2: UFs setting for VI, AR, and WB.

Service	VI	AR	WB
Th_m^{max} (Mbps)	100	100	30
Th_m^{min} (Mbps)	30	50	5

Table 5.1: Services' Th_m^{max} and Th_m^{min} requirements.

Fig. 5.2 shows the analyzed services and the sensitive UFs that affect in different proportions their QoS in terms of Th , Ec , D , and PLR [30], [120]. Considering that different UF weights characterize the service classes, we assume one NS per service. AR and WB are mapped into unicast slices. Differently, VI is mapped into a broadcast slice to exploit radio resources economically and efficiently and simultaneously serve many users. Table 5.1 shows the Th_m^{max} and Th_m^{min} requirements for each analyzed service.

5.2 The proposed E-DASA solution

This proposal is based on MADM and CGT. The different RANs of the hybrid terrestrial-airborne network act as players to make the joint best decision by selecting the best RAN in the envisioned heterogeneous environment to satisfy multiple service requests. All demanded resources in the corresponding NS are allocated if the network has enough capacity. To guarantee that all users in the football stadium enjoy the VI broadcast service, each BS reserves the required number of RBs in this NS. Therefore, all users who request the VI service can efficiently utilize the same NS resources.

5.2.1 Non-Saturated Network

Initially, we consider that the network is not saturated. For the network selection process, the algorithm computes the SF ($SF_{b,m}^u$) of all BSs in the user coverage area,

selecting the BS with the SF_{max} . The SF value is calculated as

$$SF_{b,m}^u = \psi_m^b * (w_{Th} * Th_{b,m}^{u, Norm} + w_D * D_{b,m}^{u, Norm} + w_{Ec} * EC_{b,m}^{u, Norm} + w_{PLR} * PLR_{b,m}^{u, Norm}), \quad (5.1)$$

where w_{Th} , w_D , w_{Ec} , and w_{PLR} are the UFs' weights obtained by the AHP and considering Fig. 5.2 [30]. These weights enable control of the associated parameter importance in the network decision, following the rule

$$w_{Th} + w_D + w_{Ec} + w_{PLR} = 1. \quad (5.2)$$

The $Th_{b,m}^{u, Norm}$ is calculated with the UF^{up} equation 3.9, whereas $D_{b,m}^{u, Norm}$, $EC_{b,m}^{u, Norm}$ and $PLR_{b,m}^{u, Norm}$ are calculated with the UF^{down} equation 3.10.

5.2.2 Saturated Network

In case of overloading, the BSs cooperate with the joint aim of serving the largest possible number of users and avoid abruptly decreasing the Th_{sat} delivered by one BS concerning the others. The load balancing process is based on CGT, assuming that forming a GC [85] among RANs (i.e., players) cannot be worse than acting alone.

At each saturation point, the players are evaluated according to the $Th_{sat,b}^{average}$ value among their active users and the potential resources R_{Th_b} that BS can release until all clients belonging to it have the Th_m^{min} according to the service requirements and the defined SLA. In this case, the $SF_{b,u}^*$ quantifies the preferences among different outcomes [92], and it is calculated by

$$SF_{b,u}^* = \psi_m^b * (0.5 * Th_{sat,b}^{average} + 0.5 * R_{Th_b}^{Norm}), \quad (5.3)$$

$$s.t. Th_{sat,b}^{average} \geq Th_{sat,b}^{average, min} \wedge R_{Th_b}^{Norm} > 0.$$

The normalized $R_{Th_b}^{Norm}$ is calculated using the equation 4.9. One BS outperforms another if $SF_{b,u}^* > SF_{b',u}^*$ (i.e., $BS_b \succ BS_{b'}$). Therefore, the BS with the SF_{max}^* has the best conditions to satisfy the service request at a specific saturation point.

The selected BS gradually frees up resources to satisfy the new user request with the minimal number of affected users, guaranteeing at least the Th_m^{min} of their active users according to the tariff plans and services constraints. The regular users that stay longer in the network first reduce their resources. Nevertheless, suppose all users' services with low priority reach the Th_m^{min} , and the overload situation persists. In that case, the resources of premium clients are reduced, always maintaining a superior Th_{sat} . An affected user can revert to the previous state if new resources are available on the network. The game ends when all clients get the minimum Th , and it is unfeasible to accept a new request.

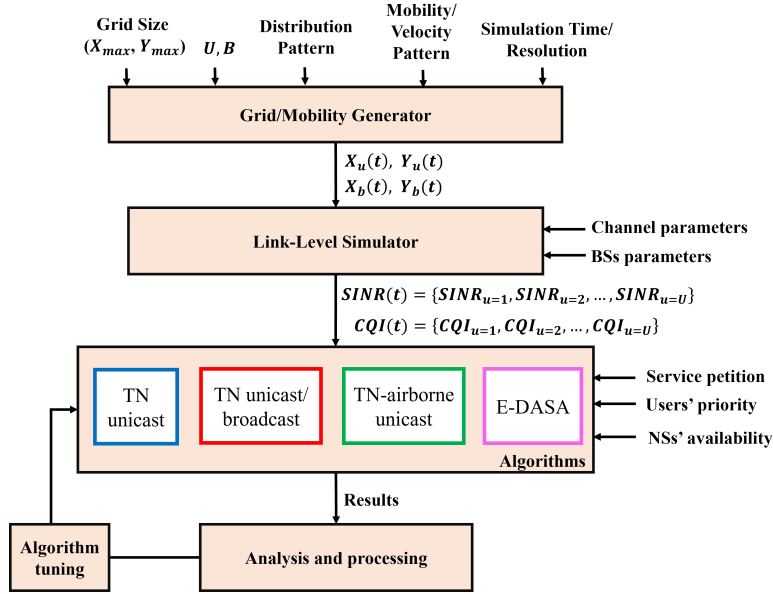


Figure 5.3: The E-DASA algorithm's validation process.

	Macro-BS	Micro-BS	UAV-BS
Operating frequency (GHz)	28	28	2.4
Bandwidth (MHz)	400	400	100
RB's bandwidth (MHz)	1.44	1.44	0.72
Subcarrier spacing (kHz)	120	120	60
Component carriers	4	2	2
BS's height (m)	25	10	100
Transmission power (dBm)	40	26	30

Table 5.2: The E-DASA simulation parameters.

5.3 Simulation and Results

Four different RANs (a macro-BS, a micro-BS, and two UAV-BSs) are placed to serve a section of the football stadium and evaluate the proposal's performance. All RANs, except the micro-BS, where the AR slice is unavailable, support all NSs. We assume that a new user requests one of the available services every two seconds for a total of 400 users. The probability that a user requests VI is 60 %, while the probability of requesting AR and WB services is set to 20 %. 90 % of the users are stationary inside the stadium, while 10 % have RWP mobility.

The main elements of the validation process are detailed in Fig. 5.3. This stage aims to evaluate the performance of our proposal E-DASA (TN-airborne unicast/broadcast) against three other scenarios: TN unicast (the DASA algorithm, Chapter 4 [30]), TN unicast/broadcast, and TN-airborne unicast. LLSs have been

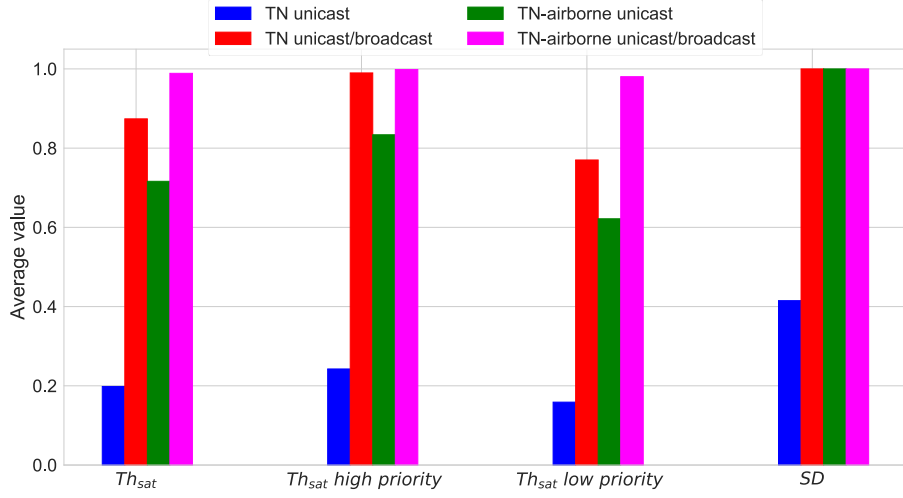


Figure 5.4: Th_{sat} and SD average values for 400 users.

carried out using an ad-hoc developed Python-based tool to obtain the SINR and CQI values for all the links between users and BSs during the simulation time [139]. Simulation parameters are specified in Table 5.2. The path loss model applied for TNs is detailed in [140], whereas the model for UAV-BSs can be found in [141]. Then, the obtained network parameters with the defined services constraints, user profile, and NSs' availability are the algorithm's inputs.

Fig. 5.4 shows the $Th_{sat}^{average}$ for the 400 users in the network, the $Th_{sat}^{average}$ for users with high priority, the $Th_{sat}^{average}$ for users with low priority, and the $SD^{average}$ values. The $SD^{average} = 0.41$ for the TN unicast scenario, meaning that this configuration can serve only 41 % of the clients due to the scarcity of resources. Differently, the other three solutions show an $SD^{average} = 1$, attending 100 % of the analyzed spectators. Regarding the $Th_{sat}^{average}$, the presented proposal outperforms the baselines with a 0.99 value. Integrating TN-airborne connectivity with unicast/broadcast capabilities increases the network capacity and optimizes resource utilization, guaranteeing a better perception for premium users according to their tariff plan.

Fig. 5.5 and 5.6 also show the outperformance of our solution in terms of Ec average (mJ) and ADR (Gbps). As Fig. 5.5 shows, the Ec average increases when the load balancing process is applied due to the scarcity of resources. In the case of ADR, for only unicast scenarios, when the first saturation point occurs, the overall ADR remains stable because the algorithm applies a load-balancing strategy to free up resources and assign them to new clients. However, exploiting broadcast capability guarantees that VI clients share the broadcast slice resources, positively impacting the performance of the network capacity and the ADR.

Fig. 5.7 details the total number of affected users due to the saturation points. All results show that the scenario with unicast services delivered via TNs considerably has the worst performance. For this scenario, the first saturation point occurs for

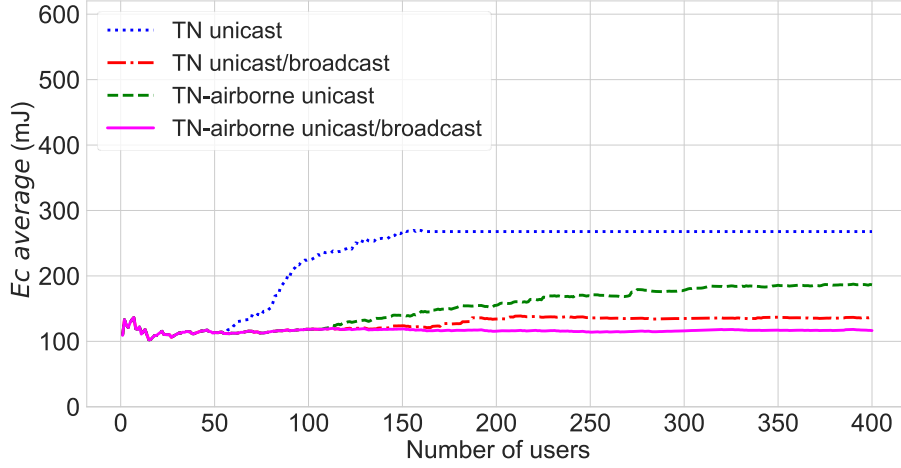


Figure 5.5: E_c average values for an incremental number of users.

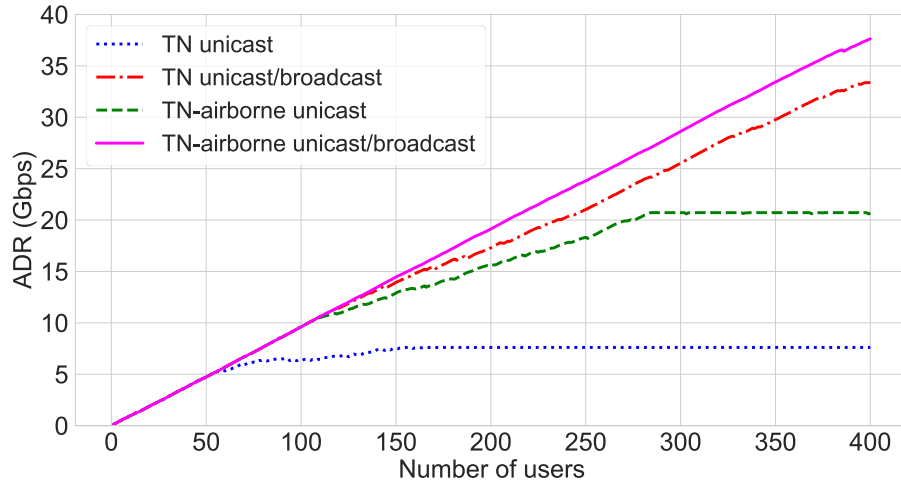


Figure 5.6: ADR for an incremental number of users.

56 users and can only serve 164 users on the network. On the contrary, the first saturation point for our proposal appears for 386 users. From this point forward, the algorithm follows a collaborative attitude to split the resources among active users at the expense of affecting the Th_{sat} performance to accept more clients on the network.

Fig. 5.8 shows the superior $Th_{sat}^{average}$ of our proposal regarding the TN unicast/broadcast scenario for an incremental number of users. It is shown how all clients experience the maximum Th_{sat} until the network reaches the first saturation point. At this moment, the load balancing starts reducing the Th from the regular clients and prioritizes the premium users with superior Th_{sat} .

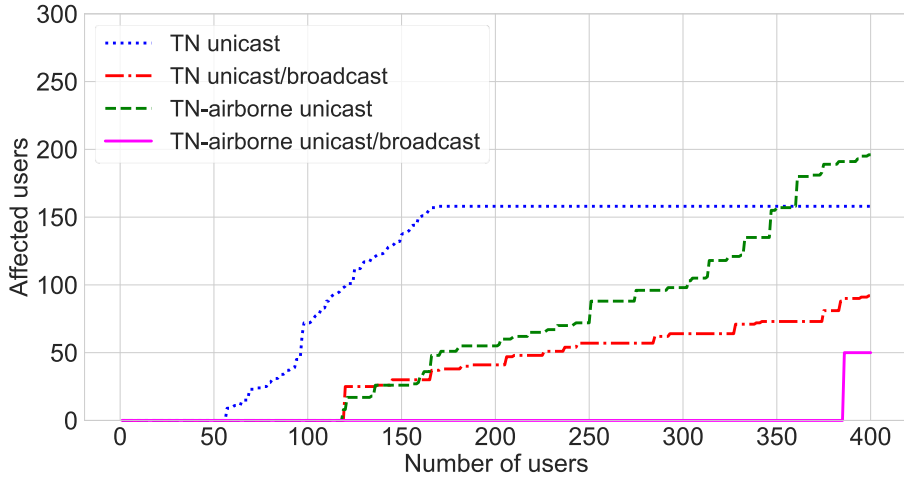


Figure 5.7: Number of affected users at each saturation point.

5.4 Conclusions

This work presents the E-DASA algorithm to select the best combination of BS/NS over a TN-airborne environment to optimize resource utilization and efficiently deliver unicast/broadcast services. The proposal is based on MADM and CGT to satisfy the service requests of multiple users with diverse priorities and mobility behaviors. In overload situations, cooperation among BSs guarantees splitting resources among active users and accepting new clients on the network without abruptly decreasing the overall Th_{sat} in one BS concerning the others. This work analyzes how the broadcast capability aided by NS and software frameworks is an effective solution in significant events like a football game, where many users request the same content simultaneously and generate peak traffic. The results show the outperformance of our proposal in terms of ADR, $Th_{sat}^{average}$, $SD^{average}$, $Ec^{average}$, and the number of affected users at each saturation point against TN unicast (the DASA algorithm), TN unicast/broadcast, and TN-airborne unicast scenarios.

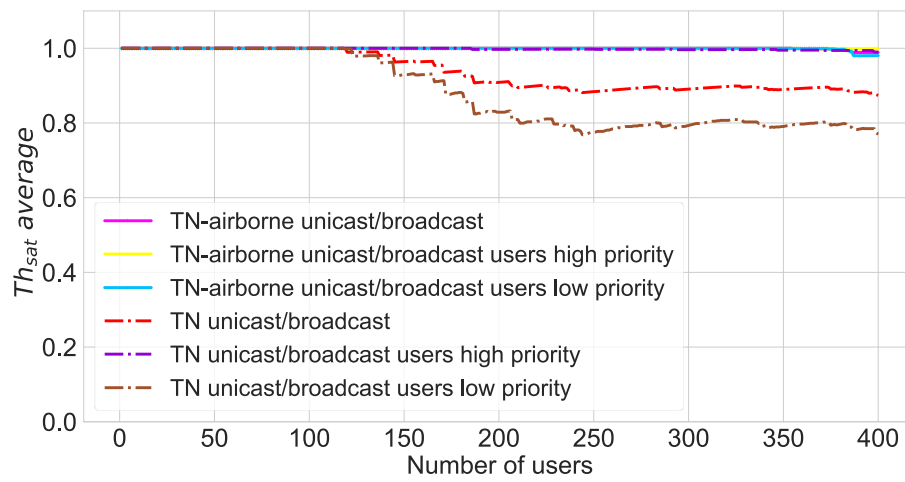


Figure 5.8: Th_{sat} average for TN-airborne unicast/broadcast and TN unicast/broadcast scenarios considering different users' priorities.

Chapter 6

ML-based solution for dynamic network selection and slice allocation in B5G O-RAN framework

This Chapter presents the eDRANS algorithm integrated within the O-RAN architecture. The proposal aims to select the best BS to satisfy multiple users' requests during diverse network conditions, improving QoS and optimizing slicing resource utilization. The solution considers multiple services with diverse requirements mapped into different NSs. The network selection process is based on F-DRL utilizing DDQN (termed in the following as federated learning with DDQN (F-DDQN)). Furthermore, the solution employs CGT as a load-balancing mechanism during overload situations. The proposal recreates a heterogeneous environment composed of terrestrial and airborne nodes. Comprehensive simulation results are obtained by optimizing resource utilization, considering multiple critical features such as throughput, delay, energy consumption, overloading, NS availability, and SLA satisfaction.

The validity and performance of the presented approaches are evaluated through rigorous network-level simulations. The proposed solution, analysis, and conclusions respond to **SO-5**. In summary, the technical contributions include the following:

1. The eDRANS algorithm is based on F-DDQN and CGT to deal with the network selection problem and guarantee a dynamic slice allocation for diverse network conditions, user types and priorities, service requirements, and mobility behaviors in B5G networks. One of the critical advantages of eDRANS is its foundation on the F-DDQN approach, which is well-suited for handling continuous state spaces and discrete action spaces while enhancing data privacy and reducing CC. On the other hand, the load balancing strategy facilitates dynamic resource adjustments to accommodate additional clients with adequate

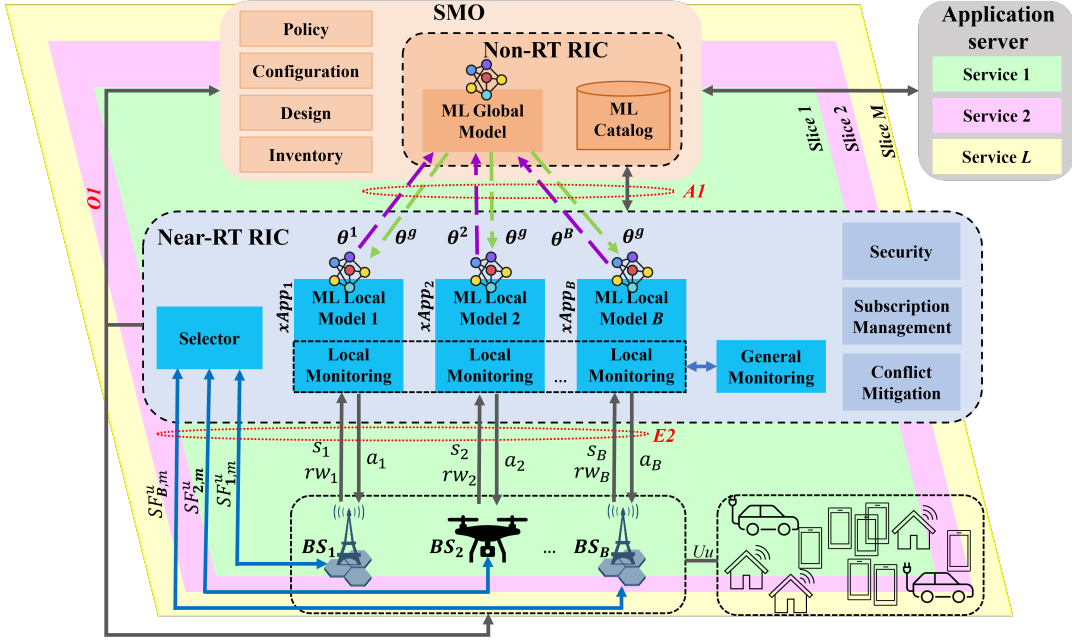


Figure 6.1: The RAN softwarized architecture based on the O-RAN framework.

QoS without abruptly compromising the active users' perception.

2. The proposed ML solution is inserted in the novel O-RAN architecture to exploit their disaggregated elements and open interfaces effectively, facilitating an ML control loop from training to model deployment. In that sense, multiple ML Local Models jointly cooperate in training an ML Global Model inserted in the RIC without sharing sensitive data and reducing communication overhead. The framework includes a Selector Module to make a final global decision considering the previous actions taken by each ML Local Model (i.e., one for each BS).

6.1 Overview of the Proposed Solution

In this Section, we illustrate the scenario and provide an overview of the proposed eDRANS algorithm.

6.1.1 The O-RAN Framework

Fig. 6.1 shows the proposed RAN softwarized high-level architecture based on the O-RAN approach [29]. We propose integrating the eDRANS algorithm in this framework to fulfill multiple users' requests over a heterogeneous environment. The proposal aims to select the best BS and optimize the utilization of NSs' resources

according to network conditions, user types and priorities, mobility patterns, and service constraints.

To handle the network selection problem, we deploy multiple $xApps$ with one ML Local Model each (i.e., one per BS). These agents use local knowledge (i.e., data from the BS they are related to) to decide whether to attend or not the service requests. Then, the Selector Module, located in the Near-RT RIC, performs the final decision based on the previous actions of the ML Local Models. Subsection 6.1.2 provides more details. Our approach assumes that the envisioned O-RAN deployment must be robust enough to collect data from multiple $E2$ interfaces and integrate $xApps$ from different vendors, guaranteeing data security and isolation. The $xApps$ ' isolation is critical for the independent operation of O-RAN services and the accurate Near-RT RIC decision-making. In this context, the Security, Conflict Mitigation, and Subscription Management components play a crucial role [29, 142].

According to the F-DRL process (described in Section 6.2), the ML model parameters locally obtained during training are collected in the Non-RT RIC to compute an enhanced ML Global Model. Next, the updated ML Global Model parameters are sent back to the local agents, so knowledge earned by all the agents is leveraged for the individual action selection. This data exchange occurs in predefined intervals that might change according to the network characteristics. No user-related or safety-critical data is transmitted among local agents or from the Near-RT RIC to the Non-RT RIC. Sending to the ML Global Model only the model parameters locally obtained enhances privacy and reduces communication overhead.

Once the ML training is finished, it undergoes a validation process to ensure efficiency. If this validation is successful, the resulting ML-trained model is published on the ML Catalog. The ML Catalog must also include under which specific conditions the ML-trained model delivers the best performance (e.g., required resources to instantiate and execute the model, input types, expected outputs, and latency requirements [143]). Then, suppose a new BS is temporally activated, such as a UAV acting as aerial BS to improve the overall network capacity and coverage during a special event. The new local agent can download and use the common ML-trained model through the $O1$ interface. According to the O-RAN specifications, the training process is offline [29]. However, this does not exclude online training. Each ML Local Model previously trained (i.e., F-DRL process) can be fine-tuned and updated based on architectural changes or inefficiencies detected through the $E2$ interface (online arrival data in the execution environment). Continuous operation is crucial in the ML workflow to improve online the previously trained ML models [144].

6.1.2 eDRANS Overview

In a HetNet composed of B BSs (TNs and NTN, where $\mathbb{B} = \mathbb{T} \cup \mathbb{N}$ as defined in Section 3.2), we consider U UEs randomly distributed and with different priorities and mobility behaviors. We consider diverse service types (i.e., services 1- L), which are

mapped into multiple RAN slices (i.e., NSs 1- M). Specifically, we assume that each UE_u can request one of these services: VI, VR, or Industrial IoT (IIoT) application. Each service is mapped into a different NS. Table 6.1 details the resulting weight values according to AHPs [30], where w_{Th} , w_D , and w_{Ec} denote the importance that each specific service gives to the QoS parameters.

Service type	w_{Th}	w_D	w_{Ec}
VI	0.65	0.1	0.25
VR	0.6	0.2	0.2
IIoT	0.15	0.15	0.7

Table 6.1: The w_{Th}, w_D, w_{Ec} values for VI, VR, and IIoT.

To evaluate the network conditions to satisfy each service request, the $SF_{b,m}^u \in [0, 1]$ is computed for each BS_b as

$$SF_{b,m}^u = \begin{cases} S_{b,m}^u, & \text{if } \psi_m^b = 1 \\ C_{b,m}^u, & \text{if } \psi_m^b = 0 \\ 0, & \text{if } (P_{RB_b}^{Norm}=0 \wedge \psi_m^b = 0) \vee D_{b,m}^{u, Norm}=0 \vee EC_{b,m}^{u, Norm}=0. \end{cases} \quad (6.1)$$

$S_{b,m}^u$ represents the score to attend the user request by the BS_b when the network has enough resources and can be defined as

$$S_{b,m}^u = \kappa_m^b * (w_{Th} * Th_{b,m}^{u, Norm} + w_D * D_{b,m}^{u, Norm} + w_{Ec} * EC_{b,m}^{u, Norm}). \quad (6.2)$$

On the other hand, $C_{b,m}^u$ is the score value during an overload situation expressed by

$$C_{b,m}^u = \frac{\kappa_m^b}{\delta''} * (w_{Th_{sat}} * Th_{sat,b}^{average} + w_{P_{RB}} * P_{RB_b}^{Norm}), \quad (6.3)$$

where $\delta'' > 1$ is a scale factor that adjust the $C_{b,m}^u$ value to benefit the BSs without overload situations.

P_{RB_b} (dimensionless) represents the potential RBs that BS_b can release until all the users belonging to it have the minimum possible Th according to the service constraints and the user priority. The normalization of P_{RB_b} ($P_{RB_b}^{Norm}$) is computed by

$$P_{RB_b}^{Norm} = \begin{cases} 0, & \text{s.t. } Cond_1 \\ \frac{P_{RB_b}}{RB_{b,m}^{u, max}}, & \text{s.t. } Cond_2 \\ 1, & \text{otherwise.} \end{cases} \quad (6.4)$$

$Cond_1$: $P_{RB_b} < RB_{b,m}^{u, min}$,

$Cond_2$: $RB_{b,m}^{u, min} \leq P_{RB_b} \leq RB_{b,m}^{u, max}$,

where $RB_{b,m}^{u, min}$ and $RB_{b,m}^{u, max}$ are the minimum and maximum number of RBs to

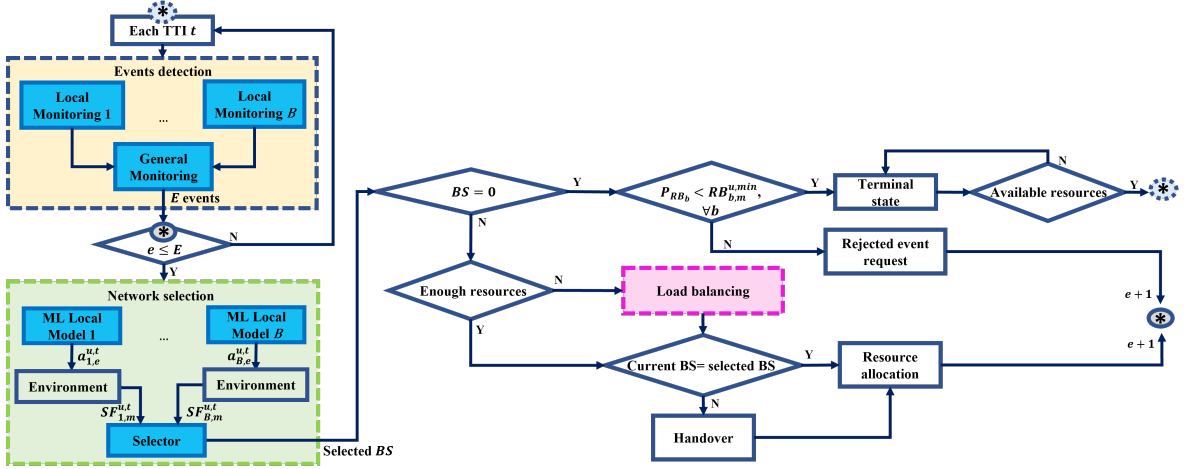


Figure 6.2: The eDRANS algorithm flowchart.

obtain the Th_m^{min} and Th_m^{max} , respectively, according to user's signal reception conditions and service's constraints. Point out that the Th_m^{min} for premium clients is higher than the Th_m^{min} for regular users, ensuring a superior perception for the clients with high priority according to the SLA (more details in Section 6.3).

Fig. 6.2 shows the algorithm flowchart, highlighting the main processes: network selection and load balancing. At each TTI t , each Local Monitoring Module collects the following events: new users' service requests, existing user's service updates, or existing user's CQI variation according to a certain threshold (to avoid the ping-pong effect preventing unnecessary handovers [55]). The events detected individually by each $xApp$ are collected by the General Monitoring Module for a total of E events. As shown in Fig. 6.2, at the end of each particular event e , the algorithm attends the next event $e + 1$ from the number of identified events in the specific TTI t . The rejected event requests are stored at the beginning of the queue for the next TTI $t + 1$.

After each ML Local Model makes its individual decision based on the specific data regarding the BS_b for the event e , the Selector Module, allocated in the Near-RT RIC, selects the BS with the highest $SF_{b,m}^{u,t}$ among all ML models that chose to attend the service request. The Selector Module does not know the BS_b 's local data. It only receives the resulting $SF_{b,m}^{u,t}$, preserving privacy and reducing communication overhead.

eDRANS considers a variable bit rate traffic according to network conditions, user priority, and service constraints. When the network has enough capacity, the algorithm assigns the number of RBs for a Th_m^{max} considering the service requirement and disregards the user's priority. On the other hand, if the selected BS does not have enough resources, eDRANS applies a load-balancing strategy according to the service performance and the SLA to benefit more users and avoid the abrupt general

QoS degradation. The load balancing aims to release resources and attend to the new user based on CGT while the general user satisfaction is kept as high as possible. Details can be found in Section 6.3. Then, if the chosen BS is not the user's current network, the handover process will be executed as shown in Fig. 6.2. However, if the service request corresponds to a new user in the network, the selected BS proceeds to the resource allocation process in the corresponding NS.

Suppose none BS is selected ($BS = 0$) because there are insufficient potential resources to release and satisfy the minimum constraints (i.e., $P_{RB_b} < RB_{b,m}^{u,min}, \forall b \in \mathbb{B}$). In that case, the system reaches a terminal state ($flag_end = 1$), and new events cannot be attended. This transitory condition holds until resources are released (e.g., a user leaves the network).

eDRANS aims to select the best BS to satisfy each user request and optimize the slicing resource utilization at each TTI t . Therefore, the algorithm can be formulated as a long-term utility optimization problem to maximize the $SF_{b,m}^{u,t}, \forall u \in \mathbb{U}$:

$$\max \lim_{T \rightarrow \infty} \sum_{t=1}^T \sum_{u=1}^U SF_{b,m}^{u,t} \quad (6.5a)$$

$$s.t. Th_m^{min} \leq Th_{b,m}^{u,t} \leq Th_m^{max}, \quad (6.5b)$$

$$D_{b,m}^{u,t} \leq D_m^{max}, \quad (6.5c)$$

$$Ec_{b,m}^{u,t} \leq Ec_m^{max}, \quad (6.5d)$$

$$\kappa_m^b = 1, \quad (6.5e)$$

$$P_{RB_{b,t}}^{Norm} > 0, \quad (6.5f)$$

where T is the total number of TTIs. The optimization variable $SF_{b,m}^{u,t}$ directly impacts QoS and user perception, considering diverse network conditions, user types, service constraints, and slice accessibility, as represented in equation 6.1. Then, to guarantee at least the minimum requirements for the UE_u 's request, the selected BS_b must ensure (6.5b-f). In that case, the $SF_{b,m}^{u,t} > 0$, and the SLA is satisfied with $I^{u,t} = 1$; otherwise, both metrics are 0. The resource allocation must always be oriented to assign the maximum possible resources without exceeding the Th_m^{max} .

6.2 Network Selection Process

The eDRANS network selection process is based on F-DDQN, building an ML Global Model cooperatively. The local agents collaborate to find the policy π^* that maximizes the long-term QoS for all the users in the network and optimizes the resource utilization, subject to the diversity of users' demands and service constraints. We consider a time-slotted system, where t' represents a specific decision interval, $t' \in \{1, 2, \dots, T'\}$, and $T' = H \times T \times E$. E is the number of events at the TTI t . In this case, T is the number of TTIs during an episode h , and H is the number of episodes during the training process.

Initially, an ML Global Model located in the Non-RT RIC initializes random global parameters θ^g and shares them with the ML Local Models situated in the Near-RT RIC. Each local agent, one for each BS_b , executes the training process for every event e in the TTI t , based on the received parameters and its dataset, obtaining new local parameters θ^b . Then, to avoid communication overhead, only for every f' decision interval, the local parameters are sent to the ML Global Model, which aggregates them via a federated averaging (FedAvg) method [78] to obtain a new global model as

$$\theta^{g,t'+1} = \frac{1}{B} \times \sum_{b=1}^B \theta^{b,t'}, \quad (6.6)$$

where B is the number of local agents participating in the training, as shown in Fig. 6.1.

Later, the resulting aggregated model weight is sent back to the ML Local Models. This iterative process is repeated until the ML algorithm converges to the optimized ML Global Model θ^{g*} . All local agents will use these same parameters $\theta^1 = \dots = \theta^B = \theta^{g*}$ without sensitive data transfer among them.

We formalize the interactions between each ML Local Model and the environment as a MDP considering the tuple of states, actions, and rewards $\langle S, \mathcal{A}, \mathcal{R} \rangle$:

State Space: It is defined for each ML Local Model as \mathcal{S}_b and contains user, application, and network data regarding BS_b . Specifically, the state observed by each ML Local Model associated with the BS_b during an event e in the TTI t is constructed as the following vector:

$s_{b,e}^t = [\rho^{u,t}, p^{u,t}, \alpha_{b,m}^u, \kappa_m^b, \psi_m^{b,t}, e_{ff_b}^{u,t}, P_{RB_{b,t}}^{Norm}, Th_{sat,b,t}^{average}, Th_{b,m}^{u,t}, Th_m^{max}, Th_m^{min}, D_{b,m}^{u,t}, D_m^{max}, Ec_{b,m}^{u,t}, Ec_m^{max}]$. As mentioned, the local information regarding BS_b is not shared with another entity to preserve privacy. Notice that several elements in the state space are continuous.

Action Space: The set of possible actions to be taken by each local agent is defined by $\mathcal{A} = \{0, 1, 2\}$. Specifically, the action taken by the local agent during an event e in the TTI t , regarding UE_u request, is termed $a_{b,e}^{u,t}$. In particular, $a_{b,e}^{u,t} = 1$ means that the BS_b can attend the service request with enough resources, whereas with $a_{b,e}^{u,t} = 2$ the BS_b can also serve the request, but it must perform a load balancing process due to overloading. In contrast, if the local agent selects $a_{b,e}^{u,t} = 0$, the BS_b cannot attend the service request, and the $SF_{b,m}^u = 0$. Then, the BS_b is not a candidate for the Selector Module. Nevertheless, if some BS can satisfy the service demand, but all actions are 0, the user request is rejected, affecting the QoS performance.

Reward: Each ML Local Model receives a reward ($rw_{b,e}^{u,t}$) due to the action performed, contributing to the learning process. The local agents are trained to maximize the cumulative reward given by

$$\mathcal{R} = \sum_t \sum_e \gamma \times rw_{b,e}^{u,t}, \quad (6.7)$$

where $\gamma \in [0, 1)$ is the discount factor that controls how future rewards are accounted for.

Suppose the local agent corresponding to the BS_b decides to attend the service request (i.e., $a_{b,e}^{u,t} = 1$). The decision is correct if the BS_b can satisfy (6.5b-e) and, consequently, $I^{u,t} = 1$ and $SF_{b,m}^u > 0$. In that case, the reward equals the $SF_{b,m}^{u,t}$ value. Moreover, suppose the agent correctly decides not to serve the request due to the BS_b 's impossibility of adjusting the resources of the current users or the inaccessibility to the requested service ($\kappa_m^b = 0$). Then, the reward is a positive value equal to 0.5. On the other hand, if the agent decides to attend the request, but it is wrong about network conditions (i.e., $a_{b,e}^{u,t} = 1$ and the BS_b presents overloading), the reward is 0.1. Other bad decisions are penalized with a -1 reward value. Mathematically, the local agent's reward is defined as

$$rw_{b,e}^{u,t} = \begin{cases} SF_{b,m}^{u,t}, & \text{s.t. } Cond_1, Cond_2 \\ 0.5, & \text{s.t. } Cond_3 \\ 0.1, & \text{s.t. } Cond_4, Cond_5 \\ -1, & \text{s.t. otherwise.} \end{cases} \quad (6.8)$$

$$Cond_1: a_{b,e}^{u,t} = 1 \wedge \psi_m^{b,t} = 1 \wedge (6.5b-e),$$

$$Cond_2: a_{b,e}^{u,t} = 2 \wedge \psi_m^{b,t} = 0 \wedge (6.5c-f),$$

$$Cond_3: a_{b,e}^{u,t} = 0 \wedge (\text{not}(6.5c) \vee \text{not}(6.5d) \vee \text{not}(6.5e) \vee (\text{not}(6.5f) \wedge \psi_m^{b,t} = 0)),$$

$$Cond_4: a_{b,e}^{u,t} = 1 \wedge \psi_m^{b,t} = 0 \wedge (6.5c-f),$$

$$Cond_5: a_{b,e}^{u,t} = 2 \wedge \psi_m^{b,t} = 1 \wedge (6.5b-e).$$

Considering our optimization problem, the continuous state space, and the discrete action space, DDQN is the DRL technique used for each ML Local Model to deal with the network selection task. DDQN is a model-free and off-policy algorithm that can effectively handle discrete action spaces [77, 145]. Compared to the traditional RL approaches, DDQN has the advantage of reducing the overestimation of Q values and thus helps us achieve faster training and more stable learning [146, 147]. The off-policy behavior enables the exploration of high-dimensional search spaces efficiently and using past experiences during training. Moreover, off-policy algorithms can be trained with either externally generated or self-generated experiences, thus reducing the possibility of getting stuck at a local minimum [148].

Fig. 6.3 shows the diagram of the local interactions of each DDQN agent with the environment. The first Q-value function $Q(s, a, \theta)$, where θ stands for the vector of NN weights, is used to make the action choice. In contrast, the second Q-value function $\hat{Q}(s, a, \theta^-)$ is used to evaluate the action reward. Initially, we assume that $\theta^- = \theta$. Then, the \hat{Q} parameters are updated based on the target network's updating rate (τ) [149].

The agents apply an epsilon (ε)-greedy strategy to select the actions and prevent stalling at a local minimum. Each agent takes the best action ($\text{argmax}_{a^*} Q_b(s, a, \theta)$)

Finally, the global loss function (\mathcal{L}_G) is

$$\mathcal{L}_G(\theta^g) = \frac{1}{\sum_{b=1}^B |\mathcal{K}_b|} \sum_{b=1}^B |\mathcal{K}_b| \times \mathcal{L}_b(\theta^b). \quad (6.12)$$

Algorithm 4 describes the F-DDQN process, where H is the number of episodes during training to guarantee an optimum θ^{g*} (i.e., $\mathcal{L}_G(\theta^{g*})$ less than or equal to some defined target). Each episode starts from an initial state (i.e., without users in the network) and runs until the network does not have enough resources to satisfy a new request ($flag_end = 1$). F' is the number of federated episodes. The FedAvg equation updates both $\theta^{g,t'}$ and $\theta^{g,t'-}$ according to the DDQN structure [151].

In the proposed F-DDQN solution, each ML Local Model runs independently and in parallel. Then, the CC regarding the local agents during training is $\mathcal{O}(H \times T \times E(\mathcal{S}_0 n_{x=1} + \sum_{x=1}^{X-1} n_x n_{x+1}) + 2|\mathcal{S}_b|^2 \times |\mathcal{A}| + \log_2 |\mathcal{B}|)$ [152, 153]. S_0 is the input layer's size, X is the number of NNs layers, and n_x is the number of neurons in the x -th layer. Specifically, we use two fully connected hidden layers with $2 \times (|\mathcal{S}_b| + |\mathcal{A}|)$ neurons [154].

In the case of the ML Global Model (Algorithm 4), the CC is $\mathcal{O}(F' \times (2 \times B))$. This term depends linearly on the number of federated episodes and agents. Factor 2 responds to the DDQN structure. Finally, the total CC for the network selection task based on F-DDQN is $\mathcal{O}(H \times T \times E(\mathcal{S}_0 n_{x=1} + \sum_{x=1}^{X-1} n_x n_{x+1}) + 2|\mathcal{S}_b|^2 \times |\mathcal{A}| + \log_2 |\mathcal{B}| + F' \times (2 \times B))$.

In our proposal, each local agent only observes the locally relevant information \mathcal{S}_b . Then, the state space is not affected by the number of BSs. On the contrary, in a centralized learning process, the unique agent must gather the information of B BSs to attend to each service request. This approach has complete knowledge of the environment with a negative impact on the privacy and communication overhead, which becomes more critical with the increment of the state space. Specifically, for a centralized ML scheme, the collected state vector for each action increases B times regarding the F-DDQN solution, negatively impacting CC. The same happens with a heuristic solution, iterating among all possibilities to select the most suitable BS. Then, the CC is affected by the number of BSs, making scalability a critical concern. In a distributed ML scheme, each agent only observes its local data \mathcal{S}_b , and there is no interaction with a central unit. Then, the increment in the number of BSs does not affect the state space. The distributed ML solution has less CC than F-DDQN, centralized DDQN, and heuristic algorithms (e.g., DASA). However, this scheme limits the agents to only learn from individual interactions with the environment, affecting algorithm performance.

6.3 Load Balancing Process

The load balancing is based on CGT and must be executed when the selected BS is overloaded. At each saturation point, the current users in the selected BS co-

Algorithm 4: The F-DDQN training process (eDRANS)

Input: $\mathcal{S}_b, \mathcal{A}, \mathcal{R}, \varepsilon, \alpha, \tau, \gamma, |\mathcal{K}_b|, f', H$
Initialize: $t' = 0, F' = 0$, ML Global Model: θ^g ,
ML Local Models: $\theta^b = \theta^{b^-} = \theta^g, |\mathcal{B}| \leftarrow \emptyset$
Output: θ^{g^*}

```

foreach episode  $h = 1, \dots, H$  do
  Initialize  $\mathcal{S}_b, flag\_end = 0$ 
  while  $flag\_end = 0$  do
    foreach TTI  $t$  do
      foreach event  $e \in E$  do
         $t' ++$ 
        Local Models (Near-RT RIC):
        foreach ML Model  $b \in B$  do
          Observe current state  $s_{b,e}^t$ 
          Agent takes  $a_{b,e}^{u,t}$  based on  $\varepsilon$ -decay
          Agent gets its  $rw_{b,e}^{u,t}$ 
          Environment changes to  $s_{b,e}^{t+1}$ 
           $\mathcal{B}$  stores  $\Xi_{b,e}^t$ 
          if  $|\mathcal{B}| > |\mathcal{K}_b|$  then
            Sample a mini-batch  $|\mathcal{K}_b|$  from memory buffer  $\mathcal{B}$ 
            Calculate  $y_{b,e}^t$  as equation (6.9)
            Calculate  $\mathcal{L}_b$  as equation (6.11)
            Update  $\theta^b$  by the  $\mathcal{L}_b$ 's backpropagation
            Update  $\theta^{b^-} \leftarrow \tau\theta^b + (1 - \tau)\theta^{b^-}$ 
          end
        end
      if  $mod(t', f') = 0$  then
         $F' ++$ 
        Global Model (Non-RT RIC):
        Collect  $\theta^{b,t'}$  and  $\theta^{b,t'-}$ 
        Apply FedAvg as equation (6.6)
        Calculate  $\mathcal{L}_G$  as equation (6.12)
        Broadcast  $\theta^{g,t'+1}$  and  $\theta^{g,t'+1^-}$  to each ML Model  $b$ 
      end
    end
  end
  if  $\varepsilon > 0.1$  then
    | Apply  $\varepsilon$ -decay strategy
  end
end

```

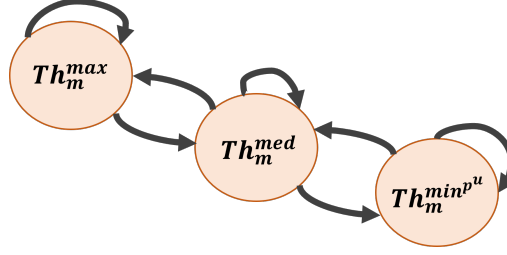


Figure 6.4: Possible actions to perform during the coalition formation.

operate to release the minimal necessary resources to achieve a specific target (i.e., the required RBs (RB_{req}) to satisfy the new service request) without abruptly compromising their perception. We consider a weighted voting game with a dynamic coalition structure [95, 97] to find the coalition (C) that better satisfies the new service request. The players can adapt their coalition structure to changes such as the arrival/departure of users, position variations, network conditions, and service constraints. Additionally, the number of resources that users can contribute to the coalition depends on their priority, potentially available resources, the service requirements, and the new user's characteristics.

The potential released resources of each user UE_u , belonging to the BS_b , can be expressed as $P_{RB_b}^u = RB_{pot1}^{u,b} + RB_{pot2}^{u,b}$. $RB_{pot1}^{u,b}$ represents the resources that a user can release to reduce the $Th_{b,m}^u$ to a medium Th value (Th_m^{med}) according to the service constraint (s.t., $Th_m^{med} < Th_{b,m}^u \leq Th_m^{max}$). On the other hand, the $RB_{pot2}^{u,b}$ are the resources that the UE_u can free up by reducing the $Th_{b,m}^u$ to the Th_m^{min} subject to the service constraint and his/her priority (s.t., $Th_m^{min} < Th_{b,m}^u \leq Th_m^{med}$). The premium users are benefited from a superior service perception, being the $Th_m^{min^{p1}} = \frac{Th_m^{med}}{2}$, where $Th_m^{min^{p1}} > Th_m^{min}$. In contrast, the minimum Th for users with low priority ($Th_m^{min^{p2}}$) coincides with the Th_m^{min} according to the service constraint.

If all users have reached the Th_m^{min} according to their priorities and service constraints, the game is over, and it is unfeasible to accept new users on the network (Fig. 6.2). This is a transitory state and holds until, for example, some users leave the network and new resources are available. In this case, new service requests can be attended, or a user whose Th has been affected due to an overload situation can revert to the previous state, as shown in Fig. 6.4.

The set of players of the CGT is formed by the RBs of the users belonging to the BS_b and can be written as

$$\mathbb{P} = \{RB_{pot1}^{1,b}, RB_{pot2}^{1,b}, \dots, RB_{pot1}^{U,b}, RB_{pot2}^{U,b}\}. \quad (6.13)$$

The influence on the outcome at each load balancing time is related to the resources in possession by the active users and the possible actions to perform according to Fig. 6.2, avoiding an abruptly $Th_{sat,b}^{average}$ degradation. During the load balancing, some users are favored according to the priority-based scheduling:

1. Users with low priority release their resources first until the $Th_m^{min^{p^2}}$ is reached.
2. Users with Th_m^{max} are selected to release their resources first regarding users with Th_m^{med} and the same priority.
3. If the service request is VI or VR, the marginal contribution of active users in the BS utilizing the IIoT service is not critical because the IIoT's Th requirement is considerably less than VI and VR applications. Therefore, if the new service request is VI or VR, the active users using these services prefer to contribute their resources to the coalition formation concerning the users utilizing the IIoT application.

It must be pointed out that two users with the same priority, service, and the same Th level can contribute differently to the game. A user with bad reception conditions requires more RBs to achieve the QoS requirements. Therefore, his/her contribution is more significant and can result in fewer affected clients during the load balancing.

Particularly, $\mathbb{P}^* \subseteq \mathbb{P}$, is a subset of \mathbb{P} obtained following the priority-based scheduling, s.t. $RB_{release}^{\mathbb{P}^*} \geq RB_{req}$, where

$$RB_{release}^{\mathbb{P}^*} = \sum_{i=1}^{|\mathbb{P}^*|} RB_{release}^i + RB_b^{av}. \quad (6.14)$$

$RB_{release}^{\mathbb{P}^*}$ represents the sum of the available resources in the BS_b and the total released resources by all the players belonging to the set \mathbb{P}^* .

\mathbb{C}_{win} is the set of possible winning coalitions from \mathbb{P}^* that satisfies the new request (RB_{req}). To find a winning coalition, it must be guaranteed that $P_{RB_b}^{Norm} > 0$ with $P_{RB_b} \geq RB_{release}^C$. The overall worth of each coalition C is described by the characteristic function $\nu(C)$

$$\nu(C) = \begin{cases} \frac{1}{4} * U_{aff}^{Norm} + \frac{3}{4} * \xi^{Norm}, & \text{if } RB_{release}^C \geq RB_{req} \\ 0, & \text{otherwise,} \end{cases} \quad (6.15)$$

with

$$\xi^{Norm} = \frac{RB_{req}}{RB_{release}^C}. \quad (6.16)$$

The U_{aff}^{Norm} is the normalized number of affected users and is calculated using the equation 4.10, and ξ^{Norm} is the normalized value of the residual RBs. $\xi^{Norm} = 1$ means that the network could release precisely the required resources for the new user. The characteristic function reflects a preference for ξ^{Norm} regarding U_{aff}^{Norm} . As a result, $C_{min} \in \mathbb{C}_{win}$ is the winning coalition with the maximum $\nu(C)$ value ($\nu^{max}(C)$), minimizing the residual RBs and the number of affected users. Point out that this kind of GT is generally not superadditive because we cannot guarantee that the GC structure, where $GC = \mathbb{P}^*$, is the C_{min} [97]. Algorithm 5 describes the load balancing process.

Algorithm 5: The load balancing process (eDRANS)

Input: \mathbb{P} , p^u , RB_{req} , RB_b^{av} , Services constraints
Initialize: $\mathbb{C}_{win} = \{\}$, $C_{min} = 0$, $\nu^{max}(C)=0$
Output: C_{min} , U_{aff} , ξ , $RB_{release}^{C_{min}}$
Apply priority-based scheduling $\mathbb{P} \rightarrow \mathbb{P}^*$
foreach $C \in \mathbb{P}^*$ **do**
 if $\sum_{i=1}^{|C|} RB_{release}^i + RB_b^{av} \geq RB_{req}$ **then**
 Compute U_{affC}, ξ_C
 $\mathbb{C}_{win}.append(C)$
 end
end
for $z \in \mathbb{C}_{win}$ **do**
 Calculate $\nu(C_z)$
 if $\nu(C_z) > \nu^{max}(C)$ **then**
 $\nu^{max}(C) = \nu(C_z)$
 $C_{min} = C_z$
 end
end
 $RB_{release}^{C_{min}} = \sum_{i=1}^{|C_{min}|} RB_{release}^i + RB_b^{av}$

6.4 Results and Discussion

To evaluate the performance of our proposal, we recreate a heterogeneous environment composed of three RANs: a macro-BS, a micro-BS, and a UAV-BS. The airborne node is opportunistically located in the grid to support the terrestrial infrastructure by increasing coverage and network capacity. All RANs support all NSs except the micro-BS, where the IIoT slice is unavailable. We assume a new user requests one of the available services every two seconds until it reaches 150 users. 90 % of the users are pedestrians with RWP mobility, while 10 % are stationary users, including SNs.

LLSs have been conducted using an ad-hoc developed Python-based tool to obtain the SINR and CQI values for all the links between users and BSs during the simulation time [139]. Simulation parameters are specified in Table 6.2. The path loss model applied for TNs is detailed in [140], whereas the model for BSs can be found in [141].

6.4.1 Training

Regarding the DDQN model of each local agent, the NN implementation has an input layer that accepts an $\mathbb{R}^{1 \times 15}$ state vector described in Section 6.2. The output layer produces an $\mathbb{R}^{1 \times 3}$ vector of Q -values corresponding with the three possible

	Macro-BS	Micro-BS	UAV-BS
Operating frequency (GHz)	28	28	28
Bandwidth (MHz)	400	400	400
RB's bandwidth (MHz)	1.44	1.44	1.44
Subcarrier spacing (kHz)	120	120	120
Component carriers	2	2	2
BS/user height (m)	25/1.5	10/1.5	100/1.5
Transmission power (dBm)	40	26	30
Small-scale fading model	Jakes	Jakes	Jakes
Large-scale fading model	[140]	[140]	[140]

Table 6.2: eDRANS simulation parameters.

Parameter	Value
Number of episodes (H)	50
Optimizer	Adam
Learning rate (α)	0.01
Exponential decay rates (β_1, β_2)	0.9, 0.999
Discount factor (γ)	0.99
Target network update (τ)	0.001
Initial ε value	1
Mini-batch size $ \mathcal{K} $	64
Maximum buffer size $ \mathcal{B} _{max}$	10000

Table 6.3: Hyperparameters configuration.

actions for each BS. We use two fully connected hidden layers with 36 neurons (i.e., $2 \times (15 + 3)$) and the rectified linear unit (ReLU) activation function in both hidden layers. The output layer uses the linear activation function to predict the long-term reward values of the actions in the given state. Tests have demonstrated that increasing the number of hidden layers does not improve the algorithm performance but increases the CC [154].

Table 6.3 details the hyperparameters' configuration. The α value, $|\mathcal{K}|$, and the optimizer were obtained experimentally through parameter tuning to provide the algorithm's best performance. We use the Adam optimizer, proven as robust and efficient for a wide range of DRL optimization problems [149, 154]. The maximum size of the experience replay buffer ($|\mathcal{B}|_{max}$) is large enough to store all experiences during the training phase. The number of episodes and the maximum number of users for each episode are selected so that the algorithm correctly converges.

Fig. 6.5 shows the loss function behavior ($\mathcal{L}_G(\theta^g)$) as a result of three ML Local Models' updates (i.e., one for each BS) to train the enhanced ML Global Model. Different results are evidenced with $\alpha = \{0.0001, 0.001, 0.01\}$, $|\mathcal{K}| = \{32, 64, 128\}$

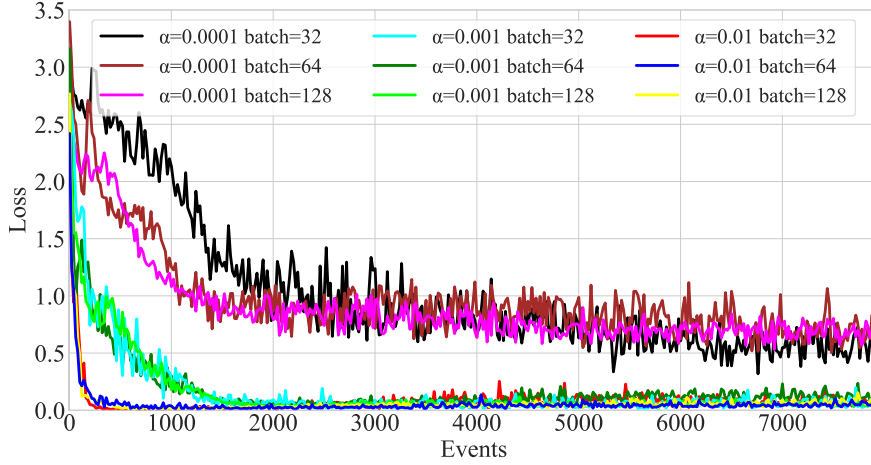


Figure 6.5: Loss function for Adam optimizer, different α values, and mini-batch sizes.

and Adam optimizer. The algorithm presents a faster convergence and lower loss values for $\alpha = 0.01$ and $|\mathcal{K}| = 64$.

Fig. 6.6 also shows the F-DDQN training process in terms of loss, but in this case, for $\alpha = \{0.0001, 0.001, 0.01\}$, $|\mathcal{K}| = 64$ and two different optimizers: Adam and stochastic gradient descent (SGD) with *momentum* = 0.9. As Fig. 6.6 illustrates, the loss function with Adam optimizer decreases faster and presents a smoother behavior than SGD with a less training cost [149, 155], especially for higher α values. Results demonstrate that the training process is slower for lower α values. Nevertheless, much higher α values may lead to instability.

Fig. 6.7 presents our proposal's reward average during training. Besides, we use the DDQN centralized and distributed ML models as benchmarks. Our F-DDQN algorithm shows a similar trend to the DDQN centralized training model regarding the reward average without the necessity to share sensitive data among agents or to the aggregation unit. In contrast, the centralized ML algorithm uses a unique central trainer responsible for collecting all data and deciding which BS best satisfies the service request based on accumulated experiences. The centralized method has complete knowledge of the environment that favors the training process but lacks privacy and causes communication overhead, which becomes more critical with the increment of the state space. On the other hand, distributed training shows the worst learning performance because each BS trains its ML model with local experiences only. There is no information exchange among agents or agents and a central unit, limiting the local models to use only individually collected data. Finally, this scheme selects the BS randomly among all BSs that decide to serve the user request based on [72].

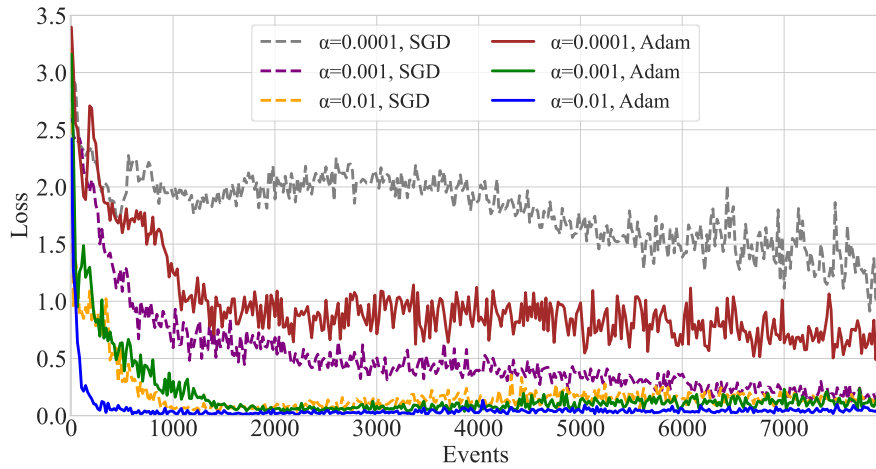


Figure 6.6: Loss function for Adam and SGD optimizers, and different α values.

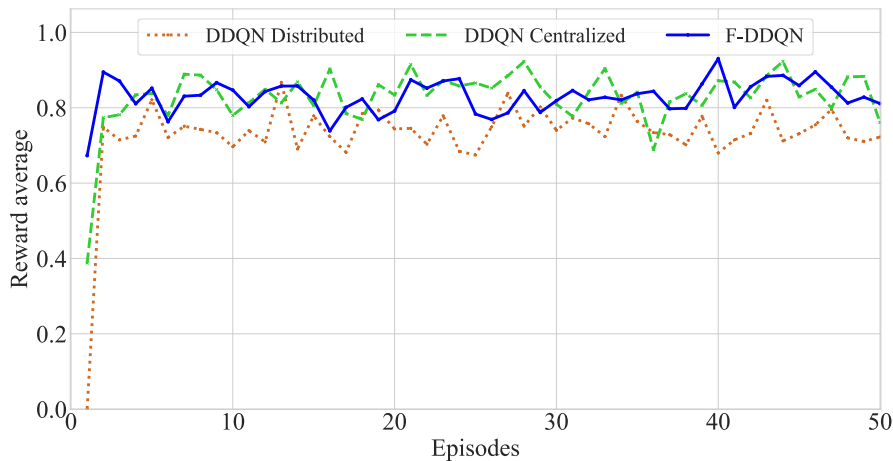


Figure 6.7: Reward average during the training process.

6.4.2 eDRANS Validation

For the eDRANS validation process, we assess its effectiveness against four state-of-the-art benchmark solutions: the Max-SINR method, a variation of the heuristic algorithm DASA presented in Chapter 4 ([30]), and the DDQN centralized and distributed ML models. Results were achieved by averaging 30 simulation runs to ensure a 95 % CV.

The baseline Max-SINR method is a variation of the traditional RSS criterion as we described in Chapter 4. We assume that Max-SINR selects the BS that provides the highest reception conditions and considers the NS accessibility without evaluating the QoS parameters and the available resources in the BSs. In contrast, the heuristic solution based on the DASA algorithm iterates among all BSs in the coverage area of the user to find the best solution for each generated event. Then,

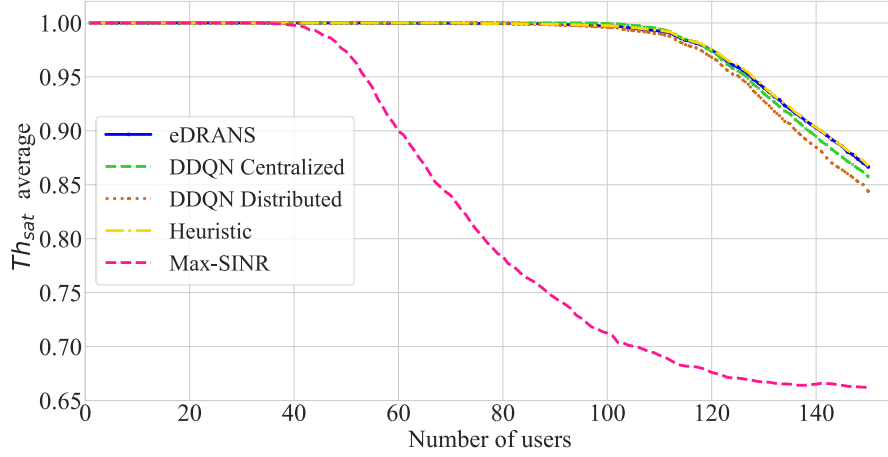


Figure 6.8: Th_{sat} average for an incremental number of users.

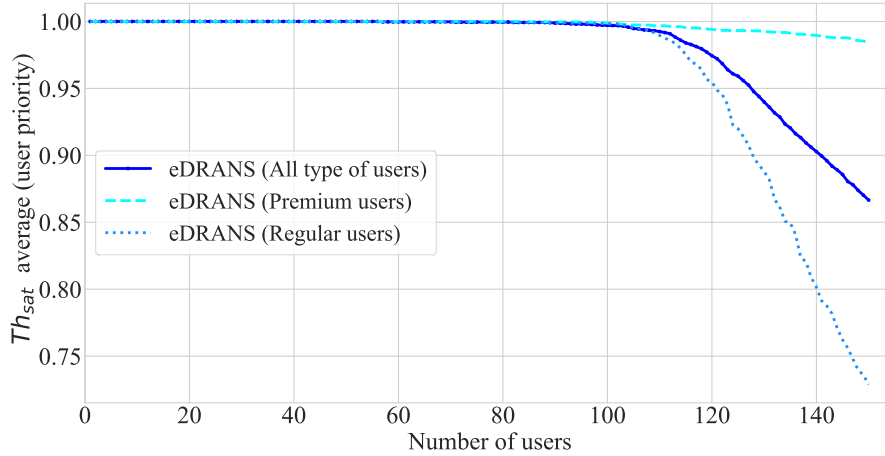


Figure 6.9: Th_{sat} for different user priorities (eDRANS algorithm).

this algorithm performs optimally in the recreated use case and provides a superior performance bound. However, this solution must collect information from all BSs in the network to make the decision. Therefore, communication overhead and CC are negatively impacted by the number of BSs. This heuristic approach suffers from reduced scalability for future massive and heterogeneous deployments.

Fig. 6.8 shows the $Th_{sat}^{average}$ of the system over time for an incremental number of users. $Th_{sat}^{average}$ remains equal to 1 until the network does not have enough resources to satisfy the new user request according to his/her priority and service constraints. Due to the scarcity of resources, the algorithm follows a collaborative attitude (i.e., bit rate adjustment), splitting the resources among active users in the selected BS_b . Then, the new service request is accepted at the expense of gradually affecting the $Th_{sat}^{average}$ performance. The Max-SINR algorithm performs

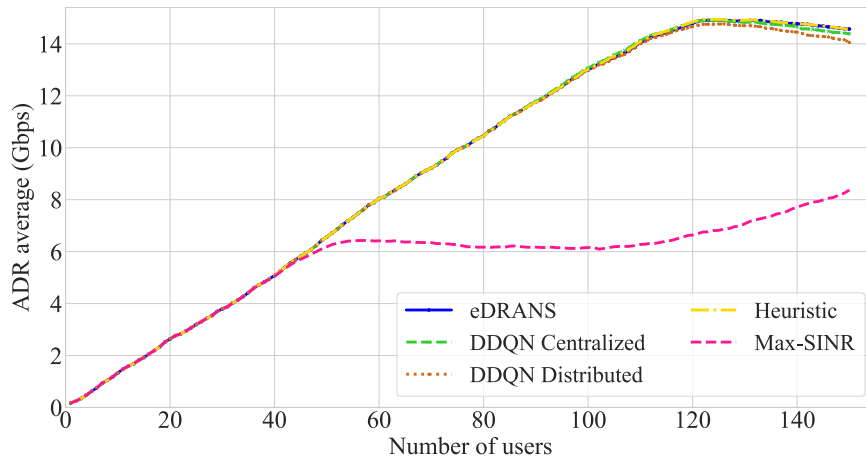
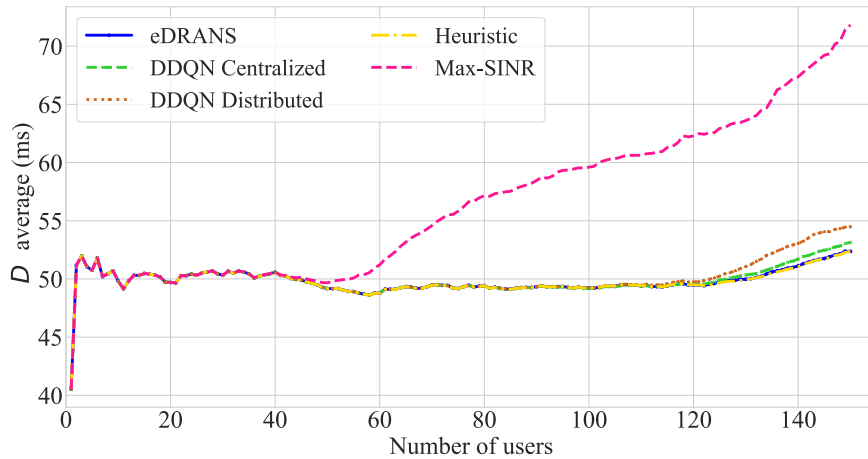
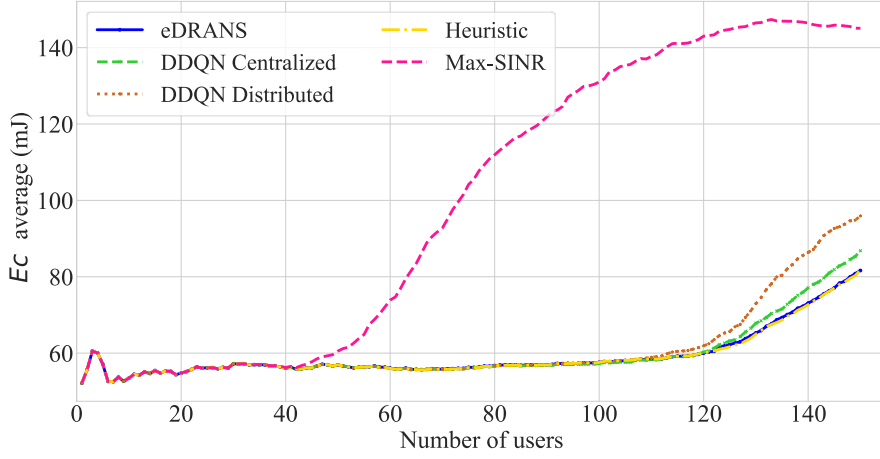
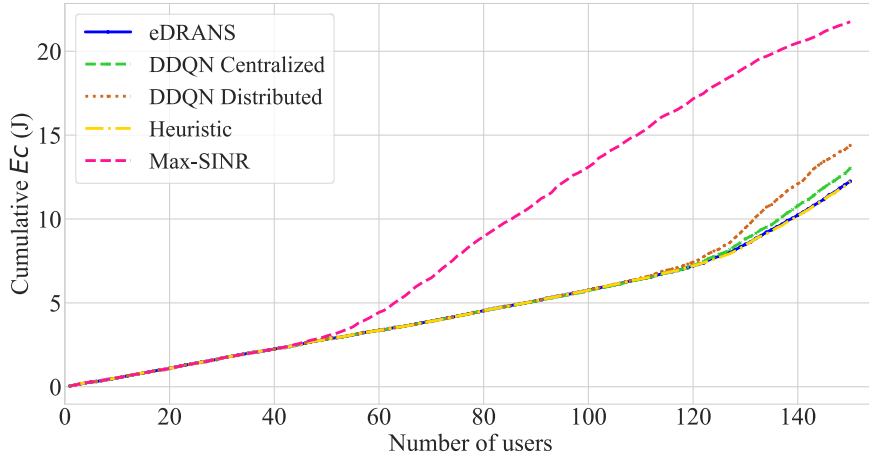


Figure 6.10: ADR average for an incremental number of users.

Figure 6.11: D average for an incremental number of users.

significantly worse because it does not consider the QoS parameters and the overload situations. This scheme only evaluates the user reception conditions to make the decision. Consequently, it has high sensibility regarding the users' mobility behavior, leading to frequent handovers, multiple clients accessing the same BS, and, therefore, degradation of the Th_{sat} from only 35 users in the network. Our proposal has a similar behavior to the heuristic algorithm and a superior performance regarding the other benchmark solutions, maintaining a higher $Th_{sat}^{average}$ value for an incremental number of users. Specifically, for 150 users in the network, our proposal and the heuristic algorithm outperform the centralized and distributed ML models and the Max-SINR criterion in terms of $Th_{sat}^{average}$ by 2 %, 3.1 %, and 24 %, respectively.

Fig. 6.9 evidences the superior service perception of premium users concerning regular users in terms of $Th_{sat}^{average}$ applying the eDRANS algorithm. While the

Figure 6.12: Ec average for an incremental number of users.Figure 6.13: Cumulative Ec for an incremental number of users.

network has enough resources, all clients maintain a Th_{sat}^{max} without a difference. However, during an overload situation, a CGT is performed among the RBs of the active users in the BS_b , prioritizing premium clients versus those of low priority. Therefore, the Th_{sat}^{max} of premium clients is equal to 1 until all regular users in the BS_b have the Th_{sat}^{min} according to the services' requirements. At this moment, the clients with high priority start to gradually release their resources to satisfy the new service request until reaching a $Th_m^{min^{p1}}$, always superior to the minimum of regular clients based on the SLA. For 150 users in the network, the $Th_{sat}^{average}$ for premium clients is 0.98, whereas for regular users is 0.73.

Then, Fig. 6.10 shows the ADR for an incremental number of users. Results evidence the superior performance of our proposal and the heuristic algorithm. An increasing trend is observed when the network has enough resources until the load

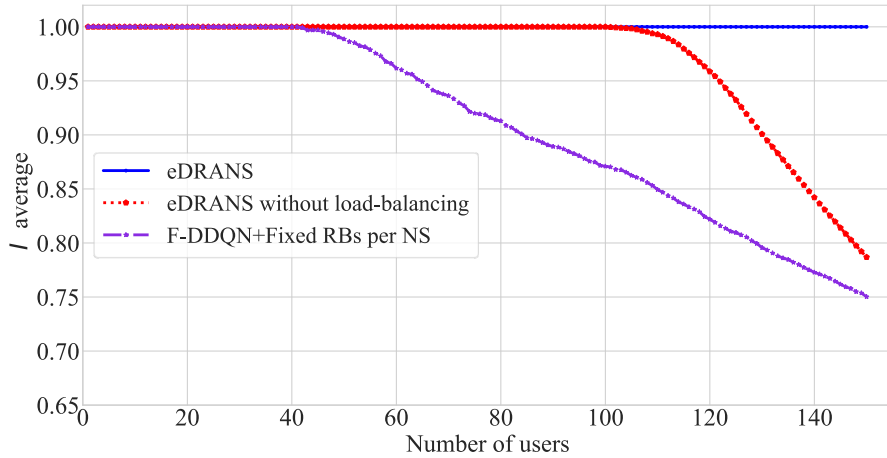


Figure 6.14: The SLA indicator (I) for an incremental number of users.

balancing starts affecting the overall ADR to satisfy new service requests. At each saturation point, the load balancing process is applied to gradually release RBs from current users to assign them to new clients, always ensuring the minimum constraints according to the service characteristics and users' priorities. Our proposal and the heuristic algorithm present higher ADR than the centralized and distributed ML models and the Max-SINR criterion by 1.2 %, 3.9 %, and 42.6 %, respectively, for 150 users in the network.

Fig. 6.11 and 6.12 display the D and Ec average for an incremental number of users. The outcome graphs show how D and Ec trends directly relate to network conditions. During overload situations and the corresponding resource reduction of active users in the selected BS_b , D and Ec are affected and increase their average values over time. The Max-SINR criterion performs poorly because it only considers user reception conditions and does not analyze the QoS parameters to make decisions. As expected, eDRANS performs similarly to the other benchmark solutions with enough network resources and guarantees less D and Ec average values during overload situations regarding the Max-SINR criterion, the centralized and distributed ML models. For example, eDRANS and the heuristic algorithm evidence 1.5 %, 3.9 %, and 27 % less D average than the centralized and distributed ML models and the Max-SINR criterion, respectively, for 150 users.

Fig. 6.13 shows the cumulative Ec for an incremental number of users averaging 30 simulation runs. Our proposal and the heuristic algorithm have the best performance. Specifically, eDRANS and the heuristic solution guarantee 6 %, 16 %, and 44 % less system's Ec than the centralized and distributed ML models and the Max-SINR criterion, respectively, for 150 users in the network.

As results show, eDRANS performs similarly to the heuristic algorithm regarding all analyzed metrics, proving its effectiveness and optimal decision under diverse network conditions. The heuristic model must centrally collect all information

and iterate among all candidate BSs to make the decision, negatively impacting communication overhead, complexity, and privacy issues. Specifically, the collected data size for each action increases B times (i.e., the number of BSs) regarding our proposal. In contrast, eDRANS benefits from collaborative ML training while enhancing data privacy and considerably reducing communication overhead compared with the centralized ML model and the heuristic solution. The presented outcomes demonstrate that F-DDQN correctly learns during multiple trial-and-error interactions with the environment to select the best BS and dynamically perform slicing resource allocation in a heterogeneous system.

Finally, Fig. 6.14 evaluates the proposed load-balancing strategy using the SLA indicator (I). We compare our proposal against two benchmarks: eDRANS without any resource adjustment during overloading and a variation of the algorithm proposed in [101] (i.e., F-DDQN with fixed RBs per NS). In the second approach, each NS (one for each service plus a master NS) is initialized with a fixed number of RBs. The master NS supports all the services available in the BS. Then, when an NS's capacity exceeds a defined threshold, the incoming traffic is allocated to the master NS. This strategy does not consider resource adjustment to already users in the overloaded NS.

For the evaluated specific conditions, eDRANS outperforms the other solutions with an I average value equal to 1, guaranteeing an effective resource adjustment. Consequently, the SLA is satisfied for the 100 % of the users in the network. The I average will remain equal to 1 until all users have the Th_m^{min} according to their priorities and the service constraints. At this point, it will be infeasible to accept new clients, which will affect the SLA satisfaction. In contrast, the eDRANS proposal, without any load-balancing strategy, presents an I average value equal to 0.79 for 150 users in the network. The average number of rejects is 32. On the other hand, the algorithm with fixed RBs for each NS shows the worst performance. Even with a master NS to alleviate saturation of the rest of the NSs, the dynamic variations in service requests, mobility behavior, and user priorities negatively impact resource usage and SLA satisfaction. Specifically, this algorithm presents an I average value equal to 0.75 and 38 rejects for 150 users in the network.

6.5 Conclusions

This work presents the eDRANS algorithm based on F-DDQN to select the most suitable BS/NSs combination over the envisioned heterogeneous environment of future wireless networks. The proposal is inserted into the novel O-RAN architecture, where multiple ML Local Models in the Near-RT RIC, one for each BS, jointly train an ML Global Model in the Non-RT RIC. The algorithm is adapted to diverse network conditions, users with different priorities and mobility behaviors, and various service constraints regarding throughput, delay, and energy consumption. eDRANS manages overload situations with a CGT strategy, splitting resources among ac-

tive users and accepting more clients without abruptly decreasing the $Th_{sat}^{average}$, as evidenced in the presented results.

Diverse simulation tests are conducted to validate the proposal. First, the impact of multiple hyperparameters during the training phase is shown. Second, the network selection process is validated by comparing it with four state-of-the-art benchmarks: the Max-SINR criterion, a variation of the heuristic DASA algorithm, and the centralized and distributed ML models. Results show that eDRANS performs similarly to the heuristic algorithm, proving its effective learning process during multiple trial-and-error interactions with the environment, enhancing data privacy and reducing communication overhead. Furthermore, our solution optimizes the overall system's QoS regarding the evaluated metrics through efficient slicing resource utilization. Specifically, eDRANS outperforms the considered ML solutions in $Th_{sat}^{average}$ by at least 2 % and the Max-SINR by 24 % for 150 users in the network. Moreover, eDRANS guarantees 6 %, 16 %, and 44 % less system's Ec than the centralized and distributed ML models and the Max-SINR criterion, respectively. On the other hand, the results show the effective treatment of users with different priorities during overloading, always prioritizing premium clients and ensuring a superior perception based on the defined SLA. Additionally, we evaluate the proposed load-balancing strategy regarding SLA satisfaction. The outcome demonstrates the necessity of applying a dynamic slicing resource adjustment in a heterogeneous environment with multiple user requests and diverse service requirements.

Chapter 7

Federated Learning-based Unicast/Multicast Service Delivery over B5G O-RAN Framework

This Chapter presents a variation of the eDRANS framework presented in Chapter 6 by deploying several collaborative local agents in a novel O-RAN scenario, suitable for applications with very low latency requirements as expected in B5G networks. Moreover, unlike Chapter 6, which only considers unicast slices, this solution takes advantage of the MBS capabilities, considering multiple unicast/multicast services mapped into different NSs. The validity and performance of the presented approaches are evaluated through rigorous network-level simulations. The proposed solution, analysis, and conclusions respond to **SO-5**. In summary, the technical contributions include the following:

1. The ML-based solution is based on F-DDQN and inserted into a novel O-RAN framework (variation of scenario 1.4 as an O-RAN extension for B5G deployment). In this case, the ML training is conducted by the collaboration of multiple terrestrial and airborne BSs and a superior entity in the RIC, enhancing privacy and reducing communication overhead. Additionally, the BSs perform the ML inference tasks, achieving an E2E delay reduction.
2. We evaluate the advantages of shared unicast/multicast service delivery over a collaborative TN-airborne connectivity to improve the QoS performance and slicing resource utilization, considering diverse types of users, priorities, and mobility behaviors.

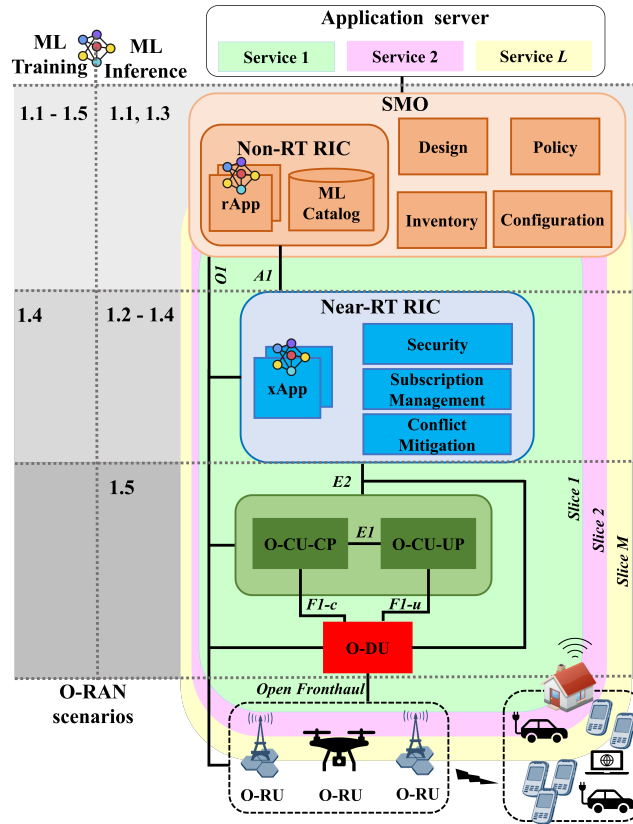


Figure 7.1: The O-RAN scenarios [26].

7.1 The O-RAN Framework

The O-RAN Alliance defines five scenarios (Fig. 7.1) detailing the allocation of ML training and inference entities [26, 29]: 1.1) Non-RT RIC performs ML training and inference functions; 1.2) Non-RT RIC performs ML training, and Near-RT RIC conducts the ML inference; 1.3) SMO performs ML training, and Non-RT RIC executes ML inference functionalities; 1.4) ML training is performed due to the collaboration between Non-RT RIC and Near-RT RIC. The ML inference is located in the Near-RT RIC; 1.5) Non-RT RIC performs ML training, and O-CUs/O-DUs assumes ML inference (i.e., through microservices called *dApps* [51]).

As B5G networks' requirements comprise very low latency, high speeds, and massive heterogeneous data, there are cases where the ML execution cannot be carried out within the timescale supported by the RICs (i.e., scenarios 1.1-1.4). Collecting sensitive data through *O1* and *E2* interfaces can negatively impact latency, overhead, and privacy. Then, elements nearer to the end-user must be capable of executing various ML inference tasks distributed at a timescale below 10 *ms* (e.g., scenario 1.5). Consequently, the O-CUs/O-DUs must have been dotted with enough resources and open interfaces to support the concurrent execution of several *dApps*

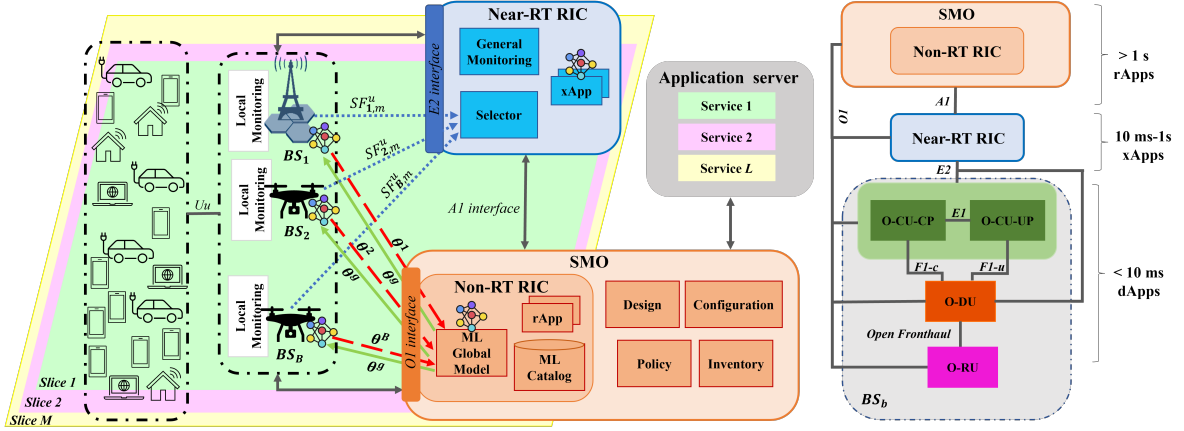


Figure 7.2: The proposed RAN softwarized architecture based on the O-RAN framework.

from different vendors without compromising their performance. The power consumption, security, CC, and storage capacity are critical concerns for future B5G ML solutions, sensibly impacting deployment costs and algorithm performance.

This research aims to select the best BS to satisfy multiple service requests and optimize the slicing resource utilization according to diverse network conditions, mobility patterns, and service constraints over a heterogeneous environment. We propose integrating the network selection algorithm in the O-RAN framework. Specifically, we propose a variation in scenario 1.4 as an O-RAN extension for B5G deployment. In this case, the ML training must be performed due to the collaboration between Non-RT RIC and O-CUs/O-DUs. The ML inference must be located in the O-CUs/O-DUs. As Fig. 7.2 shows, multiple ML Local Models are co-located within the BSs, specifically in the O-DUs. These agents use local knowledge to make individual decisions, deciding whether to attend or not the service requests. Then, the Selector Module, located in the Near-RT RIC, performs the final decision based on the ML Local Models' previous actions.

Following an F-DRL process, the agents collaborate to find the policy π^* that maximizes the long-term QoS for all the users in the network and optimizes the resource utilization, subject to the diversity of users' requests and service constraints. The ML model parameters obtained during training in the BSs are collected in the Non-RT RIC (i.e., through the *O1* interface) to compute an enhanced ML Global Model via the FedAvg method. Next, the updated ML Global Model parameters (θ^g) are returned to the local agents, so knowledge earned by all the agents is leveraged for the individual action selection. This data exchange occurs in predefined intervals to reduce communication overhead. In this process, no user-related or safety-critical data is transmitted among BSs or to the Non-RT RIC, enhancing privacy. Moreover, the local agents' location and the F-DRL design must guarantee

a timescale below 10 *ms* to enable future use cases with strict latency requirements (e.g., XR applications).

Once the ML training is finished, it undergoes a validation process to ensure efficiency. If this validation is successful, the resulting ML-trained model is published on the ML Catalog [29]. Moreover, each ML Local Module previously trained (i.e., F-DRL process) can be fine-tuned and updated based on architectural changes or inefficiencies detected (online execution environment).

7.2 Algorithm Overview

We consider a HetNet composed of terrestrial and airborne nodes to serve U end-devices requesting one of the available L services. Each service l is characterized by different requirements in terms of Th , D , and Ec . Therefore, we assume an NS per service. Moreover, taking advantage of the MBS capabilities, several services can be mapped into multicast/broadcast slices to serve many users simultaneously.

The proposed solution follows the same procedure described in Chapter 6 and is represented by Fig. 6.2. One of the main differences is the location of the ML training and inferences entities, as we detailed in Section 7.1. The network selection process is based on DDQN according to the continuous state space and the discrete action space as we discussed in Chapter 6. The proposal aims to maximize the long-term QoS of all users in the network. Specifically, the optimization target aims to maximize Th and minimize D and Ec .

When the network has enough capacity, the algorithm assigns the number of RBs for Th_m^{max} according to the service requirements. On the other hand, if the selected BS does not have enough resources, the algorithm applies the load-balancing strategy explained in Chapter 6. Another difference regarding the algorithm presented in Chapter 6 only based on unicast services, is that this solution considers multicast services mapped into multicast NSs. Then, the users requesting the same multicast service belong to the same MG. In this case, the algorithm considers the user with the worst reception conditions in the MG to perform the radio resource allocation process.

7.3 Results and Discussion

To evaluate the performance of our proposal, we recreate a heterogeneous environment composed of four RANs: a micro-BS and three UAV-BSs. The airborne nodes are opportunistically deployed in the grid to assist the terrestrial infrastructure during a temporal event by increasing coverage and network capacity. We consider 100 randomly distributed pedestrian users requesting one of the available multimedia services. The first service is mapped into a multicast (M) NS to exploit radio resources economically and efficiently and simultaneously serve many users. The

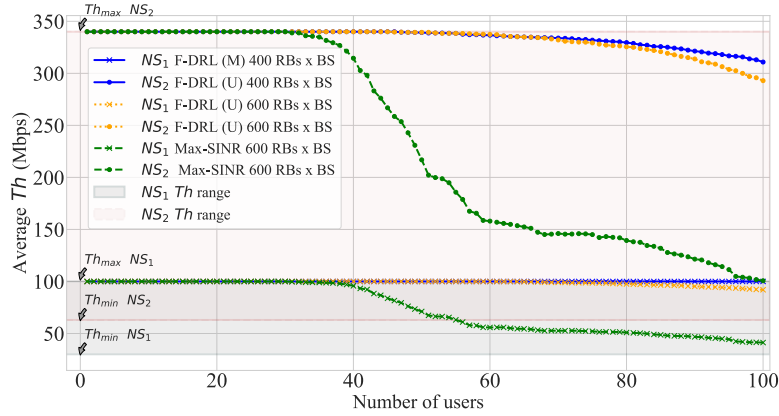


Figure 7.3: Th average per NS for F-DRL multicast (M), F-DRL unicast (U), and Max-SINR.

second service is mapped into a unicast (U) NS. Each NS has specific Th constraints (NS_1 : $Th_1^{min} = 30$ Mbps, $Th_1^{max} = 100$ Mbps; NS_2 : $Th_2^{min} = 63$ Mbps, $Th_2^{max} = 340$ Mbps).

LLSs have been conducted using an ad-hoc developed Python-based tool to obtain the SINR and CQI values for all the links between users and BSs during the simulation time [139]. The simulation parameters for the micro-BS and the UAVs are the same used in Chapter 6 and detailed in Table 6.2.

As we mentioned before, the proposed algorithm assesses the feasibility of addressing the BS/NS selection for shared unicast/MBS delivery leveraging F-DRL, the slicing paradigm, and the disaggregated O-RAN architecture. The implemented algorithm selects the most suitable BS to satisfy several concurrent requests and optimize slicing resource utilization, guaranteeing adequate QoS levels. We use two benchmark solutions: F-DRL with only unicast capabilities (i.e., both services are mapped into unicast slices) and Max-SINR. The baseline Max-SINR criterion selects the BS that provides the highest reception conditions and considers the NS accessibility without evaluating QoS parameters and available resources. Results were achieved by averaging 50 simulation runs to ensure a 95 % CV.

Fig. 7.3 shows the average Th per slice and different numbers of users. Dedicating only 400 RBs per BS, our solution outperforms the baseline, maximizing the clients' perception through effective resource management that profits from the multicast potentialities. The evaluated benchmarks using 600 RBs per BS present a similar behavior to our algorithm while they have enough resources to satisfy the users in the network. However, after a certain number of users, these algorithms must apply a load-balancing strategy. They split the resources among active users and guarantee to serve the total service petitions at the expense of affecting the average Th , always superior to the Th_m^{min} according to the service constraints. Specifically,

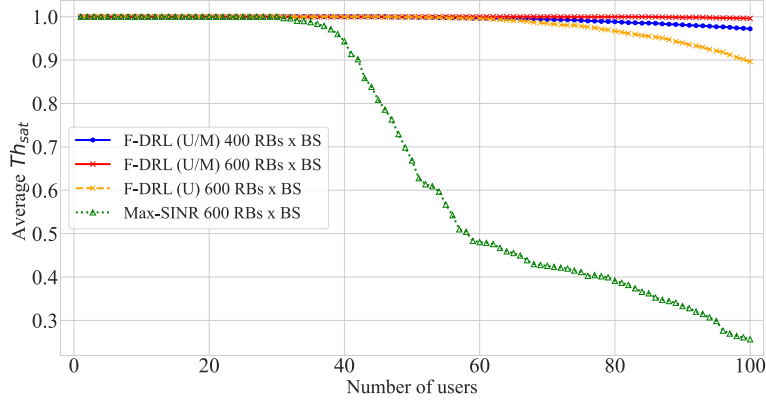


Figure 7.4: Th_{sat} average for F-DRL unicast/multicast (U/M), F-DRL (U), and Max-SINR.

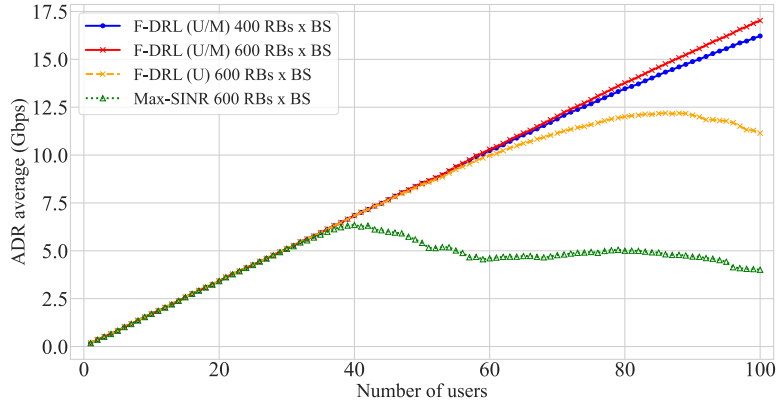


Figure 7.5: ADR average for F-DRL (U/M), F-DRL (U), and Max-SINR.

with 100 users in the network and 200 RBs less per BS, our solution outperforms the F-DRL (U) and Max-SINR in terms of average Th for NS_1 by 8 % and 58.7 %, and by 5.8 % and 67.6 % regarding NS_2 .

Fig. 7.4 and 7.5 show the $Th_{sat}^{average}$ and ADR average for different numbers of users in the network. $Th_{sat}^{average}$ remains equal to 1 until the network does not have enough resources to satisfy the new request according to the service constraints. Due to the scarcity of resources, the algorithm follows a bit rate adjustment to accept the new request at the expense of gradually affecting the $Th_{sat}^{average}$ and the overall ADR performance. The Max-SINR algorithm performs significantly worse. To make the decision, this scheme only evaluates the signal reception conditions. Consequently, it has high sensibility regarding the users' mobility behavior, leading to frequent handovers, multiple clients accessing the same BS, and, therefore, degradation of

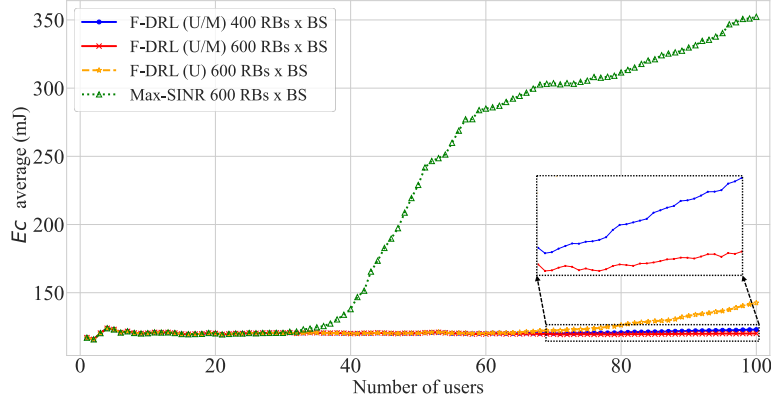


Figure 7.6: Ec average for F-DRL unicast/multicast (U/M), F-DRL unicast (U), and Max-SINR.

the Th_{sat} and ADR from only 30 users. On the contrary, our solution outperforms the baselines even with 200 RBs less per BS as demonstrated in Fig. 7.3. The MG shares the NS_1 resources, positively impacting the network performance.

Fig. 7.6 shows how the Ec directly relates to network conditions. As expected, our proposal performs similarly to the baselines when these solutions have enough network resources and guarantee less Ec average values during overload situations. Results demonstrate that a HetNet deployment with terrestrial-airborne connectivity and unicast/multicast service delivery maximizes the network capacity and optimizes resource utilization, ensuring a superior performance regarding solo unicast capabilities. Moreover, employing an F-DRL algorithm inserted in the envisioned O-RAN framework is a suitable solution to dynamically handle a complex environment with multiple requests and diverse service requirements. Finally, the same tendency is observed in Fig. 7.7 for the D average and an incremental number of users in the network.

7.4 Conclusions

This Chapter presents a dynamic network selection and slice allocation algorithm employing F-DDQN over the envisioned B5G heterogeneous environment. We consider terrestrial-airborne cooperation with unicast/multicast capability for differentiated traffic delivery. Our proposal improves the network capacity, slicing resource utilization, and satisfies multiple concurrent users with adequate QoS. The algorithm is inserted into the novel O-RAN framework, where several local agents located in the BSs jointly train an ML Global Model in the Non-RT RIC. The solution is adapted to diverse network conditions and different service constraints, enabling efficient differentiated traffic management over B5G networks. The presented simu-

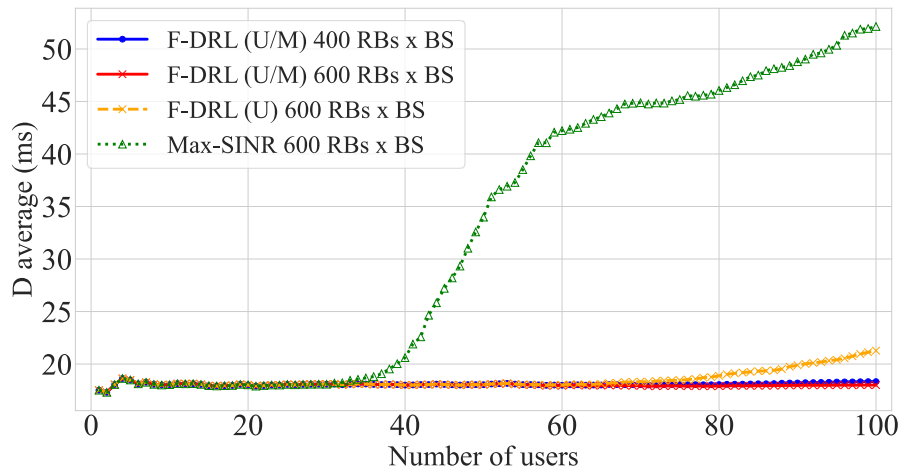


Figure 7.7: D average for F-DRL (U/M), F-DRL (U), and Max-SINR.

lation results prove the advantages of integrating F-DRL, the slicing paradigm, and MBS over a heterogeneous TN-airborne connectivity.

Chapter 8

QoE-based energy-aware resource allocation solution for video streaming B5G networks

This Chapter presents a QoE-based solution to dynamically conduct RRM in a 5G HetNet scenario. The proposed solution aims to identify the trade-off between the overall QoE- perceived by the different types of EDs when consuming video content and the overall network energy consumption, with a special focus on sustainability. In summary, the technical contributions include the following:

1. The proposed QoE-aware RRM solution ensures a dynamic resource allocation B5G HetNets for multiple EDs with different mobility behaviors requesting video streaming applications. Our findings demonstrate that allocating additional RBs does not always increase the perceived quality, but it often consumes more electricity and increases the risk of overloading. This study is based on a user-centric approach instead of only considering the QoS metrics.
2. We conduct extensive simulations for video streaming in B5G networks by considering two scenarios: serving all EDs of the same type (e.g., SPs) and serving a combination of different EDs (i.e., TVs, LPs, and SPs) with diverse mobility behaviors. These scenarios allow us to analyze the trade-off between the QoE and energy metrics for saving energy and network resources while maintaining satisfactory levels of QoE.

8.1 System Overview

Fig. 8.1 illustrates the proposed system model, which is considered to evaluate the energy consumption and QoE when streaming video content to several EDs through

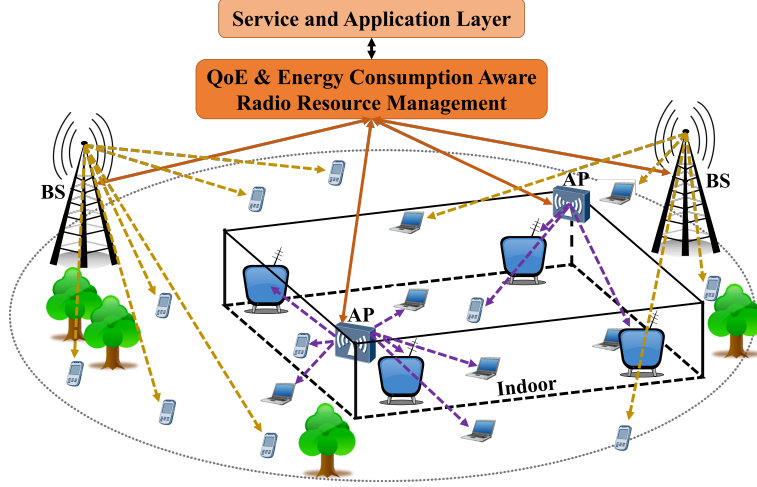


Figure 8.1: The considered HetNet deployment scenario.

a 5G RAN by varying the network setting. We assume a HetNet deployment, including a set of B NR BSs and a set of A NR APs. We assume that the network serves a set of U EDs, randomly distributed in the considered area, receiving and displaying a particular video content with a specific spatial resolution that will be characterized by a $Th_b^{u,d}$. As we explained in Section 3.2, d identifies the types of EDs, considering in this work $d \in \{TV, LP, SP\}$. The TVs and LPs are static and are connected to the APs. On the contrary, the SPs are characterized by random directional mobility and can be dynamically connected to either BSs or APs. Additionally, $BL^{u,d}$ is the backlight luminance level set on the ED and decided by the user [118].

Concerning the estimation of the QoE and energy consumption for each $ED_{u,d}$, we based on the study in [118], where a subjective assessment is conducted to investigate the impact of different luminance configurations and video resolutions on the QoE and energy consumption in video streaming. We obtain the QoE perceived by the user of an $ED_{u,d}$ in terms of the Mean Opinion Score (MOS) as a function of the $Th_b^{u,d}$ and the $BL^{u,d}$ set on the ED. The predicted MOS is defined as $MOS_p^{u,d} = f(Th_b^{u,d}, BL^{u,d})$. The details of the QoE model definition for the three considered EDs are described in Subsection 8.2.1.

We quantify the E2E (from the data center to ED) energy consumed to stream the video on the $ED_{u,d}$ in terms of the overall electricity consumption, $\Gamma^{u,d}$ (expressed in kWh), using the following equation [107]:

$$\Gamma^{u,d} = t''_{u,d} \times (P^{u,d} + \mathfrak{R}^{u,d} \times \aleph), \quad (8.1)$$

where $t''_{u,d}$ represents the streaming hours over a week, $P^{u,d}$ is the ED's power load depending on the Th of the reproduced video and, mainly, on the device's level of BL . $\mathfrak{R}^{u,d}$ is the transmitted data traffic proportional to the Th of the reproduced

ED	Resolution	\mathfrak{R}^d (GB/h)	$Th^{average}$ (Mbps)	BL^d (lx)	P^d (W)	Γ^d (kWh)
TV	4K	9.00	20	300	55.78	6.69
				5500	236.05	7.95
	FHD	2.25	5	300	53.67	1.95
				5500	243.48	3.28
LP	FHD	2.25	5	400	13.04	1.67
				4000	18.56	1.70
	HD	0.90	2	400	13.21	0.72
				4000	18.53	0.76
SP	FHD	2.25	5	200	1.85	1.59
				5000	2.46	1.59
	HD	0.90	2	200	2.98	0.65
				5000	3.19	0.65

Table 8.1: Estimated overall Γ^d per week for TV, LP, and SP [118].

video, and \aleph is a factor accounting for the electricity intensity of data traffic, including data transmission network and data center. For video encoded at HD, FHD, and 4K spatial resolution, \mathfrak{R} assumes values around 1, 2, and 9 GB/h. The power load P ranges from a few or dozens of W for SP and LP, respectively, whereas more than 200 W are needed by a 4K TV set with the brightest BL level. Setting the TV to the darkest BL level saves up to one-quarter of the consumed power. Table 8.1 shows the values of t'' , P , \mathfrak{R} , and \aleph for the three types of EDs [118].

The $MOS_p^{u,d}$ and $\Gamma^{u,d}$ depend on the $Th_b^{u,d}$ to correctly deliver the video service on the $ED_{u,d}$ and the level of $BL^{u,d}$ of the device. However, while the $Th_b^{u,d}$ can be controlled on the network management side, the level of $BL^{u,d}$ is decided by the user. We propose to optimize the $Th_b^{u,d}$ assigned to the devices connected to the network according to a SF that combines the contribution of QoE and energy and allows us to provide different weights to these two factors.

The proposed approach relies on centralized management, as depicted in Fig. 8.1. As the main objective of this work was to analyze the trade-off between energy consumption and QoE, our algorithm is simplified considering a centralized system without an O-RAN approach. Future works will be oriented to introduce an RRM solution with QoE as a target function in a distributed and softwarized environment to reduce CC and communication overhead and increase system scalability. In this case, the resource management module retrieves the CQI of each ED and, based on the importance given to QoE and energy consumption driven by the SF, decides the best BS_b to attend the request and the number of RBs to correctly reproduce the video service on that $ED_{u,d}$.

The spatial video resolutions considered for each ED are bounded by the network conditions and the native device's screen resolution, such that the highest video resolution matches the device's native resolution. Then, as we can observe in

Table 8.1, we consider for TVs the video resolutions of 4K (3840×1714) and FHD (1920×800), whereas, for LPs and SPs, the video resolutions are FHD and HD (1280×534). Moreover, we assume that the device's screen luminance $BL^{u,d}$ can be set in the darkest ($BL^{u,d} = 0$) or the brightest ($BL^{u,d} = 1$) conditions, as presented in [118].

8.2 Proposed Solution Overview

In this Section, we initially present the defined QoE models. Then, we describe the proposed resource allocation algorithm.

8.2.1 QoE Modeling

This Section presents the three QoE models designed explicitly for these considered EDs: TV (60" 4K screen, 3840×2160 pixels), LP (15.6" FHD screen, 1920×1080 pixels), and SP (5.5" FHD screen, 1920×1080 pixels). Each QoE model is obtained from the dataset of the subjective assessment conducted in [118], where a preset group of users scored the level of satisfaction of perceiving the VI service in a controlled environment. The obtained results highlight the combined contribution of the device's level of BL and the Th of the reproduced video on both the QoE and the Γ of the video streaming delivery chain. Thus, by considering changes in BL and Th , we can measure QoE and Γ changes.

We define the QoE models by considering Th and BL as dependent variables and the MOS as the variable to be predicted. We do not consider ambient and content luminances, which were two further variables included in the test conditions of the subjective assessment, because their effects on QoE and energy consumption were found to be negligible as described in [118]. Moreover, ambient and content luminances cannot be controlled because they intrinsically depend on the ambient conditions and video content, respectively.

As a result of [42], we obtained the $MOS_p^{u,d}$ models represented by the equations (8.2), (8.2) and (8.4) for TV, LP, and SP, respectively:

$$MOS_p^{u,TV} = 0.030 \times Th^{u,TV} + 0.708 \times BL^{u,TV} + 3.426 \quad (8.2)$$

$$MOS_p^{u,LP} = 0.606 \times Th^{u,LP} + 0.506 \times BL^{u,LP} + 2.797 \quad (8.3)$$

$$MOS_p^{u,SP} = -0.025 \times Th^{u,SP} + 1.975 \times BL^{u,SP} + 1.950. \quad (8.4)$$

The three applied Linear Regression (LR) models (one for each ED type) captured the relationship between $Th^{u,d}$ and $BL^{u,d}$ with $MOS_p^{u,d}$ (i.e., as a function of $f(Th^{u,d}, BL^{u,d})$).

The coefficients in the LR models represent the weights of the corresponding variables Th and BL in predicting the MOS for each ED. The BL 's impact using

the SPs is the most important, suggesting that the darkest level of BL would significantly decrease the MOS . However, the BL has a relevant impact also on the QoE perceived by users of TV and LP. In the case of the Th of the reproduced video, it has a significant impact only on the MOS of LP's users, whereas it is negligible for TVs and SPs. Additionally, the coefficient of the Th in the QoE model for SPs is negative, which can be attributed to SPs' relatively small screen sizes. According to the subjective tests conducted in [118], this type of user was not able to distinguish between the two reproduced video qualities (FHD and HD), providing slightly higher scores when watching HD videos.

8.2.2 QoE and Energy-Aware Resource Allocation Algorithm

Once the QoE models for each device d are obtained, we have implemented a heuristic solution to conduct the access network selection and optimize resource allocation in a 5G heterogeneous environment. To make the decision, we have defined a dimensionless SF ($SF_b^{u,d,t}$) that combines the $\Gamma^{u,d}$ and $MOS_p^{u,d}$ metrics for each $ED_{u,d}$. It is defined as

$$SF_b^{u,d,t} = w \times \Gamma^{u,d,Norm} + (1 - w) \times MOS_p^{u,d,Norm}, \quad (8.5)$$

where w adjusts the importance given to the electricity consumption (Γ) and QoE ($MOS_p^{u,d}$). The $\Gamma_{u,d}$ and $MOS_p^{u,d}$ metrics have different units of magnitude that make a fair comparison impossible [30]. Therefore, we normalized them to ensure their proportional contribution to the $SF_b^{u,d,t}$, adjusting its value between 0 and 1 ($SF_b^{u,d,t} \in [0, 1]$). The $MOS_p^{u,d,Norm}$ and $\Gamma^{u,d,Norm}$ are obtained based on the equations 3.9 and 3.10, respectively.

At each TTI t , the system detects if there are new EDs in the network. Then, it is executed an iterative process to associate such new devices with the BS or AP that guarantees the highest $SF_b^{u,d,t}$. Moreover, at each TTI t , if the system detects a variation in the reception conditions (i.e., $CQI_b^{u,d,t}$ feedback) of a current $ED_{u,d}$ in the network, the algorithm is re-executed. As a consequence, to maximize the $SF_b^{u,d,t}$, the device could be changed to a new BS (i.e., the handover process), or it could be updated the MCS and corresponding $RB_b^{u,d,t}$ in the current BS. The network selection and handover processes rely on more than a resource availability perspective. We consider the network and user sides, combining the QoE and Γ metrics as the decision criteria factors.

The algorithm can be formulated as a long-term utility optimization problem to maximize the $SF_b^{u,d,t}$, $\forall u \in \mathbb{U}$

$$\max \sum_t \sum_u SF_b^{u,d,t} \quad (8.6a)$$

$$s.t. Th_b^{u,d,t} \geq Th^{d,min}, \quad (8.6b)$$

where $Th^{d,min}$ is the lowest Th according to device type d (Table 8.1).

Parameter	Value
Number of BSs/APs	1/2
BS/AP Operating frequency (GHz)	28 [120, 156]
BS/AP Bandwidth (MHz)	400
NR numerology, μ	3
RB's bandwidth (MHz)	1.44
Subcarrier spacing (kHz)	120
Transmission power BS/AP (dBm)	40/26
Power spectral density of noise (dBm/Hz)	-174
Height BS/AP (m)	10/4
Small/large-scale fading models	[139]
Dynamic line of sight	Yes
Number of EDs	100
Type of EDs	TV, LP, SP
Height of EDs (m)	1.5
Mobility Model TV/LP/SP	Static/Static/Random directional [139]
Reception mode TV/LP/SP	Indoor/Indoor-Outdoor/Indoor-Outdoor
SP' speed (m/s)	0-0.8
Video resolution TV/LP/SP	FHD-4K/HD-FHD/HD-FHD
Th^{min} - Th^{max} TV/LP/SP (Mbps)	5-20/2-5/2-5
BL TV/LP/SP (lx)	300-5500/400-4000/200-5000

Table 8.2: Main simulation parameters.

8.3 Performance Evaluation

This Section presents our proposal assessment and analysis through simulation results of a recreated 5G HetNet when delivering a video service to multiple types of EDs. The simulations were carried out using an ad-hoc 5G LLS [139] developed in Python. The first Subsection details the simulation settings and considerations. Then, we present the achieved results and the corresponding analysis.

8.3.1 Simulation Settings

We recreate a 5G HetNet composed of one outdoor NR micro-BS and two indoor NR APs. We define a maximum of 100 connected EDs receiving and displaying a particular video service. Table 8.2 summarizes the main simulation parameters. While we consider this specific setting, the proposed system can be successfully applied with other network configurations.

During our simulations, we evaluate two particular scenarios that are described as follows:

- Scenario A: The 100 % of the EDs are assumed as TVs, LPs, or SPs to ana-

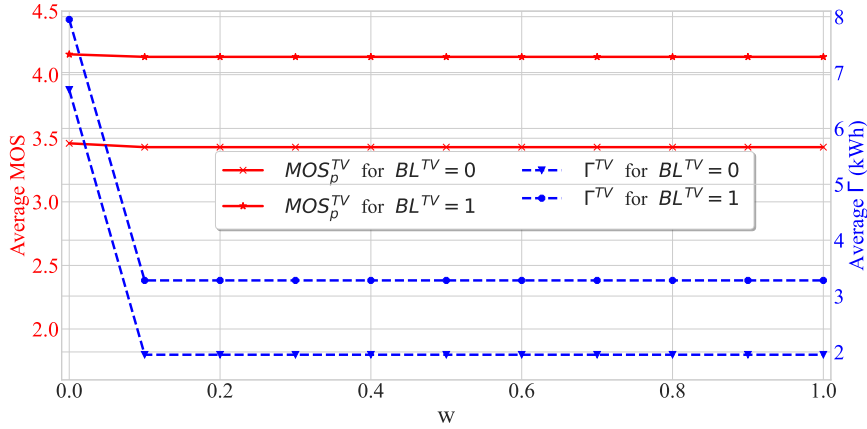


Figure 8.2: Average MOS_p^{TV} and Γ^{TV} for highest SF^{TV} and different w values.

lyze their independent behavior and impact regarding the SF considerations. Different BL configurations are evaluated.

- Scenario B: The 75 % of the EDs are SPs, and the remainder 25 % are randomly distributed between TVs and LPs. The BL is randomly assumed. This setting is oriented to assess the impact regarding the SF considerations of a heterogeneous distribution of EDs. In this case, the results were achieved by averaging 30 simulation runs to ensure a 95 % CV.

8.3.2 Results and Analysis

This Subsection presents the results and corresponding analysis of each described scenario.

Scenario A Results

Figs. 8.2, 8.3, and 8.4 show the trade-off between $MOS_p^{u,d}$ and $\Gamma^{u,d}$ for different w values. The results display the achieved $MOS_p^{u,d}$ and $\Gamma^{u,d}$ average values that maximize the $SF_b^{u,d}$ and consequently equation (8.6) for TVs, SPs, and LPs, separately. As mentioned in Section 8.1, note that $BL = 0$ and $BL = 1$ as a simple notation to indicate the darkest and the brightest values of BL set on the respective ED, whose actual BL values are reported in Table 8.2.

Particularly, Fig. 8.2 illustrates the case where all EDs are TVs. As we explained in Subsection 8.2.1, the $MOS_p^{u,TV}$ is basically determined by the BL because the Th has a minimal contribution (due to the weight coefficient value in equation (8.2)). On the contrary, a variation in $Th^{u,TV}$ directly impacts $\Gamma^{u,TV}$ because of the large difference in data traffic required by 4K compared to FHD videos. As Fig. 8.2 shows, only for $w = 0$ the MOS is prioritized, and the highest $SF_b^{u,TV}$ is reached with

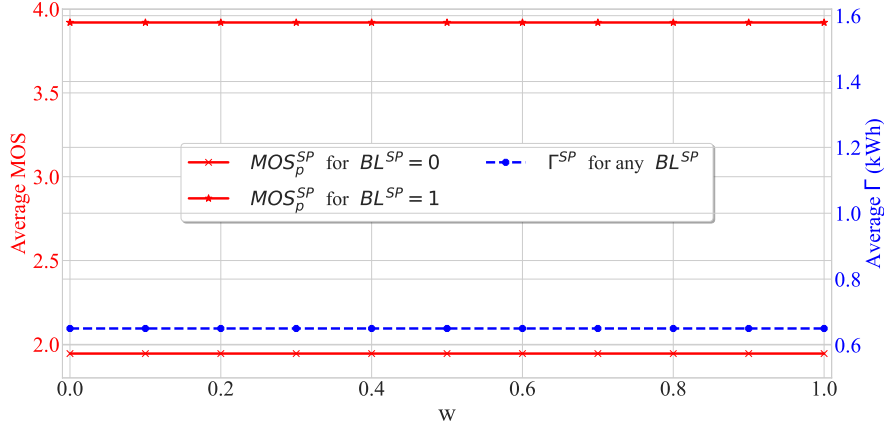


Figure 8.3: Average MOS_p^{SP} and Γ^{SP} for highest SF^{SP} and different w values.

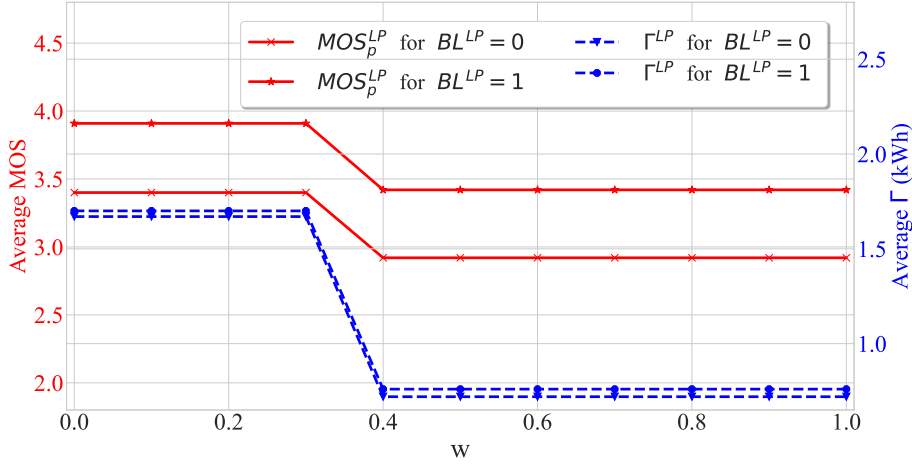


Figure 8.4: Average MOS_p^{LP} and Γ^{LP} for highest SF^{LP} and different w values.

$Th^{TV,max}$, $MOS^{TV,max}$ and $\Gamma^{TV,max}$. Then, for any $w > 0$, the $SF_b^{u,TV}$ is optimized reducing the $Th_b^{u,TV}$ and as consequence $\Gamma^{u,TV}$ and $MOS_p^{u,TV}$ values. From the $MOS_p^{u,TV}$ perspective, the reduction of the $Th^{u,TV}$ from 4K to FHD involves an insignificant MOS reduction, whereas it saves network resources and significantly decreases electricity consumption (more than halved). Setting the TV's BL from the brightest to the darkest level slightly reduces the QoE (half point of MOS) and the Γ .

Fig. 8.3 shows the result where all considered EDs are SPs. In this case, the Th also has a very small contribution to the $MOS_p^{u,SP}$, but the weight coefficient is negative, as we explained in Section 8.2.1. Then, even with $w = 0$, the highest $SF_b^{u,SP}$ is obtained with $\Gamma^{TV,min}$, $Th^{SP,min}$, and $MOS^{SP,max}$ for any $BL^{u,SP}$ configuration. It means that according to the defined QoE model for SPs in the specific

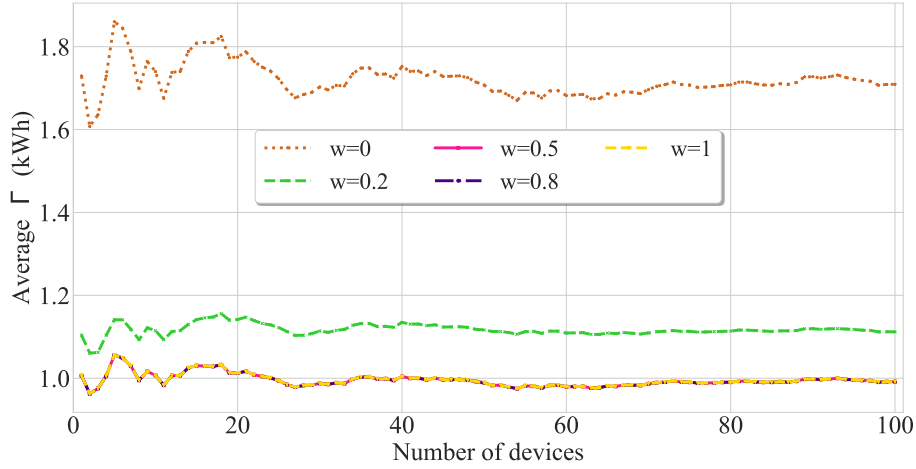


Figure 8.5: Average Γ for different numbers of EDs in the network.

recreated conditions, the optimization process always assumes a green profile. Thus, there is no need for green users to set the SP's BL from the brightest to the darkest level because this would totally decrease the MOS (from good to poor) with no electricity reduction.

On the other hand, Fig. 8.4 evidences how the Th and BL have a comparable impact on the $MOS_{u,LP}^p$, as a consequence of the QoE model presented for LPs. Specifically, for $w < 0.4$, the highest $SF_b^{u,SP}$ is achieved with $Th^{TV,max}$ and $MOS^{LP,max}$ at the expense of increasing the electricity consumption ($\Gamma^{LP,max}$). However, green users can decide to make a sacrifice in QoE (half point of MOS) to save a significant amount of energy (reduced by one-third when $w \geq 0.4$). This QoE sacrifice due to the video quality reduction would be more tolerable when the LP's BL is set to the brightest level ($3.5 < MOS \leq 4$) than to the darkest level ($3 \leq MOS \leq 3.5$).

Scenario B Results

Fig. 8.5 shows the average $\Gamma^{u,d}$ for different numbers of EDs in the network. As expected from the previous graphs, the algorithm employing $w = 0$ prioritizes the MOS , causing an increment in electricity consumption. However, Fig. 8.6 evidences that the increment in $\Gamma^{u,d}$ for $w = 0$ is not justified due to the difference in the average $MOS_p^{u,d}$ regarding $w = 0.2$ being very small. Moreover, as we presented in Figs. 8.2, 8.3 and 8.4, for $w > 0$ in the case of SPs and TVs, and for $w \geq 0.4$ in the case of LP, the $SF^{u,d}$ optimization is achieved minimizing $\Gamma^{u,d}$. Then, the resulting average $MOS_p^{u,d}$ values for the represented $w = \{0.5, 0.8, 1\}$ are less than the values observed for $w = \{0, 0.2\}$. Again, this result demonstrates how the users could opt to slightly sacrifice their own QoE to save electricity consumption.

Finally, Fig. 8.7 and 8.8 show the average ADR and $Th_{sat}^{u,d}$ for different numbers of EDs in the network. As we mentioned before, the $Th_{sat}^{u,d}$ is the ratio between

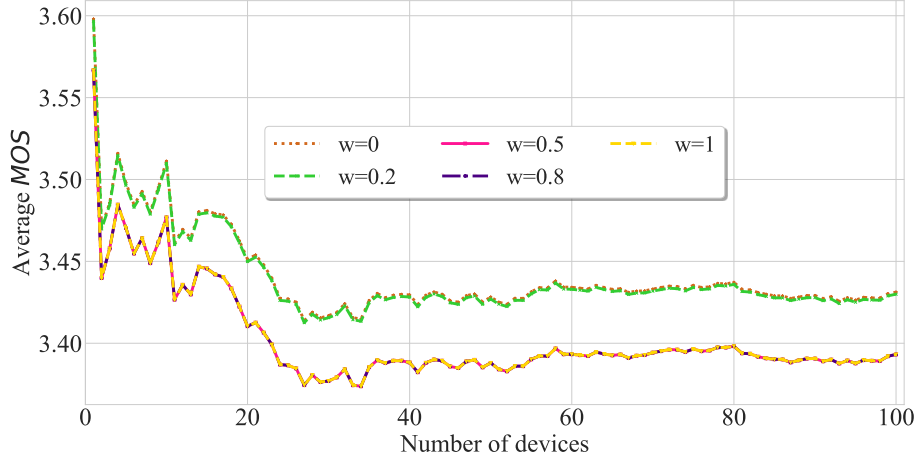


Figure 8.6: Average MOS for different a number of EDs in the network.

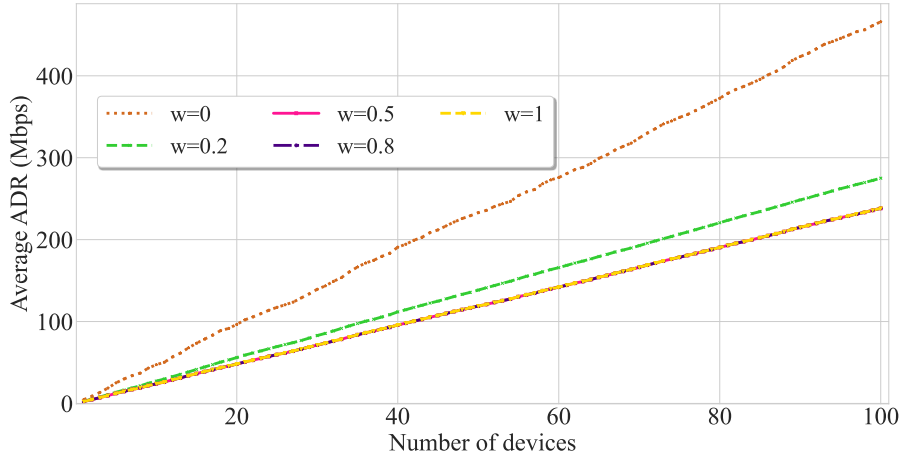


Figure 8.7: Average ADR for a different number of EDs in the network.

the assigned $Th^{u,d}$ and the $Th^{d,max}$ corresponding to the highest video resolution defined for ED_d . Then, $Th_{sat}^{u,d} = 1$ means that the network assigns to the ED_d the $Th^{d,max}$. For the recreated conditions, with $w = 0$, the average ADR presents the highest values for an incremental number of EDs, and a reduction of the ADR value of 49 % for $w = \{0.5, 0.8, 1\}$ and 100 EDs in the network. However, even with $w = 0$, $Th_{sat}^{u,d} < 0.57$ along the simulation. If we analyzed this result alone, just taking into account the Th_{sat} , it seems to be a drawback of the proposed algorithm. However, analyzing all the figures as a whole, we demonstrate that decreasing the overall $Th^{u,d}$ reduces the $Th_{sat}^{u,d}$ but it does not considerably affect the perceived QoE while saving energy and radio resources. For example, for a TV with reception conditions of $CQI^{u,TV} = 9$, the number of required RBs to achieve the $Th^{TV,max} = 20$ Mbps is $RB_b^{u,TV} = 4$, whereas for $Th^{TV,min} = 5$ Mbps is $RB_b^{u,TV} = 1$.

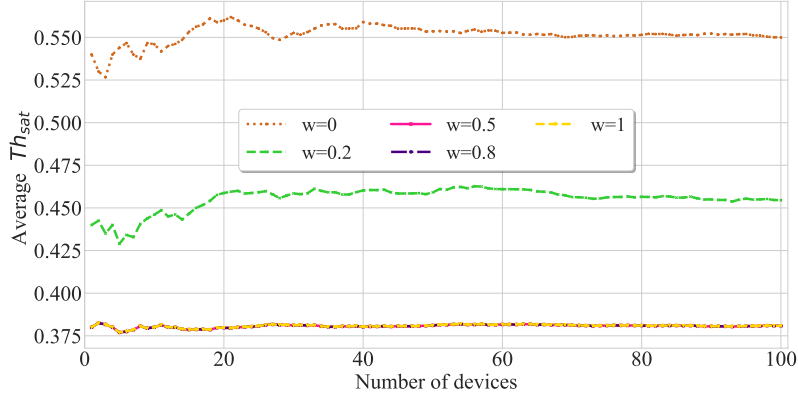


Figure 8.8: Average Th_{sat} for a different number of EDs in the network.

As demonstrated, for any considered device and $w \geq 0.4$, the $SF^{u,d}$ is optimized, minimizing $\Gamma^{u,d}$ and reducing the number of needed RBs. These released resources could be used to serve new EDs or enrich the QoE of impaired ones. For example, for the specific recreated conditions with 100 EDs in the network, using $w \geq 0.4$ reduces in 22 % the number of RBs required concerning $w = 0$. Moreover, the results demonstrated that a variation in the $Th^{u,d}$ for SPs and TVs has a very small contribution to the $MOS^{u,d}$. Nevertheless, in the case of LPs, we must manage w regarding the client's expectations and the sustainability profile they choose to follow. Then, the proposed resource allocation process is an integral solution that ensures an adequate overall QoE being aware of the electricity consumption.

8.4 Conclusion

This Chapter presents a heuristic solution to dynamically allocate resources in a 5G HetNet scenario driven by the compromise between the overall energy consumed by the E2E network infrastructure and the EDs' QoE. We based on the fact that the allocation of additional network resources does not always increase the perceived quality but it often consumes more energy. To validate the proposed solution, we set a simulation scenario involving a 5G HetNet aimed to serve 100 different EDs with diverse mobility behaviors. We defined proper QoE and energy consumption models (as a function of the Th and the device's level of BL) for each ED type. We defined a SF and conducted several simulation runs, assigning different levels of importance w to MOS and Γ variables.

When all EDs are assumed to be of the same type, we achieve different results depending on the specific QoE model. For TVs, reducing the Th implies a negligible decrease in the user's QoE, but Γ is more than halved. For SPs, the same energy level is consumed regardless of the Th and BL values, as we can observe in Table 8.1.

However, the darkest level of BL on the SP considerably reduces the QoE, which allows users with SP to be green even by setting the brightest BL . For LPs, the choice to be green is left to the user because they can decide to make a sacrifice in QoE (half point of MOS) to reduce Γ by one-third.

When simulating different EDs together (75 % SPs, 25 % between TVs and LPs), we found that a huge reduction in Γ corresponds to a tiny decrease in QoE. Specifically, by setting $w = 0.2$, the Γ is almost halved with no noticeable MOS reduction, whereas with $w = 0.5$, Γ is more than halved with slight QoE reduction (0.15 of MOS). The results are partly driven by the considered subjective data and EDs types. However, the proposed solution remains valid even with diverse and updated QoE and energy consumption models, which are currently missing in the literature.

Chapter 9

Conclusions and Future Works

9.1 Conclusions and Remarks

In line with the scaled commercial roll-out of 5G networks, the research community and the industry have begun delving into the 5G-Advanced development and the upcoming 6G. The envisioned B5G era will represent a complete paradigm shift for global communications, merging the physical, digital, and virtual worlds. It will offer unprecedented breakthroughs in media service delivery with challenging use cases and stringent QoS and QoE requirements.

In the envisioned ultra-dense B5G heterogeneous environment, multiple types of EDs with diverse tariff plans and mobility behaviors can request several applications with different requirements. Then, numerous and diverse EDs compete for finite resources, making critical a dynamic and effective RRM process. In this highly complex environment, differentiated traffic management must leverage the slicing paradigm over a softwarized framework, where decentralized and intelligent solutions must be correctly designed to reduce communication overhead and CC while preserving data privacy. On the other hand, future networks must exploit the MBS capabilities and the TNS-NTNs cooperation to achieve the ABC paradigm and optimize resource utilization.

Considering the aforementioned challenges, this Ph.D. study handled how multiple service requests in B5G HetNets can be effectively satisfied with adequate QoS and QoE. We presented diverse algorithms dealing with the network selection and slicing resource allocation processes over a heterogeneous and softwarized B5G system. Chapter 4 presented a heuristic solution based on MADM and focused on optimizing QoS metrics such as throughput, delay, and energy consumption. Moreover, this algorithm considers multiple EDs, tariff plans, and mobility behaviors. Particularly, the solution proposed in Chapter 5 is an extension of the previous Chapter, demonstrating the resource allocation improvement utilizing airborne nodes to assist the terrestrial infrastructure and exploiting the MBS capabilities.

Further, Chapter 6 presented a F-DRL solution integrated into the O-RAN archi-

ture to deal with the network selection and slicing allocation over diverse network conditions. We demonstrated that the proposed ML algorithm behaves similarly to the heuristic solution, effectively maximizing the QoS of multiple EDs. On the other hand, this solution guarantees to reduce the CC and communication overhead and enhance data privacy regarding the heuristic and traditional ML approaches (e.g., centralized DRL). Additionally, Chapter 7 analyzed how, by inserting into this solution the MBS capabilities, we can considerably save network resources and satisfy multiple concurrent EDs with adequate QoS. The above-presented solutions (i.e., Chapters 4- 7) dealt with overload situations employing CGT to adapt the network resources on-demand and satisfy numerous EDs at least with the minimum QoS requirements according to the application and user profiles.

Finally, Chapter 8 moved forward to a user-centric approach instead of only considering QoS as the optimization target. In this case, we proposed a dynamic RRM algorithm to analyze the trade-off between maximizing QoE and reducing electricity consumption over a HetNet environment. We conducted several simulations, considering diverse types of EDs with different mobility behaviors and requesting video streaming applications. Our findings demonstrated that allocating additional RBs to ensure the maximum throughput does not always increase the perceived QoE. Still, it often consumes more electricity and increases the risk of overloading.

In general, this Ph.D. study presented several dynamic RRM algorithms to satisfy multiple service requests with the ABC paradigm, aided by the TN-NTN integration, network slicing, MBS capabilities, and the O-RAN framework. We proved the importance of distributed ML solutions to make dynamic decisions with reduced CC and adequate performance. Specifically, F-DRL also reduces the risks of privacy issues. Moreover, we analyzed the importance of moving forward to a user-centric approach, jointly optimizing user perception (QoE) and QoS metrics with efficient resource usage. This research contributes to paving the way toward differentiated traffic management in B5G heterogeneous systems.

9.2 Future Works

After finishing this manuscript, several possible improvements and unsolved tasks must be conducted as future works to properly manage the identified critical challenges B5G networks. In the following, we specify our primary future works under discussion:

- Our simulations were mainly oriented to recreate heterogeneous B5G networks composed of terrestrial and airborne BSs. However, to truly analyze the 3D ecosystem over the envisioned future networks and the impact of TNs-NTNs cooperation at different altitudes, we must include in the simulations the satellite links (e.g., LEO constellations). In such a context, we must improve the capabilities of our LLS developed in Python [139] to make it more usable

and scalable. Moreover, we must analyze new B5G use cases, such as service delivery in remote areas where the NTN play a critical role.

- Regarding the proposed F-DRL algorithm (Chapter 6), future steps must consider the possible particularities of the envisioned heterogeneous B5G networks, evolving our solution to find a better balance between algorithm performance, generalization capability, and complexity. Specifically, our analysis must include the impact of additional spatial/physical input variables (e.g., BS type, size, mobility information, propagation losses) to better address the diversity among BSs (e.g., ground, airborne, and satellite nodes). Then, we must go deep inside into the impact of the dynamic and heterogeneous nature of the local agents on the F-DRL framework. Additionally, we must investigate possible synchronization issues when collecting/processing ML parameters from nodes at different altitudes.
- The MBS capability integrated into Chapter 7 is based on the traditional conventional multicast scheme (CMS), where the resource allocation process depends on the user with the worst reception conditions. Future works could be oriented to improve this solution with multicast subgrouping techniques and non-orthogonal multiple access (NOMA) [52, 69, 157] to better exploit the multicasting gain and multiuser diversity.
- Chapter 8 presented a RRM algorithm that combine the QoE and electricity consumption metrics. We employed three QoE models, one for each considered ED type. These QoE models are obtained based on subjective tests. Even if this kind of assessment guarantees a more reliable QoE prediction than objective techniques because users provide their experience directly, these methods are costly, time-consuming, and can only be conducted offline [158]. On the other hand, the reliability of the subjective tests relies on the number of participants and their diversity.

In general, due to the accelerated growth of diverse EDs, network states, and multimedia services, the QoE assessment has become increasingly complicated, evidencing the limited scope of traditional QoE methods. To handle this, recent QoE management research efforts have been conducted based on ML to provide a dynamic and real-time optimization loop for adaptive streaming applications. ML allows the modeling of complex problems with high accuracy, such as quantifying the correlation between QoS and QoE. Then, future works must be oriented to obtain an ML-based QoE prediction model for video streaming applications, without presenting a separate solution for each specific ED. Moreover, we must analyze how to estimate the QoE only based on network parameters, which is the information accessible by the MNOs. Finally, the predicted QoE values can be used as the optimization function to make dynamic resource allocation decisions, maximizing the QoE instead of traditional RRM approaches only based on QoS.

Appendices

Appendix A

Main Mathematical Notations

Table A.1: Main mathematical notations.

Notation	Definition
$\mathbb{U}(u \in \{1, 2, \dots, U\})$	Set of U users
$d \in \{TV, LP, SS, SP\}$	Types of EDs
$p^u = \{1, 2\}$	Users' priority levels
$\mathbb{B}(b \in \{1, 2, \dots, B\})$	Set of B BSs
\mathbb{T}, \mathbb{N}	Sets of TNs and NTNs
$\mathbb{M}(m \in \{1, 2, \dots, M\})$	Set of M NSs
$\mathbb{L}(l \in \{1, 2, \dots, L\})$	Set of L services
SF_b^u	Score function to evaluate network conditions
$C_{b,m}^u$	Score value with overloading
$S_{b,m,o}^u$	Score value with enough resources
$UF_{m,uf}^u, w_{m,uf}^u$	Utility function for each sensitive attribute and corresponding weight
UF^{up}, UF^{down}	Utility function upward, downward criteria
$Th_{b,m}^u, D_{b,m}^u, EC_{b,m}^u, J_{b,m}^u, PLR_{b,m}^u$	Throughput, delay, energy consumption, jitter, packet loss ratio
$D_{b,m}^{u,Tx}, D_{b,m}^{u,Q}$	Transmission and queuing delay
P^u	Power consumption
$w_{Th}, w_D, w_{Ec}, w_J, w_{PLR}$	Weight values for Th, D, Ec, J , and PLR
$\Gamma^{u,d}$	Overall electricity consumption (from the data center to the ED) to stream the video service
$MOS^{u,d}$	QoE perceived for each ED
ψ_m^b	Availability of resources in the BS_b
κ_m^b	Accessibility of the NS_m in the BS_b
St_m^b	NS_m state in the BS_b
$RB_{b,m}^u$	Number of assigned RBs

Notation	Definition
f_b	BS_b 's operating frequency
Δf	Subcarrier spacing value
μ	Numerology
e_{ffb}^u	Efficiency of a user regarding the BS_b
RB_b^{av}	Available RBs in the BS_b
BW_{RB_b}	Bandwidth of the RB
P_{RB_b}	Potential release resources
$Th_{sat,b}^u$	Throughput satisfaction
$I^{u,t}$	SLA satisfaction indicator
SD_b^u	Satisfaction degree
$w_{PRB}, w_{Th_{sat}}$	Weight values for $Th_{sat,b}^u$ and P_{RB_b}
\mathbb{P}, \mathbb{P}^*	Set of players of GT, and subset from \mathbb{P}
C_{min}	Minimal winning coalition
$RB_{release}^C$	Resources that coalition C can release
RB_{pot}^u	Resources that UE_u can release
$\nu(C)$	Coalition's characteristic function
U_{aff}	Affected users at each saturation point
\mathfrak{a}	Residual value of Ths after releasing resources
ξ	Residual value of RBs after releasing resources
\wp^u	Service request
Θ	Total requested services
$\varrho_{m,o}^u$	the priority value of the requested NS_m by the UE_u
$\varkappa_{b,m}^u$	Historical association with the NS_m via BS_b
$BL_{u,d}$	Backlight luminance level set on the $ED_{u,d}$
$t' \in \{1, 2, \dots, T'\}$	Decision intervals
E, T, H	Total events, TTIs and episodes
f', F'	Time period and number of federated episodes
$\langle S, \mathcal{A}, \mathcal{R} \rangle$	Tuple of state, action, and reward
$s_{b,e}^t, a_{b,e}^{u,t}, rw_{b,e}^{u,t}$	State, action and reward for event e in the TTI t
$Q(s, a, \theta), \tilde{Q}(s, a, \theta^-)$	Main and target neural networks (NNs)-based function
$\theta^{g,t'}, \theta^{b,t'}$	Parameters of ML Global and Local Models
$y_{b,e}^t$	Target value for each ML Local Model
$ \mathcal{K} , \mathcal{B} $	Mini-batch size, buffer size
$ \mathcal{B} $	Buffer size
$\Xi_{b,e}^t$	Experiences to store in the buffer \mathcal{B}
γ	Discount factor
$\varepsilon - decay$	Epsilon-decay strategy
τ	Target-network's updating rate
α	Learning rate

Notation	Definition
β_1, β_2	Exponential decay rates
$\mathcal{L}_G(\theta^g), \mathcal{L}_b(\theta^b)$	Loss functions (ML Global, Local Models)
X	Number of NN's layers
Ω_x	Number of neurons in the x -th layer

Appendix B

Publications

B.1 Directly Related to the Thesis

- **C. C. González**, E. F. Pupo, L. Atzori and M. Murrone, “Dynamic access control and slice allocation algorithm for diverse traffic demand over 5G heterogeneous networks,” 2021 IEEE International Symposium on Broadband Multimedia Systems and Broadcasting (BMSB), Chengdu, China, 2021, pp. 1-6, doi: 10.1109/BMSB53066.2021.9547129 [39].
- **C. C. González**, E. F. Pupo, L. Atzori and M. Murrone, “Dynamic Radio Access Selection and Slice Allocation for Differentiated Traffic Management on Future Mobile Networks,” in IEEE Transactions on Network and Service Management, vol. 19, no. 3, pp. 1965-1981, Sept. 2022, doi: 10.1109/TNSM.2022.3150978 [30].
- **C. C. González**, E. F. Pupo, D. Pereira-Ruisánchez, L. Atzori and M. Murrone, “Deep Reinforcement Learning for Dynamic Radio Access Selection over Future Wireless Networks,” 2022 IEEE International Symposium on Broadband Multimedia Systems and Broadcasting (BMSB), Bilbao, Spain, 2022, pp. 1-6, doi: 10.1109/BMSB55706.2022.9828746 [41].
- **C. C. González**, S. Pizzi, M. Murrone and G. Araniti, “Multicasting Over 6G Non-Terrestrial Networks: A Softwarization-Based Approach,” in IEEE Vehicular Technology Magazine, vol. 18, no. 1, pp. 91-99, March 2023, doi: 10.1109/MVT.2022.3232919 [15].
- **C. C. González**, E. F. Pupo, J. Montalban, S. Pizzi, E. Iradier and M. Murrone, “Hybrid Terrestrial-Airborne Connectivity for Unicast/Broadcast Services Beyond 5G,” 2023 IEEE International Symposium on Broadband Multimedia Systems and Broadcasting (BMSB), Beijing, China, 2023, pp. 1-6, doi: 10.1109/BMSB58369.2023.10211608 [19].

- **C. C. González**, E. F. Pupo, E. Iradier, P. Angueira, M. Murrioni and J. Montalban, “Network Selection over 5G-Advanced Heterogeneous Networks Based on Federated Learning and Cooperative Game Theory,” in *IEEE Transactions on Vehicular Technology*, 2024, doi: 10.1109/TVT.2024.3373638 [2].
- **C. C. González**, and M. Murrioni, “Smart radio access selection and slice allocation for differentiated traffic management over 6G heterogeneous networks,” In *Proceedings of the 15th ACM Multimedia Systems Conference*, 2024, pp. 527-53 [27].
- **C. C. González**, E. F. Pupo, J. Montalban, E. Iradier, P. Angueira, and M. Murrioni, “Federated Learning-based Unicast/Multicast Service Delivery over 6G O-RAN Framework,” 2024 *IEEE International Symposium on Broadband Multimedia Systems and Broadcasting (BMSB)*, Toronto, Canada, 2024, pp. 1-6 [40].
- **C. C. González**, E. F. Pupo, G. Bingol, A. Floris, S. Porcu, M. Murrioni, and L. Atzori, “A QoE-based Energy-aware Resource Allocation Solution for 5G Heterogeneous Networks,” 2024 *International Conference on Quality of Multimedia Experience (QoMEX’24)*, Karlshamn, Sweden, 2024, pp. 1-6 [42].

B.2 Other publications

- **C. C. González**, E. F. Pupo, D. P. Ruisánchez, D. Plets and M. Murrioni, “From MFN to SFN: Performance Prediction Through Machine Learning,” in *IEEE Transactions on Broadcasting*, vol. 68, no. 1, pp. 180-190, March 2022, doi: 10.1109/TBC.2021.3132804 [159].
- **C. C. González**, E. F. Pupo, D. P. Ruisánchez, D. Plets and M. Murrioni, “Three-stages concatenated Machine Learning model for SFN prediction,” 2021 *IEEE International Symposium on Broadband Multimedia Systems and Broadcasting (BMSB)*, Chengdu, China, 2021, pp. 1-6, doi: 10.1109/BMSB53066.2021.9547146 [160].
- E. F. Pupo, **C. C. González**, L. Atzori and M. Murrioni, “Thresholds of out-performance among Broadcast/Multicast access techniques in 5G networks,” 2021 *IEEE International Symposium on Broadband Multimedia Systems and Broadcasting (BMSB)*, Chengdu, China, 2021, pp. 1-6, doi: 10.1109/BMSB53066.2021.9547169 [161].
- D. P. Ruisánchez, D. G. Mirabal, E. F. Pupo, **C. C. González**, D. Pérez-Adán and F. A. Cesar, “Prediction of Signal Quality and SFN Interference Metrics Using Machine Learning Models,” 2021 *IEEE International Symposium on Broadband Multimedia Systems and Broadcasting (BMSB)*, Chengdu, China, 2021, pp. 1-6, doi: 10.1109/BMSB53066.2021.9547111 [162].

- E. F. Pupo, **C. C. González**, L. Atzori and M. Murrioni, “Dynamic Multicast Access Technique in SC-PTM 5G Networks: Subgrouping with OM/NOM,” 2022 IEEE International Symposium on Broadband Multimedia Systems and Broadcasting (BMSB), Bilbao, Spain, 2022, pp. 1-6, doi: 10.1109/BMSB55706.2022.9828674 [163].
- E. F. Pupo, **C. C. González**, Montalban, J., Angueira, P., Murrioni, M., & Iradier, E, ” Artificial Intelligence Aided Low Complexity RRM Algorithms for 5G-MBS,” in IEEE Transactions on Broadcasting, vol. 70, no. 1, pp. 110-122, March 2024, doi: 10.1109/TBC.2023.3311337 [52].
- E. F. Pupo, **C. C. González**, E. Iradier, J. Montalban, and M. Murrioni, “5G Link-Level Simulator for Multicast/Broadcast Services,” 2023 IEEE International Symposium on Broadband Multimedia Systems and Broadcasting (BMSB), Beijing, China, 2023, pp. 1-6, doi: 10.1109/BMSB58369.2023.10211507 [139].
- E. F. Pupo, **C. C. González**, V. Popescu, D. Giusto, and M. Murrioni, “Beyond 5G Multicast for XR Communications aided by Pre-computed Multi-beams and NOMA,” 2023 IEEE Globecom Workshops (GC Wkshps), Kuala Lumpur, Malaysia, 2023, pp. 738-743, doi: 10.1109/GCWkshps58843.2023.10465216 [23].
- E. F. Pupo, **C. C. González**, E. Iradier, J. Montalban, P. Angueira, and M. Murrioni (2023). “Dynamic Single/Multi-Rate Multicasting Aided NOMA for Addressing the Multiuser Diversity in 5G Networks”. TechRxiv. Preprint. <https://doi.org/10.36227/techrxiv.24312049.v1> [69].
- E. F. Pupo, **C. C. González**, E. Iradier, J. Montalban, P. Angueira, and M. Murrioni (2023). “Machine Learning-based Multicasting Radio Resource Management over 6G O-RAN Framework”. TechRxiv. Preprint. <https://doi.org/10.36227/techrxiv.24408250.v1> [6].
- E. F. Pupo, **C. C. González**, and M. Murrioni, “Multi-rate Multicasting Over Fixed Pre-Computed MIMO Beams,” 2024 IEEE International Symposium on Broadband Multimedia Systems and Broadcasting (BMSB), Toronto, Canada, 2024, pp. 1-6 [164].
- A. Collu, E. F. Pupo, **C. C. González**, and M. Murrioni, “Exploiting the benefits of in-band D2D communications for 5G-MBS use cases,” 2024 IEEE International Symposium on Broadband Multimedia Systems and Broadcasting (BMSB), Toronto, Canada, 2024, pp. 1-6 [165].

Appendix C

Bio

Claudia Carballo González (Student Member, IEEE) (claudia.carballogonz@unica.it) received a B.Sc. degree in Telecommunications and Electronics Engineering and an M.Sc. degree in Telecommunications and Telematics from the Havana University of Technologies in 2015 and 2020, respectively. She is a Ph.D. student at the Department of Electrical and Electronic Engineering (DIEE/UdR CNIT), University of Cagliari, Italy. Her research interests include future wireless networks, artificial intelligence, O-RAN, slicing, and multicast/broadcast.

Appendix D

Acronyms

3D	three-dimensional
3G	third-generation
3GPP	3 rd Generation Partnership Project
4G	fourth-generation
5G	fifth-generation
5GC	5G core network
6G	sixth-generation
2K	resolution of 2000 pixels
4K	resolution of 4000 pixels
8K	resolution of 8000 pixels
ABC	always best-connected
ADR	aggregated data rate
AGL	above ground level
AHP	analytical hierarchy process
AI	artificial intelligence
AP	access point
AR	augmented reality
B5G	beyond 5G

BER	bit error rate
BL	backlight luminance
BS	base station
CAN	candidate access network
CC	computational complexity
CDN	content delivery network
CGT	cooperative game theory
CI	confidence interval
CP	control plane
CMS	conventional multicast scheme
CPU	central processing unit
CQI	channel quality indicator
CU	central unit
CV	confidence value
DASA	Dynamic radio Access selection and Slice Allocation
DB Info	Database Information
DDQN	double deep Q-network
DRL	deep reinforcement learning
DU	distributed unit
E2E	end-to-end
ED	end device
eDRANS	enhanced Dynamic Radio Access Network Selection
eMBB	enhanced mobile broadband
EN-TV	enhanced television
F-DDQN	federated learning with DDQN
F-DRL	federated deep reinforcement learning

FedAvg	federated averaging
FeMBMS	further evolved multimedia broadcast multicast service
FHD	full high-definition
FIFO	First in, first out
FWA	fixed wireless access
GA	genetic algorithm
GC	grand coalition
GDPR	General Data Protection Regulation
GEO	geostationary Earth orbiting
GHG	greenhouse gas
GM	cloud gaming
gNB	gNodeB
GT	game theory
HAP	high-altitude platform
HetNet	ultra-dense heterogeneous network
HD	high-definition
ID	identification
IIoT	Industrial IoT
IMT	International Mobile Telecommunications
IoT	internet of things
KPI	key performance indicator
LEO	low Earth orbiting
LLS	link-level simulation
LP	laptop
LR	Linear Regression
MADM	multi-attribute decision-making

Max-SINR maximum SINR

MBS multicast/broadcast services

MCS modulation and coding scheme

MDP Markov decision process

MEC multi-access edge computing

MEO medium Earth orbiting

MG multicast group

MIMO multiple-input multiple-output

ML machine learning

mmWave millimeter-wave

MNO mobile network operator

MOS Mean Opinion Score

MSE mean squared error

Near-RT RIC Near-Real Time RIC

NFV network function virtualization

NG-RAN next-generation RAN

NN neural network

NOMA non-orthogonal multiple access

Non-RT RIC Non-Real Time RIC

NR new radio

NS network slice

NTN non-terrestrial network

O-CU Open-RAN central unit

O-DU Open-RAN distributed unit

O-RAN Open-RAN

O-RU Open-RAN radio unit

OFDM	orthogonal frequency-division multiplexing
PHY	physical
PS	primary service
QoE	quality of experience
QoS	quality of service
RAN	radio access network
Rel	Release
RB	resource block
ReLU	rectified linear unit
RIC	RAN Intelligent Controller
RL	reinforcement learning
RRC	radio resource control
RRM	radio resource management
RSS	received signal strength
RTT	round-trip-time
RU	radio unit
RWP	random way-point
SD	satisfaction degree
SDN	software-defined network
SF	score function
SGD	stochastic gradient descent
SINR	signal-to-interference-plus-noise ratio
SLA	service level agreement
SMO	Service Management and Orchestration
SN	sensor
SO	specific objective

SP	smartphone
SS	secondary service
SVM	support vector machine
Th	throughput
THz	terahertz
TN	terrestrial network
TOPSIS	technique for order preference by similarity to the ideal solution
TTI	transmission time interval
Tx	radio transmitter
TYDER	Traffic tYpe-based DifferEntiated Reputation
TV	televisor
UE	user equipment
UAV	unmanned aerial vehicle
UF	utility function
UP	user plane
VI	video
VMAF	video multimethod assessment fusion
VNF	virtual network function
VR	virtual reality
XR	extended reality
WB	web browsing
Wi-Fi	wireless fidelity
WLAN	wireless local area network

Bibliography

- [1] Ericsson. *Mobility report, forecasts*. www.ericsson.com/mobility-report. 2023.
- [2] C. C. González et al. “Network Selection over 5G-Advanced Heterogeneous Networks Based on Federated Learning and Cooperative Game Theory”. In: *IEEE Transactions on Vehicular Technology* 73.8 (2024), pp. 11862–11877.
- [3] X. Lin. “An overview of 5G Advanced evolution in 3GPP Release 18”. In: *IEEE Communications Standards Magazine* 6.3 (2022), pp. 77–83.
- [4] I. Rahman et al. “5G evolution toward 5G advanced: An overview of 3GPP releases 17 and 18”. In: *Ericsson Technology Review* 2021.14 (2021), pp. 2–12.
- [5] W. Chen et al. “5G-Advanced toward 6G: Past, present, and future”. In: *IEEE Journal on Selected Areas in Communications* 41.6 (2023), pp. 1592–1619.
- [6] E. F. Pupo et al. “Machine Learning-based Multicasting Radio Resource Management over 6G O-RAN Framework”. In: *Authorea Preprints* (2023).
- [7] R. Liu et al. “A Vision and An Evolutionary Framework for 6G: Scenarios, Capabilities and Enablers”. In: *arXiv preprint arXiv:2305.13887* (2023).
- [8] C.-X. Wang et al. “On the road to 6G: Visions, requirements, key technologies and testbeds”. In: *IEEE Communications Surveys & Tutorials* (2023).
- [9] M. Banafaa et al. “6G mobile communication technology: Requirements, targets, applications, challenges, advantages, and opportunities”. In: *Alexandria Engineering Journal* 64 (2023), pp. 245–274.
- [10] R. Chataut, M. Nankya, and R. Akl. “6G networks and the AI revolution—Exploring technologies, applications, and emerging challenges”. In: *Sensors* 24.6 (2024), p. 1888.
- [11] Z. Zhang et al. “6G wireless networks: Vision, requirements, architecture, and key technologies”. In: *IEEE vehicular technology magazine* 14.3 (2019), pp. 28–41.
- [12] S. Edirisinghe et al. “Recent development of emerging indoor wireless networks towards 6G”. In: *Network* 3.2 (2023), pp. 269–297.

- [13] R. Liu et al. “Beginning of the Journey Toward 6G: Vision and Framework”. In: *IEEE Communications Magazine* 61.10 (2023), pp. 8–9.
- [14] ITU. *Connect 2030 – An agenda to connect all to a better world*. 2024. URL: <https://www.itu.int/en/mediacentre/backgrounders/Pages/connect-2030-agenda> (visited on 09/02/2024).
- [15] C. C. González et al. “Multicasting Over 6G Non-Terrestrial Networks: A Softwarization-Based Approach”. In: *IEEE Vehicular Technology Magazine* 18.1 (2023), pp. 91–99.
- [16] M. M. Azari et al. “Evolution of non-terrestrial networks from 5G to 6G: A survey”. In: *IEEE communications surveys & tutorials* 24.4 (2022), pp. 2633–2672.
- [17] 3rd Generation Partnership Project. “3GPP TR 38.811 V15.4.0; Technical Specification Group Radio Access Network; Study on New Radio (NR) to support non-terrestrial networks (Release 15)”. In: (2020).
- [18] 3GPP. *3GPP TR 38.811 V15.0.0: Study on New Radio (NR) to support non-terrestrial networks (Release 15)*. Tech. rep. TR 38.811 V15.0.0. Accessed: September 30, 2024. 3GPP, 2018.
- [19] C. C. González et al. “Hybrid Terrestrial-Airborne Connectivity for Unicast/Broadcast Services Beyond 5G”. In: *2023 IEEE International Symposium on Broadband Multimedia Systems and Broadcasting (BMSB)*. IEEE, 2023, pp. 1–6.
- [20] 3GPP TR 38.821. “3rd Generation Partnership Project; Technical Specification Group Radio Access Network; Solutions for NR to support non-terrestrial networks (NTN) (Release 16), V16.2.0”. In: (2023).
- [21] R. Stuhlfauth. “5G Non-Terrestrial Networks Take Flight With New Radio and IoT Applications”. In: *Microwave Journal* 66.11 (2023).
- [22] B. Barritt and W. Eddy. “Service management & orchestration of 5G and 6G non-terrestrial networks”. In: *2022 IEEE Aerospace Conference (AERO)*. IEEE, 2022, pp. 1–11.
- [23] E. F. Pupo et al. “Beyond 5G Multicast for XR Communications aided by Pre-computed Multi-beams and NOMA”. In: *2023 IEEE Globecom Workshops (GC Wkshps)*. 2023, pp. 738–743.
- [24] V. K. Shrivastava, S. Baek, and Y. Baek. “5G evolution for multicast and broadcast services in 3GPP release 17”. In: *IEEE Communications Standards Magazine* 6.3 (2022), pp. 70–76.
- [25] N. Chukhno et al. “Approaching 6G Use Case Requirements with Multicasting”. In: *IEEE Communications Magazine* 61.5 (2023), pp. 144–150.
- [26] E. Fontes Pupo et al. “Multiuser Diversity Management for Multicast/Broadcast Services in 5G and Beyond Networks”. In: (2024).

- [27] C. C. González and M. Murrioni. “Smart radio access selection and slice allocation for differentiated traffic management over 6G heterogeneous networks”. In: *Proceedings of the 15th ACM Multimedia Systems Conference*. 2024, pp. 527–531.
- [28] A. S. Abdalla et al. “Toward next generation open radio access networks: What O-RAN can and cannot do!” In: *IEEE Network* 36.6 (2022), pp. 206–213.
- [29] M. Polese et al. “Understanding O-RAN: Architecture, interfaces, algorithms, security, and research challenges”. In: *IEEE Communications Surveys & Tutorials* (2023).
- [30] C. C. González et al. “Dynamic Radio Access Selection and Slice Allocation for Differentiated Traffic Management on Future Mobile Networks”. In: *IEEE Transactions on Network and Service Management* 19.3 (2022), pp. 1965–1981.
- [31] J. Wang et al. “Artificial Intelligence-Assisted Network Slicing: Network Assurance and Service Provisioning in 6G”. In: *IEEE Vehicular Technology Magazine* (2023).
- [32] A. Filali et al. “Multi-Access Edge Computing: A Survey”. In: *IEEE Access* 8 (2020), pp. 197017–197046.
- [33] T. Wang, X. Cao, and S. Wang. “Hierarchical Slicing: A New Paradigm of Radio Resource Management for Mobile Networks”. In: *IEEE Network* (2023).
- [34] ETSI. “ETSI EG 202 V1.3.1 (2015-07), Quality of Telecom Services, Part 3: Template for Service Level Agreements (SLA). Technical Specification”. In: (2015).
- [35] M. Xu et al. “A full dive into realizing the edge-enabled metaverse: Visions, enabling technologies, and challenges”. In: *IEEE Communications Surveys & Tutorials* (2022).
- [36] M. Ali et al. “Metaverse Communications, Networking, Security, and Applications: Research Issues, State-of-the-Art, and Future Directions”. In: *arXiv preprint arXiv:2212.13993* (2022).
- [37] S. Suyama et al. “A study on extreme wideband 6G radio access technologies for achieving 100 Gbps data rate in higher frequency bands”. In: *IEICE Transactions on Communications* 104.9 (2021), pp. 992–999.
- [38] M. V. Katwe et al. “CmWave and Sub-THz: Key Radio Enablers and Complementary Spectrum for 6G”. In: *arXiv preprint arXiv:2406.18391* (2024).

- [39] C. C. González et al. “Dynamic access control and slice allocation algorithm for diverse traffic demand over 5G heterogeneous networks”. In: *2021 IEEE International Symposium on Broadband Multimedia Systems and Broadcasting (BMSB)*. IEEE. 2021, pp. 1–6.
- [40] C. C. González et al. “Federated Learning-based Unicast/Multicast Service Delivery over 6G O-RAN Framework”. In: *2024 IEEE International Symposium on Broadband Multimedia Systems and Broadcasting (BMSB)*. 2024, pp. 1–6.
- [41] C. C. González et al. “Deep Reinforcement Learning for Dynamic Radio Access Selection over Future Wireless Networks”. In: *2022 IEEE International Symposium on Broadband Multimedia Systems and Broadcasting (BMSB)*. IEEE. 2022, pp. 1–6.
- [42] C. C. González et al. “A QoE-based Energy-aware Resource Allocation Solution for 5G Heterogeneous Networks”. In: *2024 16th International Conference on Quality of Multimedia Experience (QoMEX)*. 2024, pp. 29–35.
- [43] A. A. Barakabitze et al. “5G network slicing using SDN and NFV: A survey of taxonomy, architectures and future challenges”. In: *Computer Networks* 167 (2020), p. 106984.
- [44] T. Taleb et al. “On multi-domain network slicing orchestration architecture and federated resource control”. In: *IEEE Network* 33.5 (2019), pp. 242–252.
- [45] Z. Shu and T. Taleb. “A novel QoS framework for network slicing in 5G and beyond networks based on SDN and NFV”. In: *IEEE Network* 34.3 (2020), pp. 256–263.
- [46] F. Z. Yousaf et al. “Network slicing with flexible mobility and QoS/QoE support for 5G Networks”. In: *2017 IEEE International Conference on Communications Workshops (ICC Workshops)*. IEEE. 2017, pp. 1195–1201.
- [47] T. Ahmed et al. “On-demand network slicing using SDN/NFV-enabled satellite ground segment systems”. In: *2018 4th IEEE conference on network softwarization and workshops (NetSoft)*. ieee. 2018, pp. 242–246.
- [48] M. Chahbar et al. “A comprehensive survey on the E2E 5G network slicing model”. In: *IEEE Transactions on Network and Service Management* 18.1 (2020), pp. 49–62.
- [49] K. Park et al. “Technology trends and challenges in SDN and service assurance for end-to-end network slicing”. In: *Computer Networks* (2023), p. 109908.
- [50] O-RAN Alliance. “O-RAN.WG1.Use-Cases-Analysis-Report-R003-v10.00”. In: *O-RAN Working Group 1 (Use Cases and Overall Architecture)* (2023).
- [51] S. D’Oro et al. “dApps: Distributed applications for real-time inference and control in O-RAN”. In: *IEEE Communications Magazine* 60.11 (2022), pp. 52–58.

- [52] E. F. Pupo et al. “Artificial Intelligence Aided Low Complexity RRM Algorithms for 5G-MBS”. In: *IEEE Transactions on Broadcasting* (2023).
- [53] B. Agarwal et al. “A Comprehensive Survey on Radio Resource Management in 5G HetNets: Current Solutions, Future Trends and Open Issues”. In: *IEEE Communications Surveys & Tutorials* (2022).
- [54] C. Desogus et al. “A traffic type-based differentiated reputation algorithm for radio resource allocation during multi-service content delivery in 5G heterogeneous scenarios”. In: *IEEE Access* 7 (2019), pp. 27720–27735.
- [55] J. Montalban, G.-M. Muntean, and P. Angueira. “A utility-based framework for performance and energy-aware convergence in 5G heterogeneous network environments”. In: *IEEE Transactions on Broadcasting* 66.2 (2020), pp. 589–599.
- [56] I. Mashal et al. “A multi-criteria analysis for an Internet of Things application recommendation system”. In: *Technology in Society* 60 (2020), p. 101216.
- [57] R. V. Rosa and C. E. Rothenberg. “The pandora of network slicing: A multicriteria analysis”. In: *Transactions on Emerging Telecommunications Technologies* 31.1 (2020), e3651.
- [58] B. Bakmaz, Z. Bojkovic, and M. Bakmaz. “TOPSIS-based approach for network slice selection in 5G mobile systems”. In: *International Journal of Communication Systems* 33.11 (2020), e4395.
- [59] D. L. Olson. “Comparison of weights in TOPSIS models”. In: *Mathematical and Computer Modelling* 40.7-8 (2004), pp. 721–727.
- [60] G. Zhao et al. “Network slice selection in softwarization-based mobile networks”. In: *Transactions on Emerging Telecommunications Technologies* 31.1 (2020), e3617.
- [61] D. Whitley. “A genetic algorithm tutorial”. In: *Statistics and computing* 4 (1994), pp. 65–85.
- [62] A. Ahmed, L. M. Boulahia, and D. Gaiti. “Enabling vertical handover decisions in heterogeneous wireless networks: A state-of-the-art and a classification”. In: *IEEE Communications Surveys & Tutorials* 16.2 (2013), pp. 776–811.
- [63] A. Vince. “A framework for the greedy algorithm”. In: *Discrete Applied Mathematics* 121.1-3 (2002), pp. 247–260.
- [64] J. Montalban et al. “Broadcast core-network: Converging broadcasting with the connected world”. In: *IEEE Transactions on Broadcasting* 67.3 (2021), pp. 558–569.
- [65] G. Araniti et al. “A hybrid unicast-multicast network selection for video deliveries in dense heterogeneous network environments”. In: *IEEE Transactions on Broadcasting* 65.1 (2018), pp. 83–93.

- [66] I. Khalid et al. “An adaptive MBSFN resource allocation algorithm for multicast and unicast traffic”. In: *2023 IEEE 20th Consumer Communications & Networking Conference (CCNC)*. IEEE. 2023, pp. 579–586.
- [67] M. Zangoeei et al. “Reinforcement Learning for Radio Resource Management in RAN Slicing: A Survey”. In: *IEEE Communications Magazine* (2023).
- [68] S. Zhang and D. Zhu. “Towards artificial intelligence enabled 6G: State of the art, challenges, and opportunities”. In: *Computer Networks* 183 (2020), p. 107556.
- [69] E. Fontes Pupo et al. “Dynamic Single/Multi-Rate Multicasting Aided NOMA for Addressing the Multiuser Diversity in 5G Networks”. In: (2023).
- [70] F. Rezazadeh et al. “Intelligible Protocol Learning for Resource Allocation in 6G O-RAN Slicing”. In: *arXiv preprint arXiv:2312.07362* (2023).
- [71] H. Zhang et al. “Slicing framework for service level agreement guarantee in heterogeneous networks—a deep reinforcement learning approach”. In: *IEEE Wireless Communications Letters* 11.1 (2021), pp. 193–197.
- [72] A. Giuseppi et al. “Network selection in 5G networks based on Markov Games and Friend-or-Foe Reinforcement Learning”. In: *2020 IEEE Wireless Communications and Networking Conference Workshops (WCNCW)*. IEEE. 2020, pp. 1–5.
- [73] Y. Sun et al. “Efficient handover mechanism for radio access network slicing by exploiting distributed learning”. In: *IEEE Transactions on Network and Service Management* 17.4 (2020), pp. 2620–2633.
- [74] S. AbdulRahman et al. “A survey on federated learning: The journey from centralized to distributed on-site learning and beyond”. In: *IEEE Internet of Things Journal* 8.7 (2020), pp. 5476–5497.
- [75] Y. Shao et al. “Graph attention network-based multi-agent reinforcement learning for slicing resource management in dense cellular network”. In: *IEEE Transactions on Vehicular Technology* 70.10 (2021), pp. 10792–10803.
- [76] Z. Abou El Houda et al. “When federated learning meets game theory: A cooperative framework to secure IIoT applications on edge computing”. In: *IEEE Transactions on Industrial Informatics* 18.11 (2022), pp. 7988–7997.
- [77] Y.-J. Liu et al. “Device association for RAN slicing based on hybrid federated deep reinforcement learning”. In: *IEEE Transactions on Vehicular Technology* 69.12 (2020), pp. 15731–15745.
- [78] Y. Cao et al. “User access control in open radio access networks: A federated deep reinforcement learning approach”. In: *IEEE Transactions on Wireless Communications* 21.6 (2021), pp. 3721–3736.

- [79] S. Wang et al. “Federated learning for task and resource allocation in wireless high-altitude balloon networks”. In: *IEEE Internet of Things Journal* 8.24 (2021), pp. 17460–17475.
- [80] F. Rezazadeh et al. “On the Specialization of FDRL Agents for Scalable and Distributed 6G RAN Slicing Orchestration”. In: *IEEE Transactions on Vehicular Technology* (2022).
- [81] A. Abouaomar et al. “Federated Deep Reinforcement Learning for Open RAN Slicing in 6G Networks”. In: *IEEE Communications Magazine* (2022).
- [82] P. Tehrani, F. Restuccia, and M. Levorato. “Federated deep reinforcement learning for the distributed control of NextG wireless networks”. In: *2021 IEEE International Symposium on Dynamic Spectrum Access Networks (DySPAN)*. IEEE. 2021, pp. 248–253.
- [83] S. M. Shahid et al. “Load balancing for 5G integrated satellite-terrestrial networks”. In: *IEEE Access* 8 (2020), pp. 132144–132156.
- [84] R. Su et al. “Resource Allocation for Network Slicing in 5G Telecommunication Networks: A Survey of Principles and Models”. In: *IEEE Network* 33.6 (2019), pp. 172–179.
- [85] Z. Han et al. *Game theory for next generation wireless and communication networks: Modeling, analysis, and design*. Cambridge University Press, 2019.
- [86] B. Han et al. “Admission and congestion control for 5G network slicing”. In: *2018 IEEE Conference on Standards for Communications and Networking (CSCN)*. IEEE. 2018, pp. 1–6.
- [87] S. K. Singh et al. “Machine learning-based network sub-slicing framework in a sustainable 5G environment”. In: *Sustainability* 12.15 (2020), p. 6250.
- [88] D. Ferreira et al. “A forecasting approach to improve control and management for 5G networks”. In: *IEEE Transactions on Network and Service Management* 18.2 (2021), pp. 1817–1831.
- [89] A. Baumgartner et al. “Optimisation models for robust and survivable network slice design: A comparative analysis”. In: *GLOBECOM 2017-2017 IEEE Global Communications Conference*. IEEE. 2017, pp. 1–7.
- [90] G. Wang et al. “Reconfiguration in network slicing—Optimizing the profit and performance”. In: *IEEE Transactions on Network and Service Management* 16.2 (2019), pp. 591–605.
- [91] W. Saad, M. Bennis, and M. Chen. “A vision of 6G wireless systems: Applications, trends, technologies, and open research problems”. In: *IEEE network* 34.3 (2019), pp. 134–142.
- [92] J. Antoniou. *Game theory, the internet of things and 5G networks*. Springer, 2020.

- [93] Z. Han. *Game theory in wireless and communication networks: theory, models, and applications*. Cambridge university press, 2012.
- [94] W. A. Gamson. “A theory of coalition formation”. In: *American sociological review* (1961), pp. 373–382.
- [95] E. Elkind, G. Chalkiadakis, and N. R. Jennings. “Coalition Structures in Weighted Voting Games”. In: *ECAI*. Vol. 8. 2008, pp. 393–397.
- [96] J. Moura and D. Hutchison. “Game theory for multi-access edge computing: Survey, use cases, and future trends”. In: *IEEE Communications Surveys & Tutorials* 21.1 (2018), pp. 260–288.
- [97] M. Mash et al. “Human-computer coalition formation in weighted voting games”. In: *ACM Transactions on Intelligent Systems and Technology (TIST)* 11.6 (2020), pp. 1–20.
- [98] C. Desogus et al. “Additive logarithmic weighting for balancing video delivery over heterogeneous networks”. In: *IEEE Transactions on Broadcasting* 67.1 (2020), pp. 131–144.
- [99] M. Anedda, M. Murrioni, and G.-M. Muntean. “A novel Markov decision process-based solution for improved quality prioritized video delivery”. In: *IEEE Transactions on Network and Service Management* 17.1 (2019), pp. 592–606.
- [100] R. Botez et al. “Efficient Network Slicing with SDN and Heuristic Algorithm for Low Latency Services in 5G/B5G Networks”. In: *Sensors* 23.13 (2023), p. 6053.
- [101] S. Khan et al. “Efficient and reliable hybrid deep learning-enabled model for congestion control in 5G/6G networks”. In: *Computer Communications* 182 (2022), pp. 31–40.
- [102] Z. Zhang and A. Duan. “An Adaptive Data Traffic Control Scheme with Load Balancing in a Wireless Network”. In: *Symmetry* 14.10 (2022), p. 2164.
- [103] M. H. H. Omar et al. “Using QoE Metric as a Decision Criterion in Multimedia Heterogeneous Network Optimization: Challenges and Research Perspectives”. In: *Journal of Computer Networks and Communications* 2024.1 (2024), p. 7864757.
- [104] H.-W. Kao and E. H.-K. Wu. “QoE sustainability on 5G and beyond 5G networks”. In: *IEEE Wireless Communications* 30.1 (2023), pp. 118–125.
- [105] Y. Ding et al. “Carbon emissions and mitigation potentials of 5G base station in China”. In: *Resources, Conservation and Recycling* 182 (2022), p. 106339.

- [106] D. Xu et al. “Understanding Operational 5G: A First Measurement Study on Its Coverage, Performance and Energy Consumption”. In: *Proc. of the Annual Conf. of the ACM Special Interest Group on Data Communication on the Applications, Technologies, Architectures, and Protocols for Computer Communication*. SIGCOMM ’20. Virtual Event, USA: ACM, 2020, pp. 479–494.
- [107] P. Suski, J. Pohl, and V. Frick. “All you can stream: Investigating the role of user behavior for greenhouse gas intensity of video streaming”. In: *Proceedings of the 7th International Conference on ICT for Sustainability (2020)*.
- [108] M. T. Sultan and H. El Sayed. “QoE-Aware Analysis and Management of Multimedia Services in 5G and Beyond Heterogeneous Networks”. In: *IEEE Access* 11 (2023), pp. 77679–77688.
- [109] A. A. Barakabitze, M. Liyanage, and A. Hines. “QoESoft: QoE Management Architecture for Softwarized 5G Networks”. In: *2020 IEEE International Conference on Communications Workshops (ICC Workshops)*. 2020, pp. 1–6.
- [110] B. Agarwal et al. “QoE-Driven Optimization in 5G O-RAN-Enabled HetNets for Enhanced Video Service Quality”. In: *IEEE Communications Magazine* 61.1 (2023), pp. 56–62.
- [111] R. R. R. Rao, S. Göring, and A. Raake. “AVQBits—Adaptive Video Quality Model Based on Bitstream Information for Various Video Applications”. In: *IEEE Access* 10 (2022), pp. 80321–80351.
- [112] F. Rahdari, M. R. Khayyambashi, and N. Movahhedinia. “A QoE-aware non-linear fuzzy radio resource management approach for revenue enhancement”. In: *IEEE Systems Journal* 17.1 (2022), pp. 1407–1418.
- [113] N. Abbas et al. “Price-aware traffic splitting in D2D HetNets with cost-energy-QoE tradeoffs”. In: *Computer Networks* 172 (2020), p. 107169.
- [114] ITU. *Recommendation ITU-T P.1201 (2013). Parametric Non-Intrusive Assessment of Audiovisual Media Streaming Quality - Amendment 2: New Appendix III — Use of ITU-T P.1201 for Non-Adaptive, Progressive Download Type Media Streaming*. Tech. rep. 2013.
- [115] A. Abrol and R. K. Jha. “Power optimization in 5G networks: A step towards GrEEen communication”. In: *IEEE Access* 4 (2016), pp. 1355–1374.
- [116] T. Hossfeld et al. “A Greener Experience: Trade-offs between QoE and CO₂ Emissions in Today’s and 6G Networks”. In: *IEEE Communications Magazine* (2023), pp. 1–7.
- [117] G. Bingol, T. Hossfeld, and C. Timmerer. “Sustainability vs. Quality of Experience: Striking the Right Balance for Video Streaming”. In: *ACM SIG-Multimedia Rec* (2023).

- [118] G. Bingöl et al. “Are Quality and Sustainability Reconcilable? A Subjective Study on Video QoE, Luminance and Resolution”. In: *2023 15th International Conference on Quality of Multimedia Experience (QoMEX)*. 2023, pp. 19–24.
- [119] P. Goudarzi et al. “Joint energy-QoE efficient content delivery networks using real-time energy management”. In: *IEEE Systems Journal* 14.1 (2019), pp. 927–938.
- [120] 3GPP. “5G; NR; Physical layer procedures for data (3GPP TS 38.214 version 16.2.0 Release 16)”. In: (2020).
- [121] 3GPP. “TS 138 300 V15.8.0 5G; NR; Overall description; Stage-2”. In: (2020).
- [122] R. W. Saaty. “The analytic hierarchy process—what it is and how it is used”. In: *Mathematical modelling* 9.3-5 (1987), pp. 161–176.
- [123] G. Sutorius. “Jitter Separation in High Speed Digital Design”. In: *Agilent Technologies* (2018).
- [124] Q.-T. Nguyen-Vuong, Y. Ghamri-Doudane, and N. Agoulmine. “On utility models for access network selection in wireless heterogeneous networks”. In: *NOMS 2008-2008 IEEE Network Operations and Management Symposium*. IEEE. 2008, pp. 144–151.
- [125] S. Radouche, C. Leghris, and A. Adib. “MADM methods based on utility function and reputation for access network selection in a multi-access mobile network environment”. In: *2017 International Conference on Wireless Networks and Mobile Communications (WINCOM)*. IEEE. 2017, pp. 1–6.
- [126] R. Khoder et al. “Vertical handover network selection architecture for VLC vehicular platoon driving assistance”. In: *2020 IEEE 31st annual international symposium on personal, indoor and mobile radio communications*. IEEE. 2020, pp. 1–6.
- [127] ITU-T. “Recommendation Y.3111 (09/2017): IMT-2020 network management and orchestration framework”. In: (2017).
- [128] ITU-T. “Recommendation Y.3150 (09/20): High-level technical characteristics of network softwarization for IMT-2020”. In: (2020).
- [129] F. D. Protection. “General data protection regulation (GDPR)”. In: *Intersoft Consulting, Accessed in October* 24.1 (2018).
- [130] J. Ding et al. “IoT connectivity technologies and applications: A survey”. In: *IEEE Access* 8 (2020), pp. 67646–67673.
- [131] A. B. MacKenzie and L. A. DaSilva. *Game theory for wireless engineers*. Springer Nature, 2022.
- [132] Huawei. “Empowering consumers focused immersive VR and AR experience with mobile broadband”. In: (2016).

- [133] A. Wang et al. “5G unlocks a world of opportunities: Top ten 5G use cases”. In: *Huawei Technologies Co., Shenzhen, China* (2017).
- [134] Qualcomm. “VR and AR pushing connectivity limits”. In: (2018).
- [135] V. VYAS. “Cloud Gaming Explained: Could It Be the Next Big Change?” In: Available: <https://arcanelost.com/cloud-gaming-explained-next-big-change/> (2020).
- [136] “The INET Framework”. In: Available: <https://inet.omnetpp.org/> (2021).
- [137] E. Hyytiä and J. Virtamo. “Random waypoint mobility model in cellular networks”. In: *Wireless Networks* 13.2 (2007), pp. 177–188.
- [138] L. Bonati et al. “Open, programmable, and virtualized 5G networks: State-of-the-art and the road ahead”. In: *Computer Networks* 182 (2020), p. 107516.
- [139] E. F. Pupo et al. “5G Link-Level Simulator for Multicast/Broadcast Services”. In: *2023 IEEE International Symposium on Broadband Multimedia Systems and Broadcasting (BMSB)*. IEEE. 2023, pp. 1–6.
- [140] 3GPP TR 38.901. “5G; Study on channel model for frequencies from 0.5 to 100 GHz (3GPP TR 38.901 version 16.1.0 Release 16)”. In: (2020).
- [141] M. Alzenad et al. “3-D placement of an unmanned aerial vehicle base station (UAV-BS) for energy-efficient maximal coverage”. In: *IEEE Wireless Communications Letters* 6.4 (2017), pp. 434–437.
- [142] M. Liyanage et al. “Open RAN security: Challenges and opportunities”. In: *Journal of Network and Computer Applications* 214 (2023), p. 103621.
- [143] S. D’Oro et al. “Orchestrator: Network automation through orchestrated intelligence in the Open RAN”. In: *IEEE INFOCOM 2022-IEEE Conference on Computer Communications*. IEEE. 2022, pp. 270–279.
- [144] O-RAN Alliance. “O-RAN.WG2.AI/ML-v01.03”. In: *O-RAN Working Group 2 AI/ML workflow description and requirements* (2021).
- [145] H. Van Hasselt, A. Guez, and D. Silver. “Deep reinforcement learning with double Q-learning”. In: *Proceedings of the AAAI conference on artificial intelligence*. Vol. 30. 1. 2016.
- [146] X. Wang et al. “In-edge AI: Intelligentizing mobile edge computing, caching and communication by federated learning”. In: *IEEE Network* 33.5 (2019), pp. 156–165.
- [147] G. Rjoub et al. “A trust and energy-aware double deep reinforcement learning scheduling strategy for federated learning on IoT devices”. In: *Service-Oriented Computing: 18th International Conference, ICSOC 2020, Dubai, United Arab Emirates, December 14–17, 2020, Proceedings 18*. Springer. 2020, pp. 319–333.
- [148] R. S. Sutton and A. G. Barto. *Reinforcement learning: An introduction*. MIT press, 2018.

- [149] A. Zai and B. Brown. *Deep reinforcement learning in action*. Manning Publications, 2020.
- [150] M. Chen et al. “A joint learning and communications framework for federated learning over wireless networks”. In: *IEEE Transactions on Wireless Communications* 20.1 (2020), pp. 269–283.
- [151] R. Luo et al. “Federated deep reinforcement learning for RIS-assisted indoor multi-robot communication systems”. In: *IEEE Transactions on Vehicular Technology* 71.11 (2022), pp. 12321–12326.
- [152] H. Yang et al. “Deep reinforcement learning-based intelligent reflecting surface for secure wireless communications”. In: *IEEE Transactions on Wireless Communications* 20.1 (2020), pp. 375–388.
- [153] H. Sharma, N. Kumar, and R. Tekchandani. “Mitigating Jamming Attack in 5G Heterogeneous Networks: A Federated Deep Reinforcement Learning Approach”. In: *IEEE Transactions on Vehicular Technology* (2022).
- [154] D. Pereira-Ruisánchez et al. “Deep contextual bandit and reinforcement learning for IRS-assisted MU-MIMO systems”. In: *IEEE Transactions on Vehicular Technology* (2023).
- [155] G. Egberts et al. “A Bayesian finite-element trained machine learning approach for predicting post-burn contraction”. In: *Neural Computing and Applications* 34.11 (2022), pp. 8635–8642.
- [156] N. Chukhno et al. “Efficient management of multicast traffic in directional mmWave networks”. In: *IEEE Transactions on Broadcasting* 67.3 (2021), pp. 593–605.
- [157] S. Han, T. Xie, and C.-L. I. “Greener Physical Layer Technologies for 6G Mobile Communications”. In: *IEEE Communications Magazine* 59.4 (2021), pp. 68–74.
- [158] G. Kougioumtzidis et al. “A survey on multimedia services QoE assessment and machine learning-based prediction”. In: *IEEE Access* 10 (2022), pp. 19507–19538.
- [159] C. C. González et al. “From MFN to SFN: Performance Prediction Through Machine Learning”. In: *IEEE Transactions on Broadcasting* 68.1 (2021), pp. 180–190.
- [160] C. C. González et al. “Three-stages concatenated Machine Learning model for SFN prediction”. In: *2021 IEEE International Symposium on Broadband Multimedia Systems and Broadcasting (BMSB)*. IEEE. 2021, pp. 1–6.
- [161] E. F. Pupo et al. “Thresholds of outperformance among Broadcast/Multicast access techniques in 5G networks”. In: *2021 IEEE International Symposium on Broadband Multimedia Systems and Broadcasting (BMSB)*. IEEE. 2021, pp. 1–6.

- [162] D. P. Ruisánchez et al. “Prediction of Signal Quality and SFN Interference Metrics Using Machine Learning Models”. In: *2021 IEEE International Symposium on Broadband Multimedia Systems and Broadcasting (BMSB)*. IEEE, 2021, pp. 1–6.
- [163] E. F. Pupo et al. “Dynamic Multicast Access Technique in SC-PTM 5G Networks: Subgrouping with OM/NOM”. In: *2022 IEEE International Symposium on Broadband Multimedia Systems and Broadcasting (BMSB)*. IEEE, 2022, pp. 1–6.
- [164] E. F. Pupo, C. C. González, and M. Murrioni. “Multi-rate Multicasting Over Fixed Pre-Computed MIMO Beams”. In: *2024 IEEE International Symposium on Broadband Multimedia Systems and Broadcasting (BMSB)*. 2024, pp. 1–6.
- [165] A. Collu et al. “Exploiting the benefits of in-band D2D communications for 5G-MBS use cases”. In: *2024 IEEE International Symposium on Broadband Multimedia Systems and Broadcasting (BMSB)*. 2024, pp. 1–6.